Master thesis

Model-assisted optimization of a recombinant *Corynebacterium glutamicum* bioprocess

Schiller Katrin Lisa-Maria, Bsc

(Matrikelnummer: 01540207)

University of Natural Resources and Life Sciences, Vienna

Master program: Biotechnology (066418)

Specialization: Biochemical and Bioprocess Engineering

Supervisors:

Christoph Herwig, Univ. Prof. Dipl.–Ing. Dr. techn.

Diethard Mattanovich, Univ.Prof. Dipl.-Ing. Dr.nat.techn.

Peter Sinner, M.Sc.

Thesis conducted at Technische Universität Wien; Institute of Chemical, Environmental and Bioscience Engineering (ICEBE); Research Area Biochemical Engineering

Vienna, 2020

Declaration of Authorship

I hereby declare that I am the sole author of this work. No assistance other than that which is permitted has been used. Ideas and quotes taken directly or indirectly from other sources are identified as such. This written work has not yet been submitted in any part.

Vienna, _____ _____

Date Signature

Acknowledgments

Throughout the conduction and writing of this master thesis, I have received a great deal of support and assistance.

I would first like to thank my supervisors Professor Christoph Herwig and Professor Diethard Mattanovich for their assistance. In addition, I want to thank Professor Christoph Herwig for offering me the opportunity to conduct my master thesis at his research group and for his participation and continuous contribution of ideas.

I want to acknowledge the members of the bioprocess simulation and control team of the technical university in Vienna, for the contribution of their time and knowledge. A special thank is directed to my advisor Peter Sinner MSc for his inspiration and constant provision of help. His insightful feedback pushed me to sharpen my thinking and brought my work to a higher level. Further, I like to thank Dr. Julian Kager for his consistent assistance with MATLAB, which saved me much time and nerves.

On a more personal level, I would like to thank my parents, who always encourage me and who made it possible to follow my dreams. Further, I want to thank my partner, my friends, and my family for believing in me and for always being there.

Furthermore, I want to express my gratefulness to apl. Prof. Dr. Christian Riedel and Dr. Oliver Goldbeck from the University of Ulm for providing us with the mCherry expressing *C. glutamicum* strain. Moreover, I want to acknowledge that this project has received funding from the Bio Based Industries Joint Undertaking under the European Union's Horizon 2020 research and innovation program under grant agreement N° 790507 (iFermenter).

Abstract

Corynebacterium glutamicum is a widely used host for amino acid production in industry but its full potential for recombinant protein production is not harnessed yet. Several hypotheses were investigated to test translational as well as transcriptional limitation factors of a recombinant protein production process. Cultivations were conducted with *Corynebacterium glutamicum* ATCC13032 (pOGOduet_mCherry). It has been investigated that different inducer concentrations did not affect productivity. Thus, the process seems not to be transcription limited. To test translational limitation factors due to energy limitations two approaches were used, on the one hand, a feeding strategy with unlimited substrate supply and on the other hand, the exploitation of anaplerotic reactions. It was investigated that with unlimited substrate supply the space-time yield of the production was improved by 40 % compared to a state-of-the-art substrate-limited fed-batch process. As substrates for anaplerotic reactions acetate and carbon dioxide were analyzed. Acetate as co-substrate with glucose did negatively affect the productivity and stability of the process under the used conditions. For in-silico design of the optimal process conditions for the investigation of the cell-produced carbon dioxide as a substrate, a quantitative and dynamic model was developed. By implementing the dynamics of carbon dioxide in the liquid and gas phase of the bioreactor, a model-based process design was successfully performed. With the aid of the model, the processes were designed to achieve different ranges of dissolved carbon dioxide to investigate the effect on the processes. It was found that with a low aeration strategy, the stability and the productivity of the recombinant mCherry production process with *Corynebacterium glutamicum* were enhanced, which is hypothesized to be due to less degassing of carbon dioxide. The simulation of the influence of the dissolved carbon dioxide concentration on the production rate increased the accuracy of the product simulation, which supports this hypothesis.

Zusammenfassung

Corynebacterium glutamicum wird häufig für die Aminosäurenproduktion in der Industrie eingesetzt, das Potential für die rekombinante Proteinproduktion wurde jedoch noch nicht voll ausgenützt. Verschiedene Hypothesen über Translations- als auch Transkriptionslimitierungsfaktoren solcher rekombinanter Produktionprozesse, wurden im Zuge dieser Arbeit untersucht. Für die Bioprozesse wurde *Corynebacterium glutamicum* ATCC13032 (pOGOduet_mCherry) verwendet. Beim Testen verschiedener IPTG-Konzentrationen zur Induktion konnte keine Produktivitätssteigerung erreicht werden. Dieses Ergebnis lässt darauf schließen, dass der Produktionsprozess nicht transkriptionslimitiert ist. Um translationslimitierende Faktoren bezüglich der Energiezufuhr zu untersuchen wurden zwei verschiedene Ansätze verwendet. Einerseits, eine unlimitierte Verfügbarkeit der Kohlenstoffquelle, und andererseits die Ausnutzung von anaplerotischen Reaktionen. Es wurde ermittelt, dass unlimitierte Substratverfügbarkeit zu einer 40 % höheren spezifischen Produktleistung, verglichen mit den gängigen Substrat-limitierten Fed-Batch Prozessen, führt. Acetat und Kohlenstoffdioxid wurden als mögliche Substrate solcher anaplerotischen Reaktionen überprüft. Als Co-Substrat, hatte Acetat einen negativen Effekt sowohl auf die Produktivität als auch auf die Stabilität des Prozesses unter den getesteten Bedingungen. Für das in-silico Design der optimalen Prozessbedingungen wurde ein quantitatives und dynamisches Model erstellt. Model-basierte Prozessplanung wurde mit Hilfe der Inkludierung von den Dynamiken von Kohlenstoffdioxid in der wässrigen und gasförmigen Phase des Bioreaktors erfolgreich durchgeführt. Die Prozesse konnten mit Hilfe des Modelles so geplant werden, dass unterschiedliche Konzentrationen von Kohlenstoffdioxid im Medium erreicht wurden und der Effekt auf die Prozesse untersucht werden konnte. Es konnte festgestellt werden, dass durch niedrigere Begasungsraten eine verbesserte Stabilität und Produktivität erreicht werden konnte, wobei angenommen wird das dies auf höhere Konzentrationen von Kohlenstoffdioxid im Medium zurückzuführen ist. Durch die Simulation des Effektes der Kohlenstoffdioxidkonzentration auf die Produktivitätsrate konnte eine Verbesserung der Produktsimulation erreicht werden, dies unterstützt die aufgestellte Hypothese.

Table of contents

1 Abbreviations 1
2 List of symbols 3
3 Introduction 6
3.1 Protein production with *Corynebacterium glutamicum* 6
3.2 Anaplerotic reactions 8
3.3 Fluorescent protein mCherry 11
3.4 Bioprocess modeling 12
3.5 Aims of the study and roadmap 14
4 Material and Methods 16
4.1 Used strain 16
4.2 Chemicals and equipment 16
4.3 Media and solutions 16
4.4 Cultivation methods 20
4.4.1 Strain maintenance and pre-cultures 20
4.4.2 Shake flask cultivation 21
4.4.3 Bioreactor cultivation 21
4.5 Analytical methods 24
4.5.1 Cell dry weight 24
4.5.2 Optical density 25
4.5.3 Substrate and metabolites analytics 25
4.5.4 Fluorescence measurement 25
4.5.5 Off-gas analysis 26
4.6 Cell disruption 27
4.6.1 Homogenization 27
4.6.2 Sonication 28
4.7 Protein analysis (SDS PAGE) 28
4.8 Determination of the mass transfer coefficient of lab-scale bioreactors 29
4.9 Data analysis 31
4.9.1 Data pre-treatment 31
4.9.2 Kinetic rates and yields 31
4.10 Mechanistic modeling 31
4.10.1 Parameter estimation 31
4.10.2 Simulation errors 32
4.10.3 Sensitivity analysis 32
5 Results and Discussion 33
5.1 Effect of the inducer concentration on product formation 33

5.2 Impact of acetate as co-substrate on process stability and productivity in substrate-limited fed-batch processes 36
5.3 Process stability and productivity of a substrate-limited and a substrate-unlimited fed-batch process with glucose 38
5.4 Comparison of different modeling approaches for biomass and substrate simulation 42
5.5 Model-based analysis of oxygen and carbon dioxide dynamics in bioprocesses 49
5.5.1 Oxygen uptake rate and carbon dioxide evolution rate 49
5.5.2 Mass transfer coefficient and transfer rates 53
5.5.3 Oxygen and carbon dioxide concentration in the liquid phase 57
5.5.4 Oxygen and carbon dioxide concentration in the gas phase 60
5.6 Sensitivity analysis for selection of process parameters for affecting dissolved carbon dioxide concentration 63
5.7 Impact of different aeration rates on growth and product formation during substrate-unlimited fed-batch processes 65
5.8 Modeling of carbon dioxide influence on productivity 70
5.9 Comparison of homogenization and sonication as cell disruption methods for C. glutamicum 73
6 Summary and conclusion 76
7 Outlook 79
8 References 80
9 List of figures 85
10 List of tables 88
11 Attachments 90
11.1 Chemicals 90
11.2 Equipment 92

1 Abbreviations

ATP ..... Adenosine triphosphate

CA ..... Carbonic anhydrase

CDW ..... Cell dry weight (Biomass)

CER ..... Carbon dioxide evolution rate

C. glutamicum ..... *Corynebacterium glutamicum*

CTR ..... Carbon dioxide transfer rate

dCO_2 ..... Dissolved carbon dioxide concentration

dO_2 ..... Dissolved oxygen concentration

DoE ..... Design of experiments

DoR ..... Degree of reduction

EDTA ..... Ethylenediaminetetraacetic acid

EMP ..... Embden, Meyerhoff, Parnas pathway

eq. ..... Equation

E. coli ..... *Escherichia coli*

Fab ..... antigen-binding fragment

FP ..... Fluorescent protein

glc ..... Glucose

GRAS ..... Generally regarded as safe

GFP ..... green fluorescent protein

hEGF ..... Human epidermal growth factor

ID ..... Identification

IPTG ..... Isopropyl-β-D-thiogalactopyranoside

k_La ..... mass transfer coefficient

MOPS ..... 3-morpholino propane sulfonacid

NADH ..... Nicotinamidadenindinucleotide

NRMSE ..... Normalized root-mean-square error

OD_{600} ..... Optical density at 600 nm

OTR ..... Oxygen transfer rate

OUR ..... Oxygen uptake rate

PBS ..... Phosphate buffered saline

PCx ..... Pyruvate carboxylase

PEP ..... Phosphoenolpyruvate

RQ.....Respiratory quotient

ScFv.....Singlechain variable fragment

SDS.....Sodium dodecyl sulfate

SDS PAGE..... Sodium dodecyl sulfate-polyacrylamide gel electrophoresis

TCA.....Tricarboxylic cycle

WRSS .....Weighted residual sum of squares

2 List of symbols

α_1 ..... Van't Riet parameter [-]

α_2 ..... Van't Riet parameter [-]

β ..... Van't Riet parameter [-]

ΔH^R ..... temperature dependence constant for Henry's law [K]

ε ..... ratio between gas hold up and reactor volume [-]

μ ..... specific growth rate [1/h]

θ ..... parameter set

θ_p ..... parameter value

σ ..... measurement error

δ_p^{msqr} ..... mean square root (influence at model output)

A ..... cross sectional area [m^2]

C_i ..... concentration of component i in the reactor [g/L]

$C_{k,i}$ ..... concentration of component i in the kth feed [g/L]

CER ..... carbon dioxide evolution rate [mol/h]

CTR ..... carbon dioxide transfer rate [mol/h]

d ..... number of measuring points of states [-]

D ..... stirrer diameter [m]

D_k ..... dilution rate [1/h]

D_{O2} ..... diffusion coefficient for oxygen in water [m^2/s]

dO_2 ..... dissolved oxygen [mol/L]

dO_2^* ..... dissolved oxygen in equilibrium according to Henry's law [mol/L]

D_{CO2} ..... diffusion coefficient for carbon dioxide in water [m^2/s]

dCO_2 ..... dissolved carbon dioxide [mol/L]

dCO_2^* ..... dissolved carbon dioxide in equilibrium according to Henry's law [mol/L]

DoR_{O2} ..... degree of reduction of oxygen [-]

DoR_X ..... degree of reduction of biomass [-]

DoR_{Glc} ..... degree of reduction of glucose [-]

E ..... conversion matrix of yield coefficients

$F_{AIR, in}$ ..... inlet air flow [L/h]

F_{gas} ..... gas flow rate [L/h]

F_{in} ..... Feed flow rate into reactor [L/h]

F_{out} ..... Harvest flow rate out of reactor [L/h]

$F_{O2,\,in}$ ..... inlet oxygen flow [L/h]

Glc_{met} ..... glucose metabolized [g]

H ..... Henry's law constant [atm L/mol]

H^0 ..... Henry's law constant at standard conditions [atm L/mol]

$[H^+]$ ..... hydronium concentration [mol/L]

$[HCO_3^-]$ ..... bicarbonate ion concentration [mol/L]

K ..... Van't Riet parameter [-]

k_1 ..... forward rate constant for r_1 [1/s]

k_{-1} ..... backward rate constant for r_1 [L/mol/s]

k_2 ..... forward rate constant for r_2 [L/mol/s]

k_{-2} ..... backward rate constant for r_2 [1/s]

K_1 ..... equilibrium constant of carbon dioxide hydration with water [mol/L]

K_2 ..... equilibrium constant of carbon dioxide hydration with hydroxide ion [mol/L]

K_i ..... inhibition parameter for glucose uptake rate decrease [$g_{Glucose}$]

K_s ..... substrate saturation constant [g/L]

k_La ..... mass transfer coefficient [1/h]

lag ..... decrease parameter for glucose uptake rate [$1/g_{Glucose}$] or [$1/g_{Biomass}$]

MW_{Glc} ..... molecular weight of glucose per carbon-mole [$g_{Glucose}/mol_C$]

MW_X ..... molecular weight of biomass per carbon-mole [$g_{Biomass}/mol_C$]

n ..... number of states [-]

N ..... stirrer speed [rpm]

NRMSE ..... Normalized root-mean-square error [%]

RMSE ..... root-mean-square error

OUR ..... oxygen uptake rate [mol/h]

OTR ..... oxygen transfer rate [mol/h]

p_{CO2} ..... partial pressure of carbon dioxide [bar]

p_{O2} ..... partial pressure of oxygen [bar]

p_{total} ..... total pressure in the reactor [bar]

P_{out} ..... product concentration in harvest [g/L]

q ..... reaction rate [g/g/h]

q_p ..... product formation rate [$g_{Product}/h$]

$q_{p,0}$ ..... specific product formation rate [$g_{Product}/g_{Biomass}/h$]

q_s ..... specific substrate uptake rate [$g_{Substrate}/g_{Biomass}/h$]

$q_{s,max}$ ..... maximum specific substrate uptake rate – Monod kinetic [$g_{Substrate}/g_{Biomass}/h$]

r_1 ..... rate of reaction of carbon dioxide hydration with water [mol/L/s]

r_2 ..... rate of reaction of carbon dioxide hydration with hydroxide ion [mol/L/s]

Ra_{inert} ..... Inert gas ration [-]

RQ..... respiratory quotient [-]

S ..... Substrate concentration in reactor [g/L]

S_{in}..... Sugar concentration in feed [g/L]

S_{out} ..... Sugar concentration in harvest [g/L]

T..... Temperature [K]

T_0 ..... standard temperature (298.15 K) [K]

t..... time [h]

V ..... Reactor volume [m^3]

V_{air} ..... gas hold up [m^3]

V_m..... molar volume of gas at norm condition (20 °C, 1 atm) [L/mol]

WRSS ..... Weighted residual sum of squares

X ..... biomass concentration [g/L]

X_{out} ..... Biomass concentration in harvest [g/L]

$y_{i,j}$ ..... measured state variable

$\hat{y}_{i,j}$ ..... estimated state of the model

y_{CO2} ..... mole fraction of CO_2 at the gas-liquid interface [%]

$y_{CO2, AIR}$ ..... mole fraction of CO_2 in air [%]

$y_{CO2, out}$ ..... mole fraction of CO_2 in exhaust gas [%]

$y_{O2, AIR}$ ..... mole fraction of O_2 in air [%]

$y_{O2, in}$ ..... mole fraction of O_2 in O_2 tank [%]

$y_{O2, out}$..... mole fraction of O_2 in exhaust gas [%]

$y_{O2, wet}$ ..... O_2 concentration diluted by water content [%]

$Y_{CO2/X}$..... Carbon dioxide yield [$mol_{Carbon}/g_{Biomass}$]

$Y_{O2/X}$ ..... Oxygen yield [$mol_{Oxygen}/g_{Biomass}$]

$Y_{P/X}$..... Product yield coefficient [$g_{Product}/g_{Biomass}$]

$Y_{X/S}$..... Biomass yield coefficient [$g_{Biomass}/g_{Substrate}$]

3 Introduction

3.1 Protein production with *Corynebacterium glutamicum*

The soil bacterium *Corynebacterium glutamicum* (*C. glutamicum*) shows a broad metabolic diversity. It is a gram-positive, short rod-shaped bacterium, which grows aerobic and facultative anaerobic on various sources of sugars and organic acids (Kalinowski et al., 2003; Michel et al., 2015). Furthermore, it is recognized to be non-endotoxic (absence of lipopolysaccharide), non-sporulating and belongs to the generally recognized as safe (GRAS) bacteria, which are the reasons it has been widely used as a host in industry (Lee et al., 2016). Moreover, it is a fast-growing expression system, which shows maximum growth rates up to 0.6 h^{-1} (Grünberger et al., 2013). It shows low extracellular protease activity and therefore it is a favorable host for secreted protease-sensitive proteins (Liu et al., 2013). The fact of the absence of lipopolysaccharides is favorable for the production of therapeutics, compared to gram-negative bacteria. This makes also the downstream process less demanding, which can increase the product yield of the processes (Lee & Kim, 2018). Due to the multilayered peptidoglycan layer of *C. glutamicum*, the cell disruption is more challenging than for gram-negative bacteria, as Liu et al. (2018) reported. This is an important factor, which has to be considered for the downstream processes of intracellular products.

In 1975 it was discovered that *C. glutamicum* is capable to produce L-glutamic acid from glucose. With optimized fermentation conditions, even the wild type can produce the amino acid in an industrial feasible scale (Kinoshita et al., 1957). Because of further improvements in the fermentation process and metabolic engineering of the strain, also L-lysine can be industrially produced with *C. glutamicum* (Graaf et al., 2001). Those amino acids have major importance for industry: L-glutamate and L-lysine show annual market volumes of around 2.5 and 1.5 million tons, respectively, and predicted market growth of 6 – 8 % per year (Becker & Wittmann, 2012). *C. glutamicum* is also widely used for the production of nucleic acids, alcohols and organic acids, and xylitol under oxygen deprivation conditions (Inui et al., 2004; Lee & Kim, 2018; Okino et al., 2005; Sasaki et al., 2010).

In 2003, the whole genome sequence of *C. glutamicum* ATCC13032 was published, which makes it even more valuable for the biotechnology industry, because targeted metabolic engineering is then capable. Thus, methods like reconstructing the metabolic flow of carbon into products are possible and make processes more economic (Kalinowski et al., 2003). To modify the metabolic processes there are three approaches, first the amplification of enzymes to increase product formation, second the reduction of the by-product formation, and third the introduction of enzyme feedback controls. Production methods include cytosolic, surface-

displayed enzyme, and secreted expression (Lee & Kim, 2018). There are several successful examples for metabolite production with *C. glutamicum*, like L-Alanine for animal feed, lactate for food packaging, and also polymers like cadaverine and rare sugars like D-Tagatose (Lee & Kim, 2018).

In contrast to metabolite production, protein production involves more steps, starting from the transcription of DNA to mRNA, to the translation to a polypeptide or protein, ending with some posttranslational modifications. Thus, recombinant production of enzymes or other proteins is more demanding than the production of metabolites, like amino acids. The recombinantly produced protein can be either the wanted end product or a tool to increase the productivity of a metabolite production process. As an example, by overexpression of enzymes of the biosynthetic pathway metabolite production can be increased, or by the recombinant introduction of enzymes, foreign metabolites can be produced. As an example, Okino et al. (2008) expressed D-lactate dehydrogenase from *Lactobacillus delbrueckii* to overcome limitations of lactic acid bacteria and showed a high D-lactate production in *C. glutamicum.* Other examples of cytosolic protein expressions are listed in the review of Lee and Kim (2018), like alanine dehydrogenase for L-Alanine production or glutamate decarboxylase from *Escherichia coli* (*E. coli*) for Gamma-aminobutyric acid production for foods and pharmaceutical products.

For the secreted expression, *C. glutamicum* has two native protein secretion mechanisms, the secretory and the twin-arginine translocation pathway (Lee et al., 2016). This is a main advantage of this microorganism, because with gram-negative bacteria like *E. coli* the production of secreted proteins is more complicated, due to the second cell membrane and secretion into the periplasmic space. Intracellular productions have the drawback of proteolytic degradation, the necessity of cell lysis, and the building of inclusion bodies, which must be refolded and lead to a higher effort in the downstream process (Srivastava & Deb, 2005). There are some successful examples for the recombinant protein production, where the secreted protein is the desired product. Date et al. (2006) demonstrated that the protein human epidermal growth factor (hEGF) can be secreted in an active form by *C. glutamicum* with a yield of 156 mg/L/day. *C. glutamicum* is also a possible alternative for mammalian cells, for the production of proteins that do not need glycosylation like single-chain variable fragment (scFv) and antigen-binding fragment (Fab), like Yim et al. (2014) showed in their work.

Compared with one of the leading hosts for recombinant protein production *E. coli, C. glutamicum* shows a much lower transformation efficiency and there are fewer expression systems available. Therefore, the development of the genetic engineering toolbox is needed to establish *C. glutamicum* as a protein production host for industry (Lee et al., 2016).

The lower product yields, which are obtained with *C. glutamicum*, can be increased by identification and subsequent optimization of critical process parameters to regulate bioprocess performance. Possible bioprocess parameters for adaptation are pH, aeration, temperature, and feed rates (Hermann, 2003).

A recombinant production process can be limited due to some transcriptional or translational factors. Transcriptional limitations can be investigated with different inducer concentrations, as Rittmann et al. (2008) described for engineering a glycerol utilization pathway for a *C. glutamicum* bioprocess. Translational limitations can be caused by deficient energy supply. To ensure a sufficient energy supply during a recombinant protein production process it would be possible to provide an unlimited supply of the main carbon source as example glucose or by refueling the precursor metabolites as described in the next section 3.2.

3.2 Anaplerotic reactions

Metabolism consists of the reactions of catabolism and anabolism. The degradation of macromolecules to smaller molecules is called catabolism, the opposite, the synthesis of complex molecules is called anabolism. During the catabolism energy is generated, most often in the form of adenosine triphosphate (ATP), which is used during the anabolism (Fromm & Hargrove, 2012). Reducing equivalents, like nicotinamide adenine dinucleotide (NADH) occupy an important role in metabolism. Those transfer the equivalent of one electron in redox reactions. The oxidized form NAD^+ gets reduced during the tricarboxylic acid cycle (TCA), and the reduced form NADH is then used as cofactor for example during oxidative phosphorylation or polymerization of metabolites.

Thus, central carbon metabolism fulfills three functions:

1. Production of reducing equivalents like NADH
2. Generation of high energy molecules like ATP
3. Provision of precursor metabolites for the generation of macromolecules (Kappelmann, 2018)

Each metabolic pathway produces one or more products, which can be end products or precursors for other pathways. For example, glycolysis, which is also called the Embden, Meyerhoff, Parnas Pathway (EMP), is not only the conversion of glucose to pyruvate but also produces ATP and precursors for the synthesis of macromolecules, like proteins and lipids. Within the TCA, the precursor pyruvate is oxidized to CO_2, water, and energy (Fromm & Hargrove, 2012). In addition to that, the TCA provides precursors for the synthesis of amino acids. These precursors have to be ‘refilled’, otherwise there would be a lack of the acceptor molecule oxaloacetate and the cycle cannot go on (Blombach et al., 2013). Those ‘refilling’

reactions are called anaplerotic reactions. Anaplerotic reactions are especially important for production processes of metabolites or proteins, where the precursors get drained. Amino acids are synthesized from metabolites of the EMP and the TCA (see Figure 1), and subsequently, amino acids are used for protein production. Thus, anaplerotic reactions are important to refill precursors to obtain a stable metabolism.

CO_2 and HCO_3^- are products of decarboxylation reactions, therefore their concentration in the culture medium increases during a growing culture process. To refuel the TCA CO_2 and HCO_3^- can be used via anaplerotic reactions. Each organism has some carboxylases, which uses CO_2 or HCO_3^- as substrates, and some decarboxylases, which produce CO_2 (Blombach & Takors, 2015).

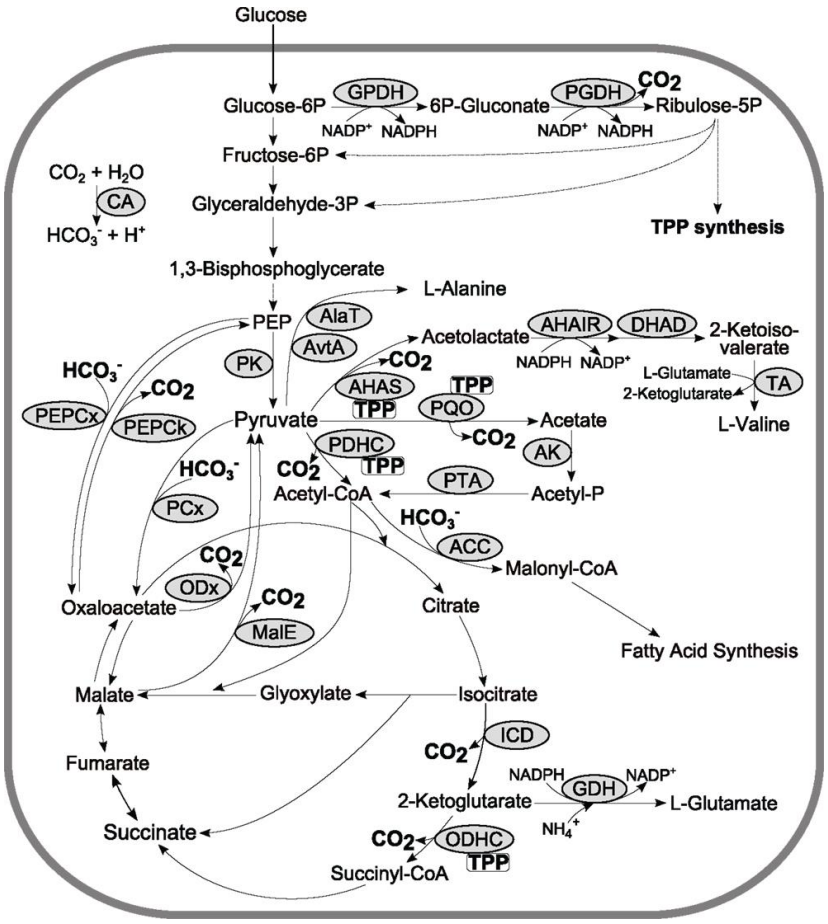

Figure 1: Central metabolism of C. glutamicum (Blombach & Takors, 2015); ACC, acetyl-CoA carboxylase; AHAIR, acetohydroxyacid isomeroreductase; AHAS, acetohydroxyacid synthase; AK, acetate kinase; AlaT, alanine aminotransferase; AvtA, valine-pyruvate aminotransferase; CA, carbonic anhydrase; DHAD, dihydroxy acid dehydratase; GDH, glutamate dehydrogenase; GPDH, glucose-6P dehydrogenase; ICD, isocitrate dehydrogenase; MalE, malic enzyme; ODHC, 2-ketoglutarate dehydrogenase complex; ODx, oxaloacetate decarboxylase; PCx, pyruvate carboxylase; PDHC, pyruvate dehydrogenase complex; PEP phosphoenolpyruvate; PEPCk, PEP carboxykinase; PEPCx, PEP carboxylase; PGDH, 6P-gluconate dehydrogenase; PK, pyruvate kinase; PQO, pyruvate:quinone oxidoreductase; PTA, phosphotransacetylase; TA, transaminase B; TPP, thiamine pyrophosphate

Figure 1 shows the central metabolism of *C. glutamicum*. Important for the carbon flux distribution are the carboxylating and decarboxylating enzymes at the node of phosphoenolpyruvate (PEP)-pyruvate-oxaloacetate. *C. glutamicum* is equipped with biotin-dependent pyruvate carboxylase (PCx) and PEP carboxylase. Interestingly, both enzymes have about 30-fold higher values for the Michalis-Menten constants (K_M) for bicarbonate, than the value of PEP carboxylase of *E. coli*. Thus, it is important to make sure that there are sufficient CO_2 and HCO_3^- availabilities, especially at the beginning of a bioprocess, where the biomass, and therefore the carbon evolution rate (CER) is low. This is especially important for products that need high anaplerotic flux, like succinate and L-lysine (Blombach & Takors, 2015). For instance, if due to high aeration, the carbon dioxide is stripped out, anaplerotic reactions can get substrate limited, which can subsequently cause reduced growth and productivity. Both, PEP carboxylase and pyruvate carboxylase are important anaplerotic enzymes. In addition, Figure 1 shows, that zinc-dependent carbonic anhydrases (CAs) catalyze the reversible hydration of CO_2. This is advantageous for the organisms, due to the low diffusive potential of CO_2 and the slow chemical conversion of CO_2 to HCO_3^- (Blombach & Takors, 2015). The importance of CAs is shown by Mitsuhashi et al. (2004). The inactivation of CAs caused severely reduced growth under atmospheric conditions, but with increased CO_2 concentrations in the aeration gas flow, growth was possible.

CO_2 and HCO_3^- can create transcriptional responses. (Blombach & Takors, 2015). The impact of different CO_2 and HCO_3^- levels on metabolism and regulation have been shown by Blombach et al. (2013). They observed an increased biomass to substrate yield during the initial growth phase under high CO_2 levels above 300 mbar. Different levels of pCO_2 between 0.2 – 0.3 bar do not influence growth rates of *C. glutamicum* if growing on glucose. In contrast to that, if lactate is used as a substrate, the maximum growth rates could be enhanced due to higher levels of pCO_2. The influence of adding bicarbonate on the product-yield of organic acids was investigated by Okino et al. (2005). Under oxygen deprivation *C. glutamicum* produces organic acids, when bicarbonate is added, the glucose consumption rate was increased which thus led to higher production rates. At higher bicarbonate concentrations, the succinic acid yield increased, and the lactic acid yield decreased. With higher CO_2 concentration in the process air, the formation of organic acids during L-lysine production with a leucine and homoserine auxotrophic *C. glutamicum* can be decreased (Hadj Sassi et al., 1996).

As mentioned in section 3.1, *C. glutamicum* is able to use different carbohydrates and organic acids as substrates. Glucose and acetate are used as substrates for amino acid production. As Figure 1 shows, after the uptake of acetate, it gets activated to acetyl coenzyme A. If acetate is the sole substrate, the glyoxylate cycle is needed as an anaplerotic pathway. Thus, the

involved enzymes in the glyoxylate cycle are essential if acetate is the sole substrate. On a medium with a mixture of acetate and glucose, *C. glutamicum* shows a nondiauxic growth, which means that both substrates are metabolized simultaneously, where total carbon consumption rates are comparable to those if one of the sugars is used as the sole substrate (Wendisch et al., 2000). If acetate is the sole substrate, the TCA shows higher activity than compared with the mixture or glucose. As mentioned above, during growth on glucose, the TCA cycle is refilled with carboxylation reactions of PCx and PEP carboxylase. During growth on acetate, the anaplerotic function is fulfilled via the glyoxylate cycle (Wendisch et al., 2000). Paegle and Ruklisha (2003) observed that although small amounts of acetate (added to a glucose pulse) decreases growth but it increases the cell-specific rate of lysine production and the lysine yield by *C. glutamicum* RC 115. Higher amounts of acetate resulted in decreased values of the production rate and yield. Therefore, acetate in low concentrations can be beneficial when used as a co-substrate to glucose.

3.3 Fluorescent protein mCherry

Fluorescent proteins (FPs) are an important tool in the field of cell biology research. mCherry belongs to the group of mFruits, which are second-generation monomeric red fluorescent proteins. The emission (550 – 650 nm) and excitation (550 - 650 nm) maxima are largely distributed (Shu et al., 2006). mFruits are mainly used as markers for in vivo applications in mammalian cell imaging. Those monomeric variants avoid oligomerization, which leads to perturbations in cellular activities during their use for tagging purposes (Regmi et al., 2013). mCherry, which was published in 2004, has a molecular weight of 26.7 kDa, and it is derived from *Discosoma sp.*. It is rapidly maturing and shows low acid sensitivity (Lambert, n.d.). mCherry is used as a fluorescent tracer for transfection and transgenic methods. It is derived from DsRed, which is a red FP related to the green fluorescent protein (GFP). (Neuromics, n.d.). All of those FPs need molecular oxygen to form chromophores (Regmi et al., 2013).

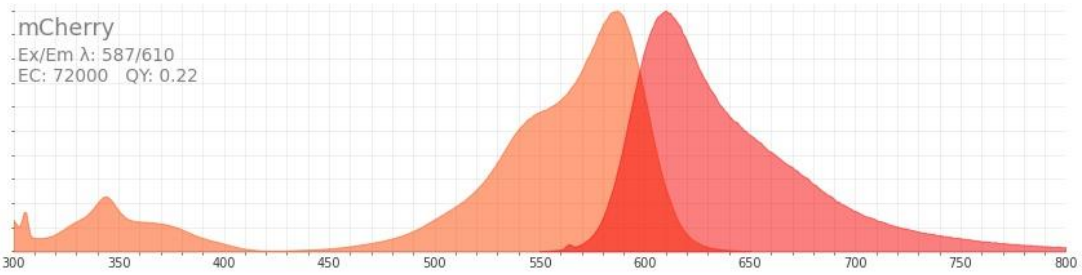

Figure 2: Fluorescence spectra of mCherry (Lambert, n.d.)

As shown in Figure 2, the maximum extinction and emission wavelengths of mCherry are 587 and 610 nm, respectively. The maturation requires 15 minutes and shows a half-life time of 68 seconds (Lambert, n.d.). For the maturation of the chromophore, two moles of oxygen are

needed, in contrast to the maturation of GFP, where only one mole oxygen is needed (Remington, 2006).

mCherry and other fluorescence proteins are often used as model proteins for investigations of recombinant protein production (section 3.1). To produce mCherry with *C. glutamicum* recombinantly, inducible promoters can be used. The Tac-promoter is a combination of the promoters trp and lac, it is inducible with Isopropyl-β-D-thiogalactopyranoside (IPTG) because the hybrid promoter uses the lac repressor and can be derepressed with IPTG. pTac is frequently used and is regarded as semi-strong (Boer et al., 1983). The Tet-promoter is inducible with the antibiotic tetracycline because in the presence of tetracycline, the tetracycline repressor binds to the antibiotic instead of the operator site and due to a conformational change, gene expression is possible (Carroll et al., 2005).

3.4 Bioprocess modeling

An important part of Bioprocess Engineering is on-line monitoring and controlling of bioprocesses. One strategy for this is based on mathematical modeling, to describe the dynamics of the bioprocess (Bastin, 1990). Model is a collective term for ‘representations of essential system aspects, with knowledge being presented in a workable form’ (van Waveren, 1999, p. 29). Models are used to simulate processes over time in order of changes in input parameters.

Due to the purpose of the model, it can be distinguished between simulation models and models for monitoring and control design. In contrast to complex simulation models, also called structured bioprocess models, that work with details about metabolic pathways, unstructured bioprocess models work with macroscopic mass balances, which include the main substrates and metabolites which are consumed and produced (Bastin & van Impe, 1995). By using bioprocess models, the development costs can be reduced and the process efficiency can be increased, compared to trial-and-error bioprocess development (Solle et al., 2017).

To describe the system, assumptions can be made to make the model more ‘usable’ (van Waveren, 1999). A model describes the biological behavior with mathematical expressions, like ordinary differential equations and non-linear and interacting reaction kinetics. Due to the structure of the model, it can be distinguished between mechanistic and data-driven models, although the distinction is sometimes blurred. Data-driven models describe input-output correlations, mechanistic models describe causal relationships utilizing process knowledge. The main parts of a typical mechanistic model are the reaction scheme with the reaction kinetics and model parameters. Model parameters are values that are supposed to be constant but are not exactly known. Within mechanistic models, typically parameters with a physical or qualitative meaning are used. In contrast to that, within data-driven models, the parameters

are just based on correlations to the process data. A combination of those two model types is called hybrid modeling (Solle et al., 2017). Modeling of a process starts with some basic knowledge and then gets extended until meeting the predefined demands (Daume et al., 2020).

As mentioned above, the bioprocess behavior can be described with a set of ordinary differential equations. Those describe the system states over time starting from a given initial state value. Material balances can describe some important process states like volume (equation (1)), biomass, substrate, and product (equation (2)) over time. The first term of the material balance (equation (2)) describes the dilution by the feed, where k denotes for the different feeds and i for the different components like as example glucose. The dilution D_k is determined by the feed rate and the current reactor volume. The second term describes the reaction kinetics, where E is a conversion matrix consisting of the yield coefficients (Daume et al., 2020).

$$\frac{dV}{dt} = \sum_{k=1}^{m} F_{in} - F_{out} \tag{1}$$

$$\frac{dC_k}{dt} = \sum_{k=1}^{m} \left(D_k \left(C_{k,i} - C_i \right) \right) + E \cdot q \cdot X \tag{2}$$

The used reactions rates q in equation (2) are often described with parameters. As an example, the substrate uptake rate q_s can be described with a Monod kinetic, which can be seen in equation (3). According to this equation, the substrate uptake rate is described by the glucose concentration with the aid of the parameters $q_{s,max,}$ and K_s, which represents the maximal uptake rate and the substrate saturation constant, respectively.

$$q_s = \frac{q_{s,max} * S}{S + K_S} \tag{3}$$

Values for those parameters can be determined from experimental data or by simulating and thereby minimizing the error between process data and the model prediction (Solle et al., 2017).

3.5 Aims of the study and roadmap

As mentioned in section 3.1 the recombinant protein production with *C. glutamicum* as expression host is not very established yet, although it is a GRAS bacteria that is extensively used in the industry mainly for amino acid production. The reasons for this are on the one hand the lower transformation efficiency and the less developed genetic engineering toolbox compared with the gram-negative *E. coli* and on the other hand, the lower product yields which can be obtained. Low yields are caused among other reasons by little knowledge of metabolic bottlenecks, which are limiting recombinant protein production. Therefore, a deeper process-understanding and knowledge about cell metabolism during production processes within bioreactors are needed (Liu et al., 2013).

Four hypotheses were tested to investigate translation as well as transcriptional limitation factors of a recombinant protein production process with *C. glutamicum*.

A. 'Different inducer concentrations are affecting productivity.'
   Different inducer concentrations were tested to overcome some potential transcriptional limitations. This approach was used for the improvement of an amino acid production process with *C. glutamicum* (Rittmann et al., 2008), thus it should be investigated if a positive effect could be achieved also with the *C. glutamicum* ATCC13032 (pOGOduet_mCherry) production process.

To overcome possible production limitations due to the energy supply two approaches were used.

B. 'A substrate-unlimited production process shows benefits compared with substrate-limiting processes.'
   An unlimited substrate supply should ensure the energy supply during recombinant protein production. Razak and Viswanath (2015) published an optimized initial glucose concentration of 80 g/L for lysine production in *C. glutamicum* MH 20-22 B during a batch process.

The second approach investigates the exploitation of anaplerotic reactions with two different substrates.

C. 'The addition of acetate as co-substrate to glucose influences the productivity and stability of the process by utilizing anaplerotic reactions.'
D. 'Lower aeration rates lead to higher carbon dioxide concentrations in the medium and therefore, to higher productivity and process stability by utilizing anaplerotic reactions.'
   As stated in section 3.2 several publications investigated the influence of carbon dioxide or acetate by exploiting anaplerotic reactions on product yields and growth of *C.*

glutamicum during amino acid or organic acid productions, but not during recombinant protein production.

A quantitative and dynamic model for describing biomass, substrate, and product during bioprocesses is made for in-silico design of process conditions. The model is used for bioprocess optimization of the protein production process and is experimentally verified. For the investigation of the influence of different carbon dioxide concentrations, the model gets extended to describe the dynamics of carbon dioxide in the liquid and gas phase of the bioreactor. For this issue also the mass transfer coefficient of the used bioreactors is determined. The model was used to determine the optimal process parameter to affect the dissolved carbon dioxide concentrations. Moreover, it was possible to design the process conditions to achieve different ranges of carbon dioxide during the experiments to investigate the effect on the process. Thus, trial-and-error experiments were avoided.

For the roadmap of the thesis see Figure 3:

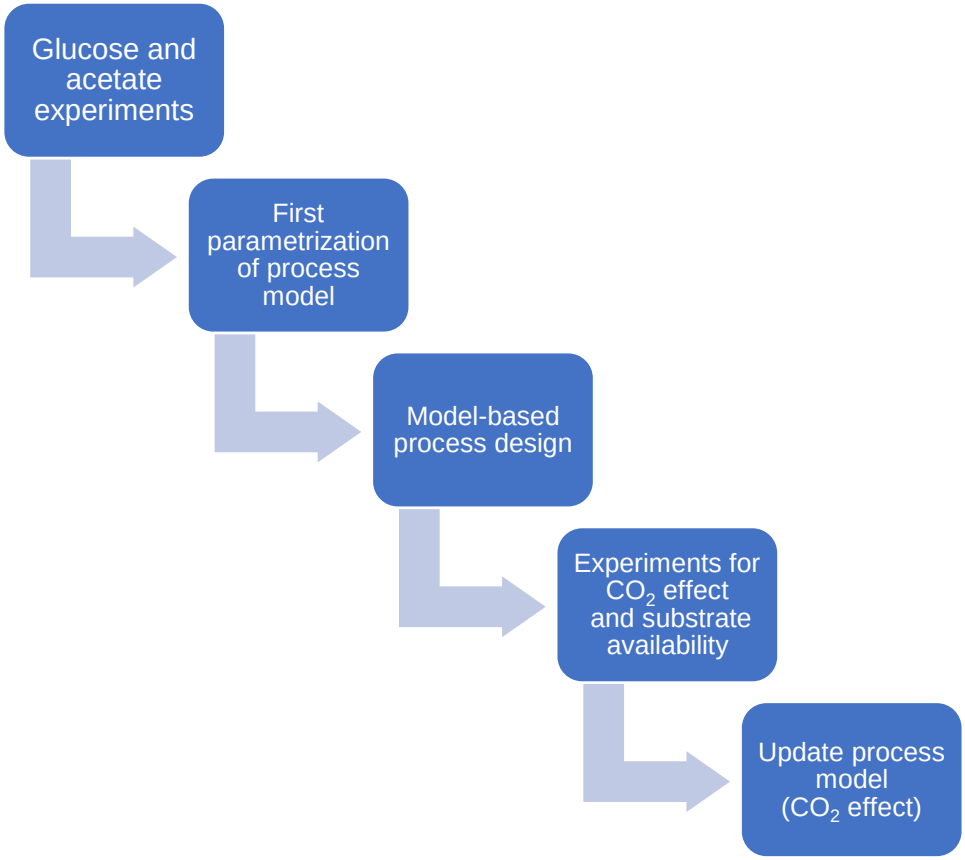

Figure 3: Roadmap of the thesis

4 Material and Methods

4.1 Used strain

For cultivations with mCherry production, the strain *Corynebacterium glutamicum* ATCC13032 (pOGOduet_mCherry) was used. pOGOduet is an expression vector for *C. glutamicum* with two independently inducible promoters Ptac and Ptet which are followed by two unique multiple cloning sites (Goldbeck & Seibold, 2018).

4.2 Chemicals and equipment

The lists of chemicals and equipment used in this work can be found in the attachments (Table 26, Table 27).

4.3 Media and solutions

2TY - complex media; used for preculture

Preparation: Components are dissolved in deionized water and autoclaved. A filter-sterilized antibiotic solution is added afterward. Agar is only added for agar plate preparation.

Table 1: Media composition 2TY

Chemical	Concentration	Unit
Tryptone	16	g/L
Yeast extract	10	g/L
Sodium chloride	5	g/L
Agar	18	g/L
Kanamycin sulfate (50 g/L)	50	µg/mL

CGXII - Minimal media; used for bioprocess

Preparation: Components were dissolved in deionized water and pH adjusted to 7 with 5 M KOH (for feed preparation: pH 6.5) and autoclaved. Magnesium sulfate heptahydrate, Calcium chloride dehydrate, Biotin, Trace element solution, and the Kanamycin were added after autoclaving (all as filter-sterilized stock solutions). As antifoam, polypropylene glycol 2000 was added to media used for bioreactor cultivations before autoclaving with a concentration of 0.5 mL/L. Urea and MOPS were only used for preculture steps in shake flasks, but not in the bioreactor. As Carbon source glucose and when indicated acetate as co-substrate was used,

the concentrations were varied for the experiments. IPTG was used for induction of the plasmid-encoded gene expression, the used concentrations were varied for the experiments.

Table 2: Media composition CGXII

Chemical	Concentration	Unit
Dipotassium hydrogen phosphate	1	g/L
Potassium dihydrogen phosphate	1	g/L
Ammonium sulfate	10	g/L
Urea	5	g/L
MOPS	21	g/L
Magnesium sulfate heptahydrate (1000x)	0.25	g/L
Calcium chloride dehydrate (1000x)	0.01	g/L
Biotin (1000x)	0.2	mg/L
Trace element solution (1000x)	1	mL/L
Kanamycin sulfate (50 g/L)	50	µg/mL

Acid - 6 M Ammonium hydroxide

Preparation: First water and then the acid is added, this is filled up to 1 L with deionized water and filled into a sterile bottle subsequently.

Table 3: Media composition base

Chemical	Concentration	Unit
deionized water	450	mL/L
Ammonium hydroxide (25 % (w/w), 13,30 M)	451	mL/L

Base - 1M Phosphoric acid

Preparation: First water and then the base is added, this is filled up to 1 L with deionized water and filled into a sterile bottle subsequently.

Table 4: Media composition acid

Chemical	Concentration	Unit
deionized water	250	mL/L
Phosphoric acid (85 % (w/w), 14,62 M)	68.42	mL/L

Phosphate buffered saline (PBS)

Preparation: For PBS, the chemicals are dissolved in deionized water and then autoclaved.

Table 5: Media composition phosphate-buffered saline

Chemical	Concentration	Unit
Sodium chloride	8	g/L
Potassium chloride	0.2	g/L
Disodium hydrogen phosphate dehydrate	1.8	g/L
Potassium dihydrogen phosphate	0.24	g/L

Trace elements solution (1000x)

Preparation: Components are dissolved in deionized water, the pH is adjusted to 1 by adding 32 % (v/v) hydrochloric acid, and the solution is sterile filtered subsequently.

Table 6: Media composition trace elements solution

Chemical	Concentration	Unit
Iron(ll) sulfate heptahydrate	16.4	g/L
Manganese sulfate monohydrate	10	g/L
Copper(ll) sulfate pentahydrate	0.2	g/L
Zinc sulfate heptahydrate	1	g/L
Nicke(ll) chloride hexahydrate	0.02	g/L

SDS – Laemmli buffer (4x)

Preparation: The chemicals are mixed and filled up with deionized water, then Bromophenol and β-Mercaptoethanol is added.

Table 7: Media composition 4xLaemli buffer

Chemical	Concentration	Unit
Tris (tris(hydroxyethyl)aminomethane)	250	mL/L
SDS (sodium dodecyl sulfate)	100	g/L
Glycerol	500	mL/L
Bromophenol	2.5	g/L
β-Mercaptoethanol	5	mL/L

SDS running buffer (10x)

Preparation: Dissolve glycine and tris base in deionized water, add SDS, and fill it up to 1L with deionized water. For usage, the solution is diluted 1:10.

Table 8: Media composition 10xSDS running buffer

Chemical	Concentration	Unit
Glycine	144	g/L
Tris base	30.2	g/L
SDS	10	g/L

Coomassie Brilliant Blue staining solution

Preparation: After dissolving the stain, the solution is stirred for several hours and then filtered.

Table 9: Media composition Coomassie brilliant blue staining solution

Chemical	Concentration	Unit
Coomassie Brilliant Blue	1	g/L
Methanol	500	mL/L
Acetic acid	100	mL/L
Deionized water	400	mL/L

Coomassie destaining solution

Table 10: Media composition Coomassie destaining solution

Chemical	Concentration	Unit
Methanol	200	mL/L
Acetic acid	100	mL/L
Deionized water	700	mL/L

Lysis buffer

Preparation: The chemicals are dissolved in deionized water, the pH is adjusted to 7.4 with hydrochloric acid, then the protease inhibitor is added.

Table 11: Media composition lysis buffer

Chemical	Concentration	Unit
TRIS (tris(hydroxyethyl)aminomethane)	12.1	g/L
EDTA (Ethylenediaminetetraacetate)	3.72	g/L
cOmplete™, Mini, EDTA-free Protease Inhibitor Cocktail	3	tablets/L

4.4 Cultivation methods

4.4.1 Strain maintenance and pre-cultures

The strain was stored as cryopreservative in a -80 °C freezer. The first pre-culture (step A) was done on a 2TY agar plate with the antibiotic kanamycin, which was incubated for about 30 hours at 30 °C. A single colony from step A was transferred to 5 mL 2TY medium with kanamycin (step B), which was incubated for about 15 hours in a rotary shaker (30 °C; 230 rpm). The culture of step B was then distributed to five 5 mL 2TY medium with kanamycin (step C), which was again incubated for about 8 hours in a rotary shaker (30 °C; 230 rpm).

For bioreactor cultivations: Next, the culture of step C was transferred to four 1 L total volume shake flasks without baffles with 150 mL CGXII medium with 10 g/L Glucose as carbon source (step D). This was incubated for about 15 hours in a rotary shaker (30 °C; 230 rpm). To remove the cultivation supernatant, the culture was transferred to 50 mL falcon tubes, which were centrifuged with 3240 g for 10 minutes at room temperature. The supernatant of 300 mL preculture of step D got discarded and the pellet was resuspended in 50 mL fresh CGXII reactor medium. This was used for the inoculum of the bioreactor.

For shake flask experiments: The culture from step C was transferred to 500 mL CGXII medium in an Ultra Yield™ 2.5 L flask with 15 g/L Glucose as carbon source. This was incubated for about 10 hours in a rotary shaker (30 °C; 230 rpm). For inoculum preparation, preculture supernatant was removed as described above for bioreactor cultivations.

4.4.2 Shake flask cultivation

To investigate the impact of different inducer concentrations the pre-culture from the previous section 4.4.1 was divided into six shake flasks, with each 150 mL of CGXII media (same used for pre-culture, but with 20 g/L Glucose as carbon source) to yield an initial optical density at 600 nm (OD_{600}) of about 7.7. Testing conditions are listed in Table 12.

Table 12: Shake flask cultivation conditions with different inducer concentrations

Shake flask	IPTG-concentration [µM]
1	0
2	20
3	100
4	200
5	500
6	1000

The shake flasks were incubated at 30 °C at 230 rpm for 72 hours. During incubation, six samples were drawn sterile (after 3, 6, 24, 52, and 72 hours). Metabolites and glucose as substrate were measured (see section 4.5.3), as well as the fluorescence (section 4.5.4) and the dry cell weight (section 4.5.1).

4.4.3 Bioreactor cultivation

4.4.3.1 Bioreactor setup

For the bioreactor cultivations, a 3.5 L stirred tank reactor with double Rushton turbines and baffles (Infors Labfors 5, microbial configuration) was used. The temperature was controlled with a heating/cooling system to 30 °C, the stirrer speed was bounded between 400 and 1200 rpm and the pH was controlled to 7 with 6 M ammonium hydroxide and 1 M phosphoric acid. Offline analytics like biomass (section 4.5.1), product (section 4.5.4), and substrate concentrations (section 4.5.3), as well as on-line analytics, were conducted. On-line signals like pH, dO_2, O_2, and CO_2 concentrations in the off-gas and feed, base, acid, and reactor weights were recorded with the process information management system Lucullus (Securecell, Switzerland). An illustration of the bioreactor setup is shown in Figure 4.

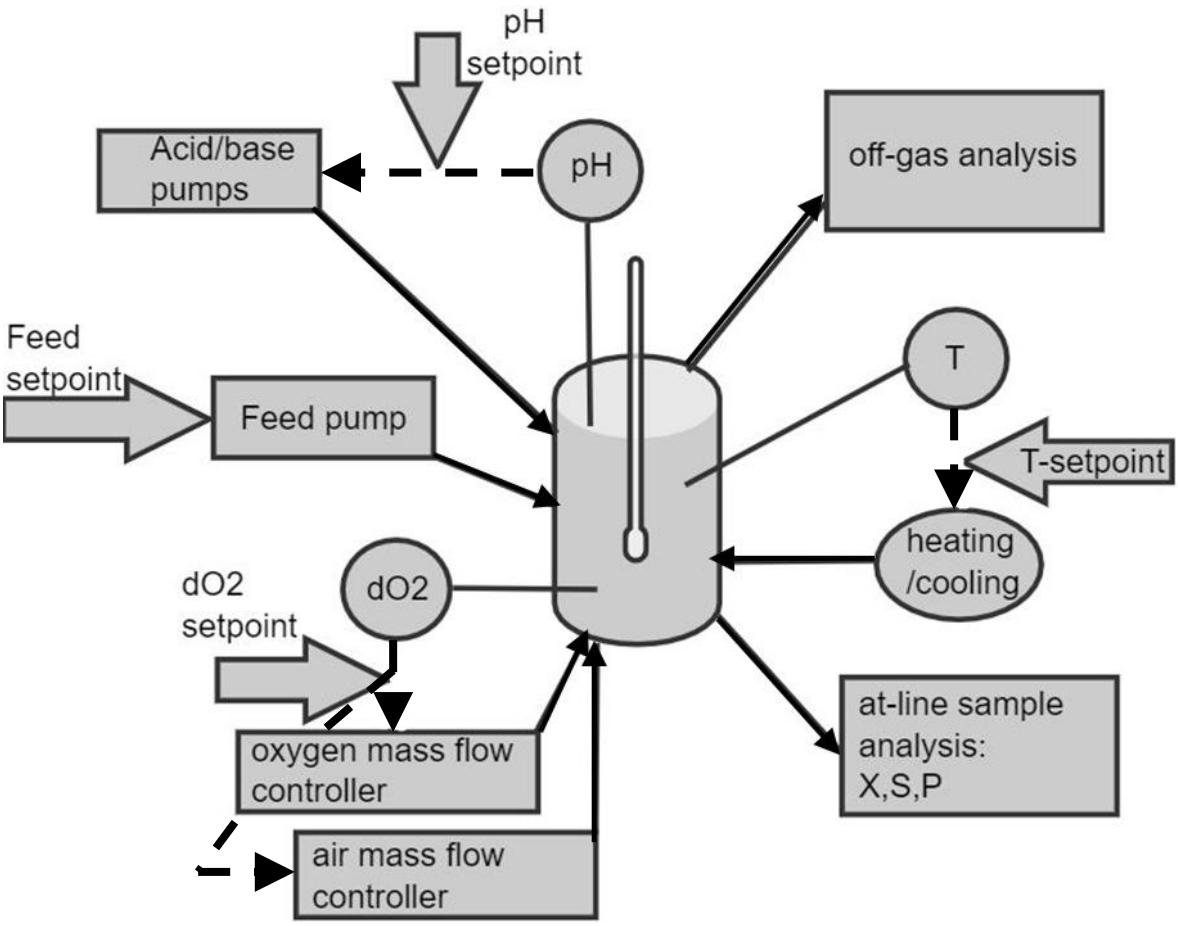

Figure 4: Simplified bioreactor setup with measurements of temperature, pH, and dO_2 and with off-gas analysis and at-line analysis of biomass, substrate, and product. Temperature is controlled with a heating and cooling jacket, the pH with acid and base pumps, and the dO2 with the gas flow controller and the stirrer speed.

4.4.3.2 Substrate-limited fed-batch processes with glucose and acetate as substrates

To analyze the effect of acetate as co-substrate of glucose during fed-batch processes two bioreactor cultivations were performed. The dissolved oxygen level was controlled to a value above 30 % by adapting the stirrer speed and the gas flowrate of sterile air and oxygen. As reactor batch medium 1.6 L of CGXII medium with 20 g/L glucose was used, which were inoculated with the preculture of section 4.4.1 to an OD_{600} of about 1.1. After the glucose was consumed, which was indicated by a sharply increasing dO_2 value, the feed was started. For the reactor with glucose as the sole carbon source, CGXII medium with 350 g/L glucose as feed was used. For the reactor with acetate as co-substrate, two feeds were used, both CGXII medium, one with 350 g/L glucose, and one with 50 g/L acetate. The feed rates for both bioprocesses are shown in Figure 5 and Figure 6. Both reactors were conducted with an exponential substrate-limited feed with a regulated growth rate of 0.07 h^{-1}. For the process with acetate as co-substrate, a ratio of 0.3:1 of acetate to glucose was used. To ensure the comparability of the experiments, other process conditions that may influence cellular growth or carbon dioxide availability were kept constant, for example, total pressure (about 1 bar), pH

(pH 7), and temperature (30 °C) (see section 4.4.3.1). At about 10 g/L CDW the reactors were induced with 0.5 mM IPTG. For induction, the IPTG was diluted in 8 mL deionized water and injected with a syringe into the bioreactor. Samples were taken one time during the batch phase and about every three hours during the fed-batch phase. Metabolites and glucose as substrate were measured (see section 4.5.3), as well as the fluorescence (section 4.5.4) and the dry cell weight (section 4.5.1).

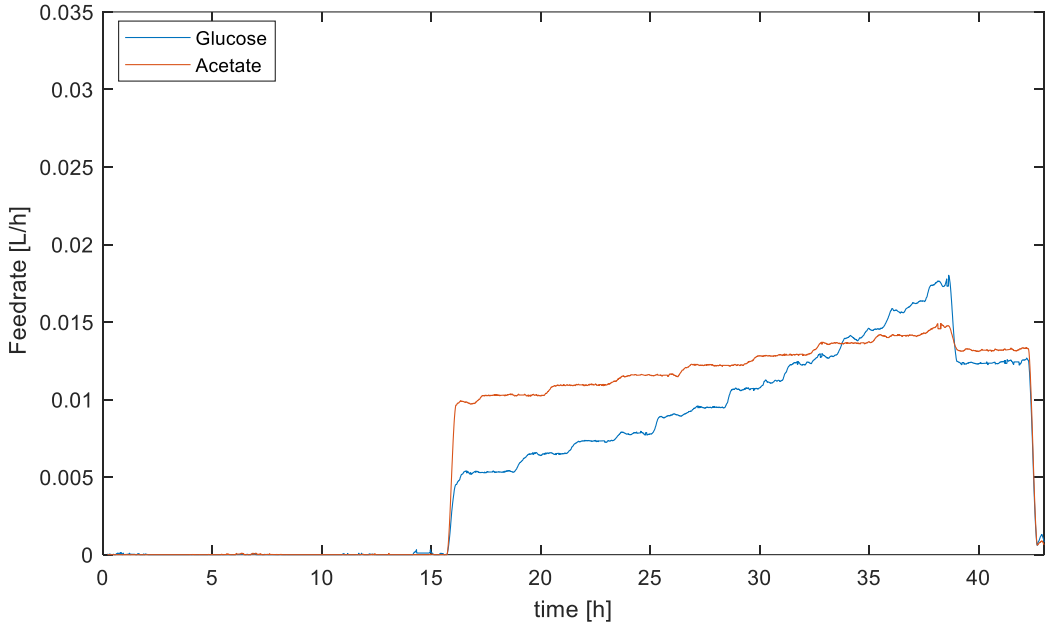

Figure 5: Feed rate of the substrate-limited fed-batch process with glucose and acetate

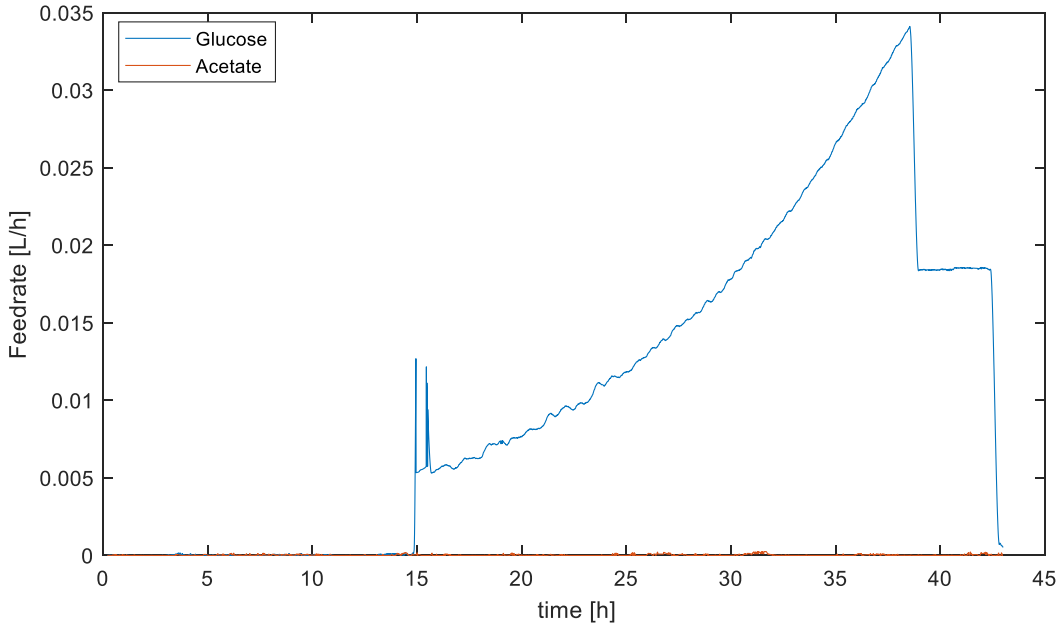

Figure 6: Feed rate of the substrate-limited fed-batch process with glucose

4.4.3.3 Fed-batch processes with different aeration rates

To investigate the effect on productivity and stability of processes with different aeration rates, four experiments in bioreactors were conducted. Three different aeration rates, 1.6 L/min, 0.8 L/min, and 0.25 L/min were examined (process conditions were in-silico designed with the model of section 5.5). The low aeration rate experiment was conducted two times, with different antifoam concentrations of 0.5 mL/L and 0.05 mL/L, the process with 0.8 L/min were conducted with 0.05 mL/L antifoam and the process with 0.25 L/min with 0.5 mL/L. To ensure the comparability of the experiments, other process conditions that may influence cellular growth or carbon dioxide availability were kept constant, for example, total pressure (about 1 bar), pH (pH 7), and temperature (30 °C) (see section 4.4.3.1). The dissolved oxygen level was controlled to a value of above 30 % by adapting the split of sterile air and pure oxygen and by altering the stirrer speed. All four experiments were conducted as unlimited-substrate fed-batch processes. For the batch phase, the minimal medium CGXII was used with a glucose concentration of 20 g/L. The feed was started when about 5 g/L glucose was left (estimated with substrate measurement and assumed growth rate of 0.4 h^{-1}). As feed, minimal medium CGXII with 350 g/L glucose was used. The bioprocesses were induced with 0.5 mM IPTG at about 10 g/L CDW. The IPTG was diluted in 8 mL deionized water and then injected with a syringe. Samples were taken at the beginning every 4 hours and after induction every 3 hours. Metabolites and glucose as substrate were measured (see section 4.5.3), as well as the fluorescence (section 4.5.4) and the dry cell weight (section 4.5.1). To achieve a substrate-unlimited process, real-time control with a soft sensor was utilized (described in section 5.3). During the process, glucose concentration should not exceed a limit of about 50 g/L. This maximum limit was chosen because of potential substrate inhibition effects and the carbon dioxide solubility is influenced by increasing glucose concentrations. Below 50 g/L the relative difference in solubility is below 5 %.

4.5 Analytical methods

4.5.1 Cell dry weight

1.8 mL of the culture sample was transferred in a pre-dried and pre-weighed 2 mL reaction tube and centrifuged at 11880 g at 4 °C for 10 minutes. The supernatants were collected and used for further measurements (sections 4.5.3 and 4.5.4). The cell pellets were washed with 1.8 mL PBS buffer and were centrifuged with the same parameters again. The supernatants were discarded, and the pellets were dried at 110 °C for at least 72 hours. The weights were determined with an analytical balance. The cell dry weight was determined in triplicates during the bioreactor experiments and in duplicates during the shake flask experiment.

4.5.2 Optical density

The OD was determined to observe the biomass formation during the cultivation. Therefore, the samples were measured in a photometer Genesys 20 (ThermoScientific, United States) at 600 nm. Because the linear range of the measurement is between 0.2 and 0.8, the samples were diluted with PBS to this range.

4.5.3 Substrate and metabolites analytics

Depending on the experiment, various substrates and metabolites were measured from the samples taken during the cultivation, like glucose, acetate, ammonium, glutamate, and lactate. 400 µL of the supernatant yielded from the centrifugation of the cell dry measurement (section 4.5.1) were measured at-line with CEDEX Bio HT Analyzer (Roche, Switzerland). Substrates and metabolites were measured with enzymatic photometry. For the measurements different enzymes were used: for acetate (AC2B 068) acetate kinase, phosphotransacetylase, citrate synthase, and L-malate dehydrogenase; for glucose (GLC3B 938) hexokinase and glucose-6-phosphate dehydrogenase; for glutamate (GLU2B 894) L- glutamate oxidase and peroxidase; for lactate (LAC2B 933) lactate oxidase and peroxidase; for ammonium (NH3B 914) glutamate dehydrogenase. Either NADH/NADPH or a formed chromogen was then measured photometrically.

4.5.4 Fluorescence measurement

To quantify matured mCherry as ‘active’ protein fraction, each whole broth sample (200 µL) and supernatant (200 µL; from section 4.5.1) was measured with an Infinite M200 PRO TECAN (TECAN, Switzerland) in black 96-well plates with flat bottom without a lid. Measurement was done at an excitation wavelength of 570 nm (bandwidth 9 nm), with a gain of 80, an emission wavelength of 600 nm (bandwidth 20 nm), in top reading mode with a number of reads of 25, with 20 µs integration time, 0 µs for lag and settle time. Z-position was at 20000 µm.

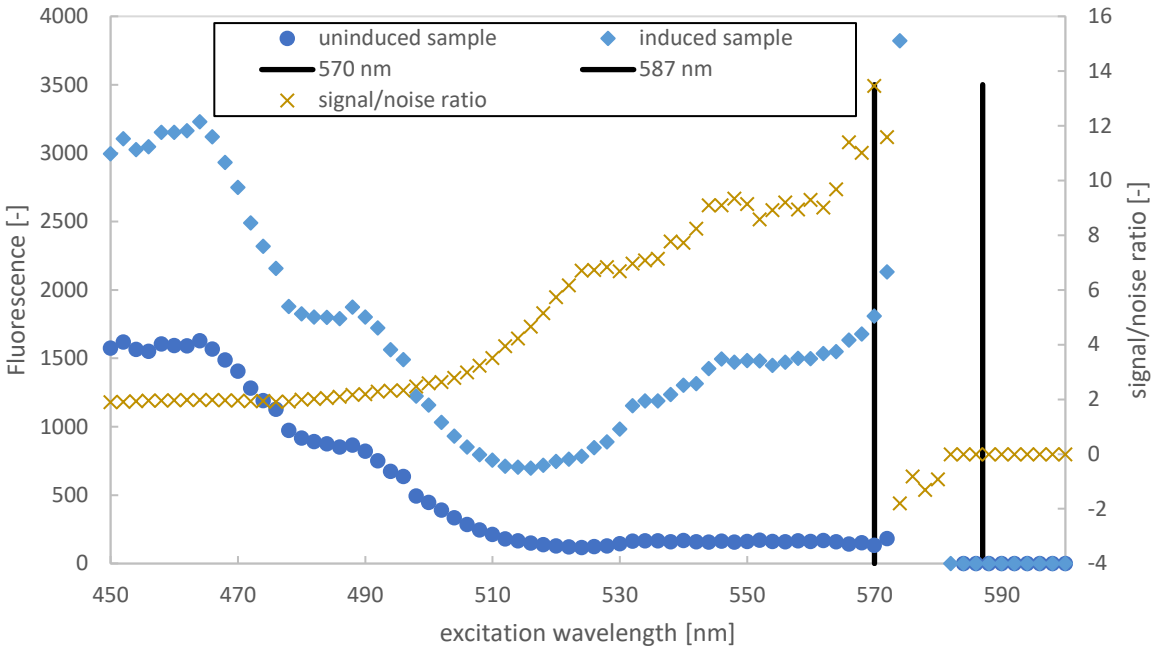

Figure 7: Signal to noise ratio of a fluorescence spectra, calculated with an uninduced and an induced sample of a recombinant mCherry bioprocess with C. glutamicum ATCC13032

Figure 7 shows, that the excitation wavelength 587 nm, which is used in literature (see section 3.3), is beyond the measurement range in the given setup (from 584 nm on values were out of range, denoted as zero in the diagram). Therefore, a value with a high signal to noise ratio was chosen, which was determined from the spectra of an uninduced and an induced sample with equation (4). The data set was obtained from the bioprocess experiment with low aeration with low antifoam concentration from section 4.4.3.3.

$$signal/noise\ ratio = \frac{value\ of\ induced\ sample}{value\ of\ uninduced\ sample} \qquad (4)$$

The highest signal/noise ratio was determined for the excitation wavelengths 568, 570, and 572 nm with values of 11.0, 13.5, and 11.6 respectively. Therefore, for further measurements of fluorescence, the excitation wavelength of 570 nm was chosen.

4.5.5 Off-gas analysis

During each bioreactor cultivation, off-gas analysis was conducted. For this issue, the oxygen and carbon dioxide mole fractions in the exhaust gas were measured with the BlueInOne or the BlueVary Ferm gas analyzer. Therefore, oxygen, as well as carbon dioxide, could be measured on-line and in real-time. The Ferm gas analyzer uses infrared (IR) spectroscopy for the carbon dioxide and zirconium dioxide for oxygen measurement. (BlueSens gas sensor GmbH, n.d.)

To calculate the CER, the oxygen uptake rate (OUR), and the respiratory quotient (RQ) the following equations (5), (6), (7), (8) were used in MATLAB (MathWorks, United States):

$$Ra_{inert} = \frac{1 - \frac{F_{O2,in} \cdot y_{O2,in} + F_{AIR,in} \cdot y_{O2,AIR} - F_{AIR,in} \cdot y_{CO2,in}}{F_{AIR,in} + F_{O2,in}}}{1 - y_{O2,out} - y_{CO2,out} - 1 - \frac{y_{O2,wet}}{y_{O2,AIR}}} \quad (5)$$

$$OUR = \frac{F_{AIR,in} + F_{O2,in}}{V_m} \cdot (Ra_{inert} \cdot y_{O2,out} - \frac{F_{O2,in} \cdot y_{O2,in} + F_{AIR,in} \cdot y_{O2,AIR}}{F_{AIR,in} + F_{O2,in}}) \quad (6)$$

$$CER = \frac{F_{AIR,in} + F_{O2,in}}{V_m} \cdot (Ra_{inert} \cdot y_{CO2,out} - \frac{F_{AIR,in} \cdot y_{CO2,in}}{F_{AIR,in} + F_{O2,in}}) \quad (7)$$

$$RQ = -\frac{CER}{OUR} \quad (8)$$

4.6 Cell disruption

4.6.1 Homogenization

For testing different cell disruption methods, frozen cell pellets (from 10 mL culture broth, centrifuged at 3240 g at 4°C for 10 minutes) were resuspended in 40 mL lysis buffer. Samples with lysozyme were incubated for 2 hours at 37 °C and 230 rpm. The homogenizer PandaPLUS 2000 (GEA Niro Soavi, Germany) was used for cell disruption. Homogenization was done with 120/1200 bar. The following conditions were tested:

Table 13: Cell disruption methods – tested conditions of homogenization

Time [min]	Lysozyme concentration [mg/mL]
5	15
5	0
20	0

After homogenization, the samples were centrifuged (4 °C, 9800 rpm, 10 minutes). The supernatant was stored in the freezer for further measurements (section 4.7). The pellets were washed with 30 mL deionized water (same conditions for centrifugation), the supernatants

were discarded. The pellets were resuspended in 10 mL deionized water and distributed to ten tubes, which were centrifuged (10 minutes; 14 000 rpm, 4 °C). The supernatants were discarded, and the pellets were stored in the freezer for further measurements (section 4.7).

4.6.2 Sonication

For testing different cell disruption methods, frozen cell pellets (from 10 mL culture broth, centrifuged at 3240 g at 4°C for 10 minutes) were resuspended in 15 mL lysis buffer. Samples with lysozyme were incubated for 2 hours at 37 °C and 230 rpm. The samples were treated with a sonication lance (Bandelin, Germany), with a 75 % amplitude and 30 s pulse. The following conditions had been tested:

Table 14: Cell disruption methods – tested conditions of sonication

Time [min]	Lysozyme concentration [mg/mL]
30	15
20	15
30	5
20	5
45	0
30	0

For the cell disruption analysis (section 4.7), the samples were centrifuged (10 minutes; 14 000 rpm at 4°C). Pellets and supernatants were stored in the freezer.

For the protein analysis of the bioprocess experiments with different aeration rates (section 4.4.3.3), the pellets (from 1.8 mL broth) got resuspended in 1.8 mL lysis buffer. The samples were treated with a sonication lance (Bandelin, Germany), with a 75 % amplitude and 30 s pulse for 30 minutes. The whole broth was used for protein analysis as described in section 4.7.

4.7 Protein analysis (SDS PAGE)

An SDS PAGE (sodium dodecyl sulfate-polyacrylamide gel electrophoresis) was done with the samples from the cell disruption test:

For the SDS PAGE, the pellets from the centrifuged lysed broth of section 4.6 were resuspended in 1.8 mL lysis buffer. The supernatants of section 4.6 were used undiluted. 60 µL sample and 20 µL Laemmli buffer (4x) were mixed and incubated for ten minutes at 95 °C. 10 µL of the mixture were added to a 4 - 15 % Mini-PROTEAN TGX gel (BIORAD, United

States). 10 µL PageRuler Prestained marker 10-250 kDa (ThermoScientific, United States) was used. The gels were run for about 45 minutes at 170 V. The gels were dyed with a Coomassie blue stain for 30 minutes and were destained one time for 10 minutes and then a second time for about one hour at room temperature on a rotary shaker.

A second SDS PAGE gel was made for the protein analysis of the experiments with different aeration rates:

The 1.8 mL treated broth of section 4.6.2 was diluted with lysis buffer, intending to reach an OD_{600} of 20 on the SDS PAGE. 60 µL sample and 20 µL Laemmli buffer were mixed, and 10 minutes incubated at 95 °C. 10 µL of the mixture were added to a 4 – 15 % Mini-PROTEAN TGX gel (BIORAD, United States). 4 µL of the marker 'Precision Plus Protein Unstained' (BIORAD, United States) was used. The gels were run for about 45 minutes at 170 V. The gels were dyed with a Coomassie blue stain for 30 minutes and were destained one time for 10 minutes and then a second time for about one hour at room temperature on a rotary shaker.

4.8 Determination of the mass transfer coefficient of lab-scale bioreactors

The mass transfer coefficient (k_La) was determined for both reactors which were used during the conduction of this thesis. The mass transfer coefficient is, as Van't Riet (1979) stated, dependent on the gas flow rate and the stirrer speed. The relevant mathematical relationship is shown in equation (9).

$$kLa_{O2} = K \cdot N^{\alpha 1} \cdot D^{\alpha 2} \cdot \left(\frac{F_{AIR,in}}{A}\right)^{\beta} \quad (9)$$

A design of experiments (DoE) according to Figure 8 was chosen to cover all conditions used during the bioreactor cultivations. Therefore, the limits for the gas flow rate were set to 0.2 till 2 L/min and the limits for the stirrer speed to 400 till 1200 rpm. Altogether, 13 conditions were tested in triplicates.

For the determination, minimal medium CGXII with 20 g/L glucose was used. The bioreactor setup and conditions shown in the section 'Bioreactor setup' were used. The DoE shown below was tested for two concentrations of antifoam: 0.05 mL/L and 0.5 mL/L.

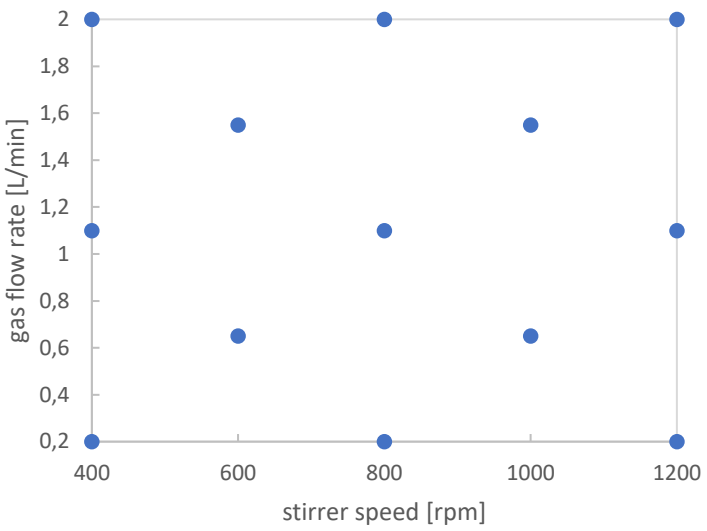

Figure 8: Design of experiments for the determination of the mass transfer coefficient of bioreactors

The k_La was measured using a dynamic method. For this, the changes in the dissolved oxygen values were measured with an oxygen electrode. The dO_2 sensor was two-point calibrated at 1000 rpm, the 100 % point was calibrated with 2 L/min airflow and the 0 % point with 1 L/min nitrogen. Each measurement started with degassing, where nitrogen was sparged to degas oxygen in the fermenter. When the dO_2 value was below 0.2 % the measurement started with one parameter set of gas flow and stirrer speed as stated in the DoE. The change of dO_2 was measured until a value above 97 % (assumed as dO_2*, the dissolved oxygen in equilibrium according to Henry's law) was reached. According to equation (10), the k_La values were calculated for each measurement point using the MATLAB (MathWorks, United States) function fminsearch.

$$\frac{d\ dO_2}{d\ t} = kLa \cdot (dO_2{}^* - dO_2) \qquad (10)$$

This function is used to find a local minimum of a function by varying a parameter (MathWorks Deutschland, n.d.–a). In this case, the parameter k_La is varied until the error between the observed change of dO_2 and the calculated change according to equation (10) is minimal.

For parameter estimation of α1, α2, β, and K from equation (9) also the fminsearch function in MATLAB (MathWorks, United States) was used.

4.9 Data analysis

4.9.1 Data pre-treatment

To use the obtained data of the bioprocess experiments for further calculations some pre-treatment was necessary. To remove outliers caused by manual sampling from the data sets obtained by the balances (feed, acid, base, reactor) the MATLAB (MathWorks, United States) function Hampel filter was used. This function determines the median of a window (data point including surrounding data points) and if the data point differs from the median more than three standard deviations, it is replaced with the median value (MathWorks Deutschland, n.d.–b). During data analysis in this thesis, a window of 200 data points was used.

4.9.2 Kinetic rates and yields

Calculations of substrate uptake and other growth characteristics in MATLAB (MathWorks, United States) are based on the following equations (11), (12), (13), and (14). Those equations can be used for common cultivation types, like batch, fed-batch, and continuous cultivation, with the assumption that there are no products or biomass in the feed. Terms for rates in and out of the reactor can be neglected depending on the cultivation type.

$$\mu = \frac{r_X}{X} = \frac{\frac{dX}{dt} + \frac{F_{out}}{V} \cdot X_{out}}{X} \tag{11}$$

$$q_S = \frac{r_S}{X} = \frac{\frac{dS}{dt} - \frac{F_{out}}{V} \cdot S_{out} + \frac{F_{in}}{V} \cdot S_{in}}{X} \tag{12}$$

$$Y_{X/S} = \frac{\Delta X}{\Delta S} \tag{13}$$

$$q_P = \frac{r_P}{X} = \frac{\frac{dP}{dt} + \frac{F_{out}}{V} \cdot P_{out}}{X} \tag{14}$$

4.10 Mechanistic modeling

4.10.1 Parameter estimation

Parameters of the model were estimated to minimize the error between the observed and the simulated states. This was done by using the function of Weighted Residual Sum of Squares

(WRSS, see equation (15)), which can determine a set of parameters that gives a minimal WRSS as a compromise for all given states (equation (16)) (Daume et al., 2020).

$$WRSS = \sum_{i=1}^{n} \sum_{j=1}^{d} \left(\frac{y_{i,j} - \widehat{y_{i,j}}}{\sigma_{i,j}}\right)^2 \quad (15)$$

$$\hat{\theta} = argmin\,[WRSS(\theta)] \quad (16)$$

The same equations were used for the estimation of a global parameter set for the multiple data sets.

4.10.2 Simulation errors

To determine the deviations of the simulated states ŷ to the experimental states y throughout the whole period, the Normalized Root-Mean-Square Error (NRMSE, see equation (17)) was used.

$$NRMSE = \frac{\sqrt{\frac{1}{d}\sum_{j=1}^{d}(y_j - \hat{y}_j)^2}}{max(y) - \min(y)} \quad (17)$$

4.10.3 Sensitivity analysis

To determine the effects of process and model parameters on the carbon dioxide concentration, a sensitivity analysis was conducted. Whereby sensitive parameters have a high impact on the output. The local sensitivity S was determined by numerical approximation. Here small parameter deflections of few percentages were used to determine the overall impact on the model output.

$$\delta_p^{msqr} = \sqrt{\frac{1}{n}\sum_{i=1}^{n} \overline{S_{i,p}}} \quad (18)$$

$$\overline{S_{i,p}} = \frac{\partial\, y_i}{\partial \theta_p} \cdot\, \theta_p \quad (19)$$

A high value of δ_p^{msqr} is caused by a high influencing parameter θ_p on the selected model output y_i (Daume et al., 2020).

5 Results and Discussion

5.1 Effect of the inducer concentration on product formation

To determine if mCherry is an intra- or extracellular product, the results of the fluorescence measurement of supernatants were compared to those of the whole broth. The data was obtained from the shake flask with 0.5 mM IPTG inducer concentration.

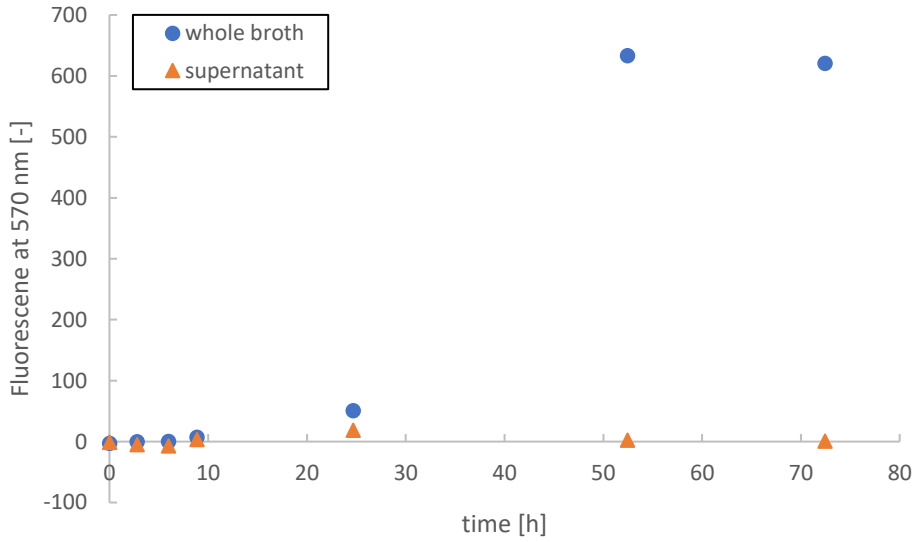

Figure 9: Comparison of fluorescence measurements values of supernatants and whole broth samples of shake flask cultivation with C. glutamicum ATCC13032 (pOGOduet_mCherry) with 0.5 mM IPTG for determination of product location

Figure 9 shows that the supernatant obtained much lower fluorescence values than the broth. The last two samples showed fractions below one percent. Therefore, it was assumed that mCherry is produced as an intracellular product in *C. glutamicum* ATCC13032 (pOGOduet_mCherry). The following results of fluorescence refer always to the whole broth measurements unless otherwise stated.

Figure 10 and Figure 11 show the time courses of the CDW and the fluorescence at 570 nm measurements of the cultivations with different inducer concentrations. All tested inducer concentrations lead to similar high CDW, therefore no difference in the growth could be detected due to the different induction. The cultivation with 500 µM IPTG showed a high CDW value after about two days, but as the high standard deviation of this sample point indicates, this is most likely a measurement error, due to uncertainties during sample treatment.

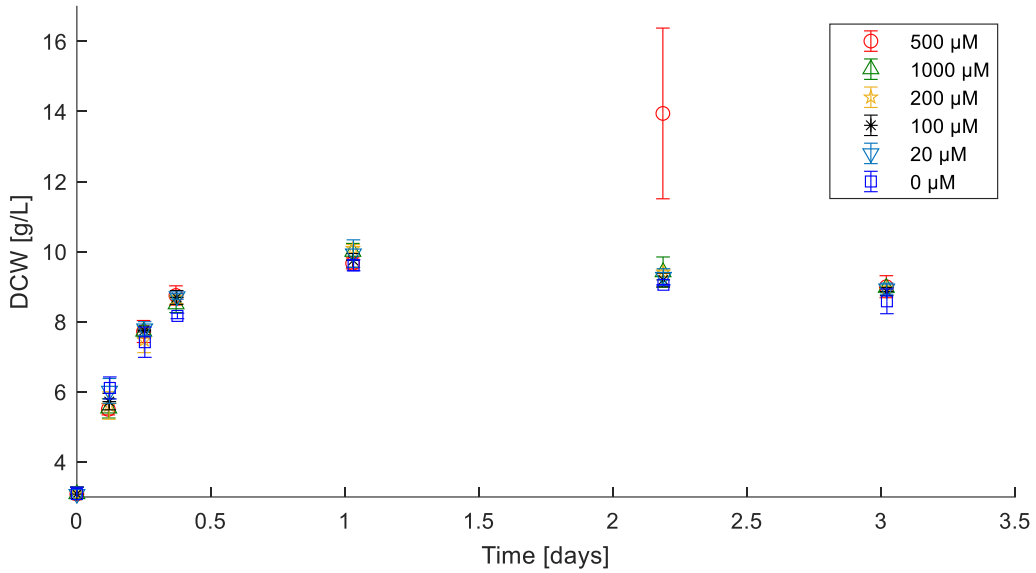

Figure 10: Time course of CDW measurements of shake flask cultivation of C. glutamicum ATCC13032 (pOGOduet_mCherry) with different inducer concentrations (500 µM, 1000 µM, 200 µM, 100 µM, 20 µM, and 0 µM IPTG)

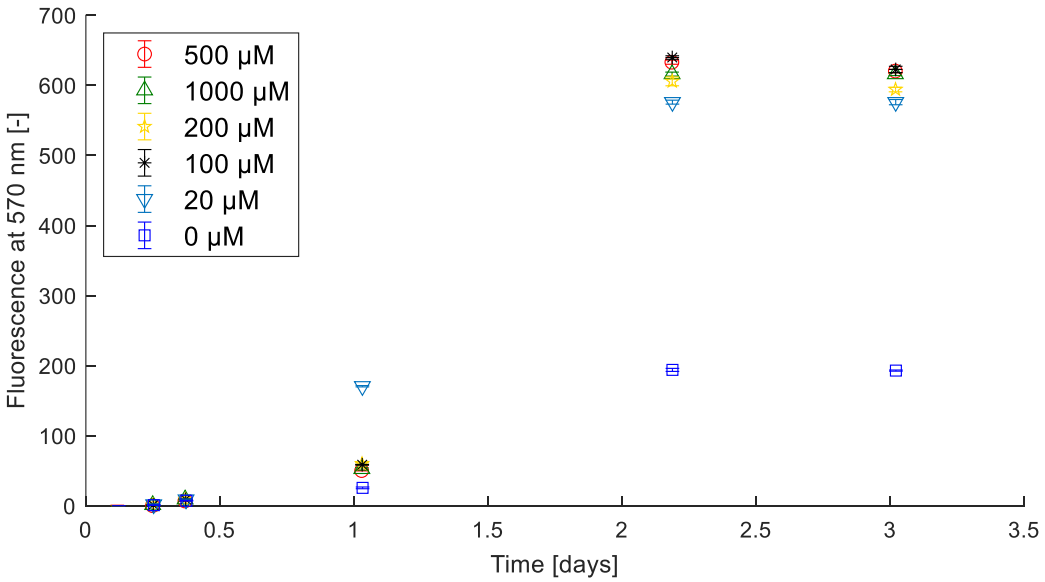

Figure 11: Time course of fluorescence measurements at 570 nm of shake flask cultivation of C. glutamicum ATCC13032 (pOGOduet_mCherry) with different inducer concentrations (500 µM, 1000 µM, 200 µM, 100 µM, 20 µM, and 0 µM IPTG)

If both figures (Figure 10, Figure 11) are compared, it can be seen that although the induction was done at the process beginning, the fluorescence values started increasing as recently as the growth stopped. This is most probable, because the maturation of mCherry needs oxygen (see section 3.3), and the growth during shake flask cultivation is oxygen-limited. Therefore, mCherry maturated when there was no oxygen uptake from the culture anymore and thus, oxygen was available. These results show that for further investigation of the inducer effects, an inducer screening under oxygen unlimited concentration would be necessary, this could be achieved by using another cultivation system, like a laboratory-scale bioreactor system.

Figure 12 illustrates, that the different inducer concentrations did not influence the product formation at a high level. Except for the negative control cultivation (0 mM IPTG), all cultivations reached a similar maximal fluorescence value. Low production yields can be caused by limitations of translation or transcription as described in section 3.1. The observed fluorescence is the last step of a complex product formation process, starting from transcription to translation, and with final posttranslational modifications. From this initial shake flask cultivations, it is difficult to determine which step is the rate-limiting one. Due to the similar results of different inducer concentrations, it could be an indication, that translation is the limiting step instead of transcription. In other cases, ITPG concentration influenced productivity, as Rittmann et al. (2008) showed in their work about recombinant glycerol kinase expression in *C. glutamicum*. In this investigation, varying IPTG concentrations led to different growth rates, due to different glycerol kinase activities.

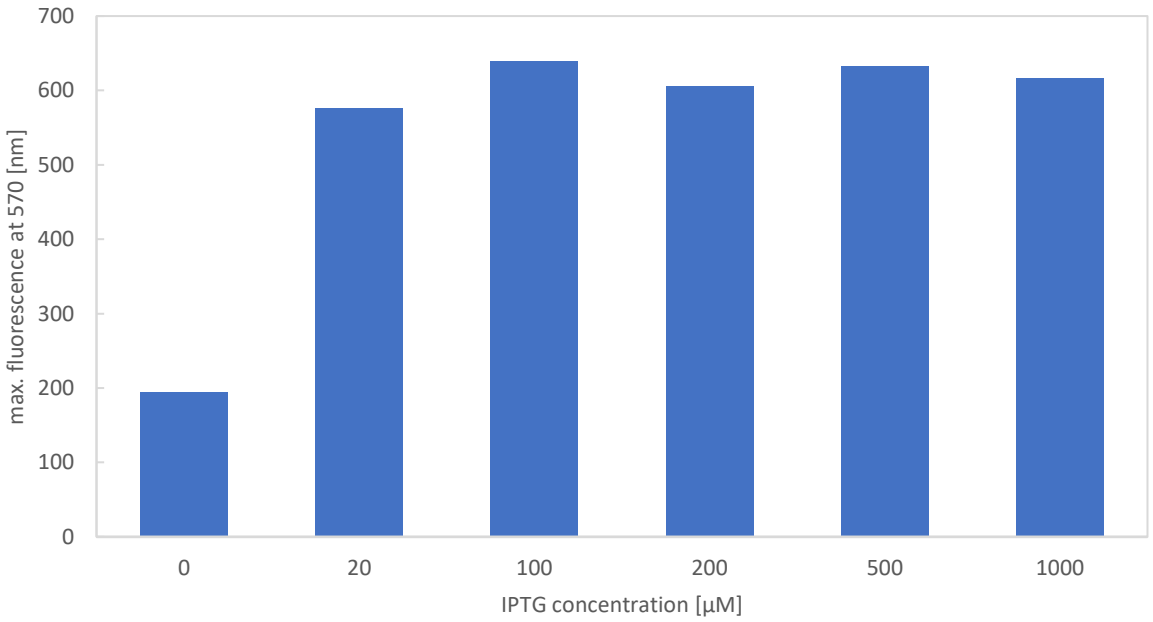

Figure 12: Comparison of maximal reached fluorescence values at 570 nm of shake flask cultivation of C. glutamicum ATCC13032 (pOGOduet_mCherry) with different inducer concentrations (500 µM, 1000 µM, 200 µM, 100 µM, 20 µM, and 0 µM IPTG)

The negative control seems to show a remarkably high fluorescence value, compared to the induced cultivations. This may indicate that the promotor is leaky and mCherry is produced although the culture was not induced. It would be also possible, that during the cultivations it came to degradation of the mCherry before the matured proteins could be measured, and therefore, the induced cultivations showed a lower result.

To sum up, the different IPTG concentrations influenced neither the growth nor the observed product formation of mCherry and therefore, the adaption of the inducer concentration is likely not to considerably improve the bioprocess in this case.

5.2 Impact of acetate as co-substrate on process stability and productivity in substrate-limited fed-batch processes

Figure 13 shows the time courses of growth rate and the substrate uptake rates for glucose and acetate, which are important process variables. The growth rates of both processes were similar, despite the process with glucose as sole substrate showed a slightly faster growth. Although the growth rate should have been 0.07 h^{-1} due to the adjusted feed rate, both processes showed a fast decrease below this value during the fed-batch phase, which displays poor process stability. The uptake rates of the process with acetate and glucose in the feed medium, reflect the set ratio of 0.3:1 acetate to glucose. If the uptake rates of glucose and acetate are summed up, the carbon uptake rates of both processes were in a comparable range. Moreover, the changes in the rates over time were similar. This means that no improvement of the process stability due to the addition of acetate as co-substrate could be detected.

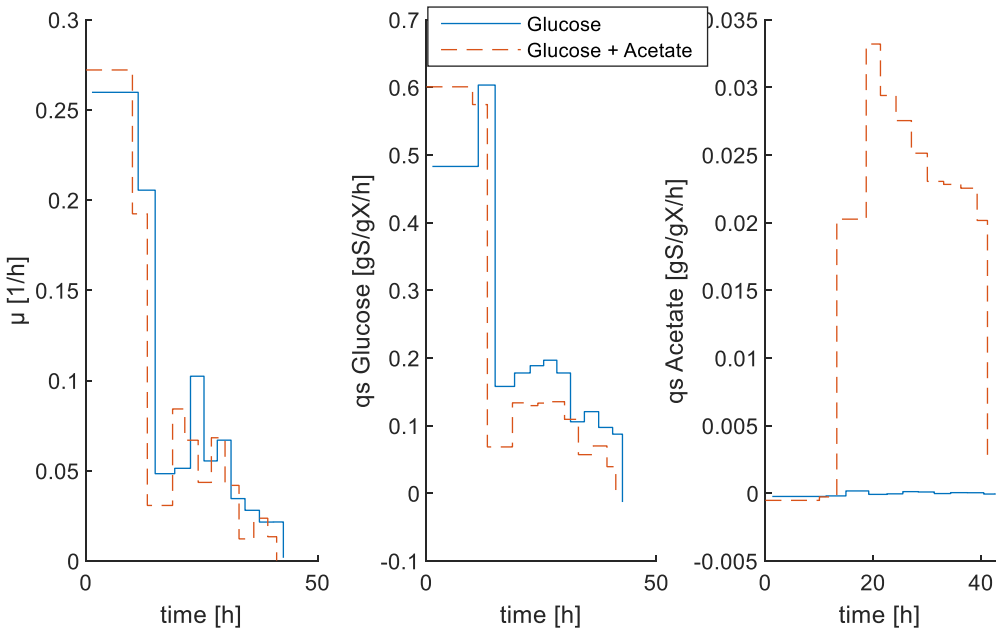

Figure 13: Time course of growth rate and substrate uptake rates of glucose and acetate during substrate-limited fed-batch processes of C. glutamicum ATCC13032 (pOGOduet_mCherry) with and without acetate as co-substrate both induced with 0.5 mM IPTG after 19 hours

The production rates of the two cultivations after induction are shown in Figure 14, the production rate of the process with acetate as co-substrate was most of the time smaller and the production broke down earlier, compared with the process with glucose as the sole carbon source.

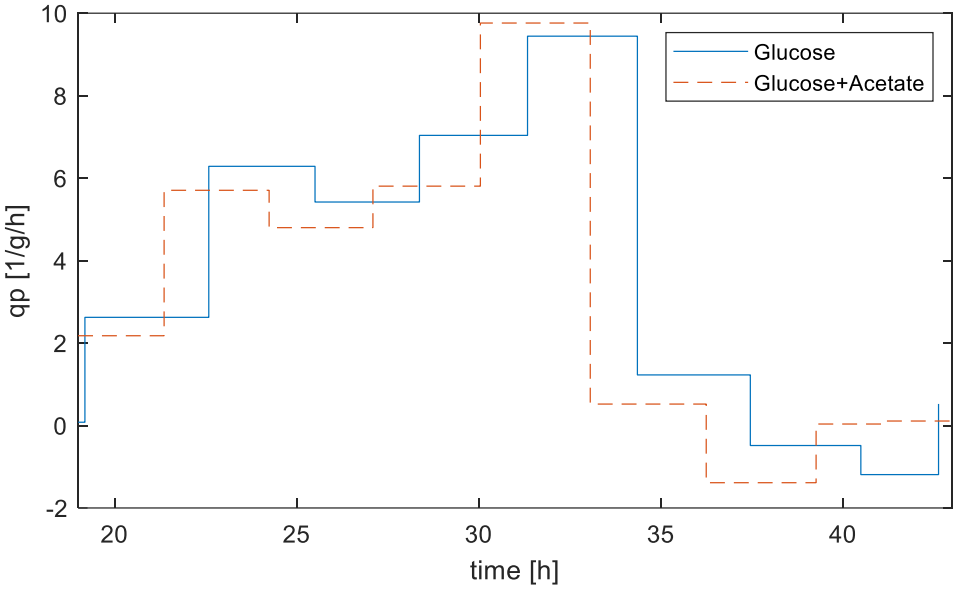

Figure 14: Time course of production rate during substrate-limited fed-batch processes of C. glutamicum ATCC13032 (pOGOduet_mCherry) with and without acetate as co-substrate both induced with 0.5 mM IPTG after 19 hours

As Figure 15 shows, the higher maximal CDW value as well as the higher maximal fluorescence value were achieved with the cultivation with glucose as the sole carbon source. The space-time yield was calculated according to equation (20). This value shows that the process with glucose as the sole substrate yielded a higher fluorescence value in the same period and reactor volume.

$$Space/_{Time}\, Yield = \frac{max.\ FU}{V_{Reactor} * t_{Process}} \qquad (20)$$

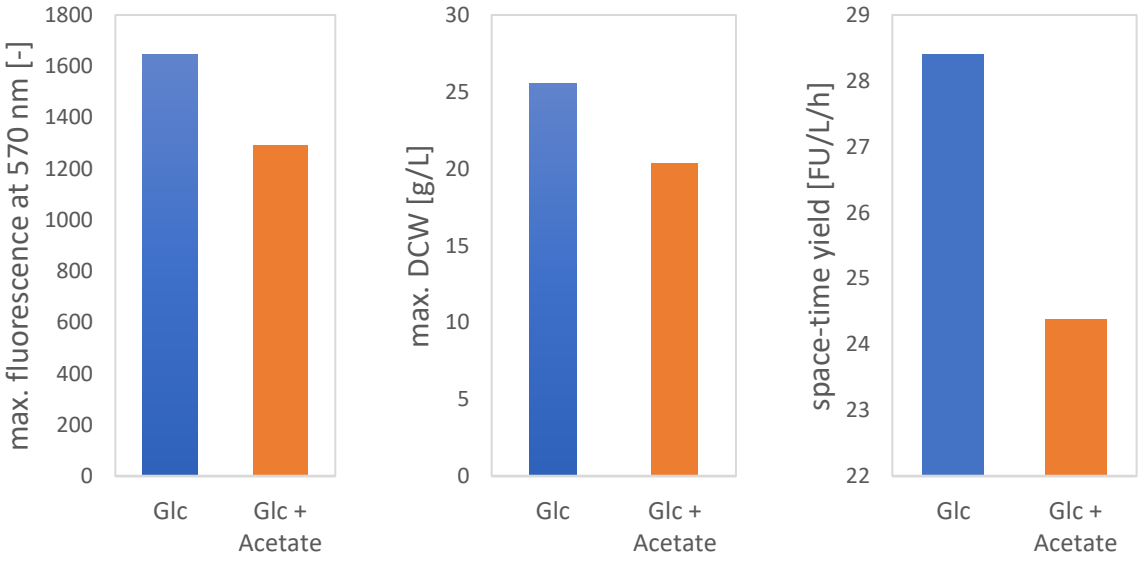

Figure 15: Evaluation of the effect of acetate as co-substrate on growth, the maximal fluorescence value, and the space-time yield during substrate-limited fed-batch processes of C. glutamicum ATCC13032 (pOGOduet_mCherry) both induced with 0.5 mM IPTG after 19 hours

Due to the results of the space-time yield and the early break down of the production rate of the process with acetate as co-substrate, it seems that acetate had a negative effect on the productivity of the production process of mCherry. As mentioned in section 3.2, Paegle and Ruklisha (2003) investigated, that only small amounts of acetate as co-substrate (ratio 9:1 of glucose to acetate) had a positive impact on the lysine yield and production rate. In contrast, higher amounts (ratio 2:8 of glucose to acetate) showed a negative impact on those values. Considering those investigations, a reason for the observed negative effect on productivity could be the too low ratio of glucose to acetate (3.3:1). To review this assumption, different ratios of glucose to acetate should be tested. As mentioned before, both processes showed bad process stability, thus a further possibility would be to investigate the effect of acetate as co-substrate also with a substrate-unlimited feeding strategy as described in section 5.3.

5.3 Process stability and productivity of a substrate-limited and a substrate-unlimited fed-batch process with glucose

The substrate unlimited fed-batch process was realized with a real-time control with the aid of a soft sensor. With the use of an off-gas analyzer (section 4.5.5) the carbon dioxide concentration in the off-gas is accessible in real-time and thus also the CER can be calculated (see section 5.5.1). With knowledge of a simplified stoichiometry of the reaction with the assumption that intracellular product accumulation does not change the biomass elemental composition, the consumed glucose, and the growth rate can be determined. For simplification also possible by-products of the process were not included in the stoichiometry. With those values, the feed rate can be regulated to prevent substrate limitation. A schematic overview of the procedure is shown in Figure 16.

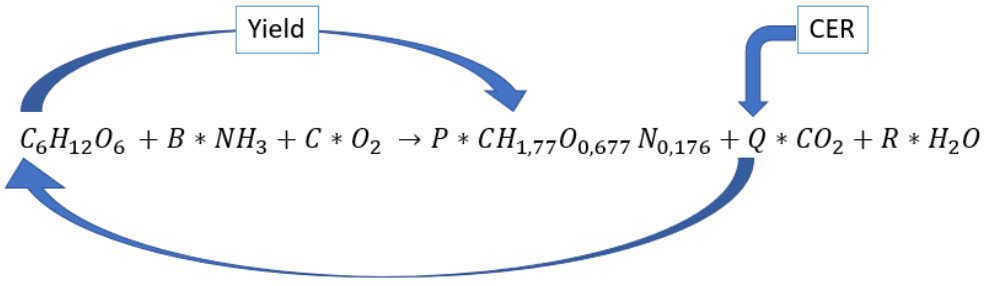

Figure 16: Schematic overview of the procedure of real-time control of substrate-unlimited feeding strategy

For this issue, the biomass composition of *C. glutamicum* ATCC13032 (on CGXII medium) was derived from the publication of Eggeling and Bott (2005). For simplification, a constant biomass yield coefficient of 0.3 gX/gS was used, determined as mean from previous bioprocesses.

Figure 17 displays the comparison of the real-time determined growth rate of the soft-sensor with the subsequent calculated growth rate with the process data (sections 4.5.1 and 4.9.2). The real-time determination of the growth rate was sufficient to accomplish a substrate-unlimited fed-batch process without exceeding 50 g/L glucose concentration in the reactor. However, especially after 20 hours, the real-time growth rate calculated based on the CER was overestimated. Thus, for further application, the soft sensor should be improved. This could be achieved by the integration of by-products such as glutamate and lactate into the stoichiometry (Figure 16), or by integrating the influence of the intracellular product on the biomass composition.

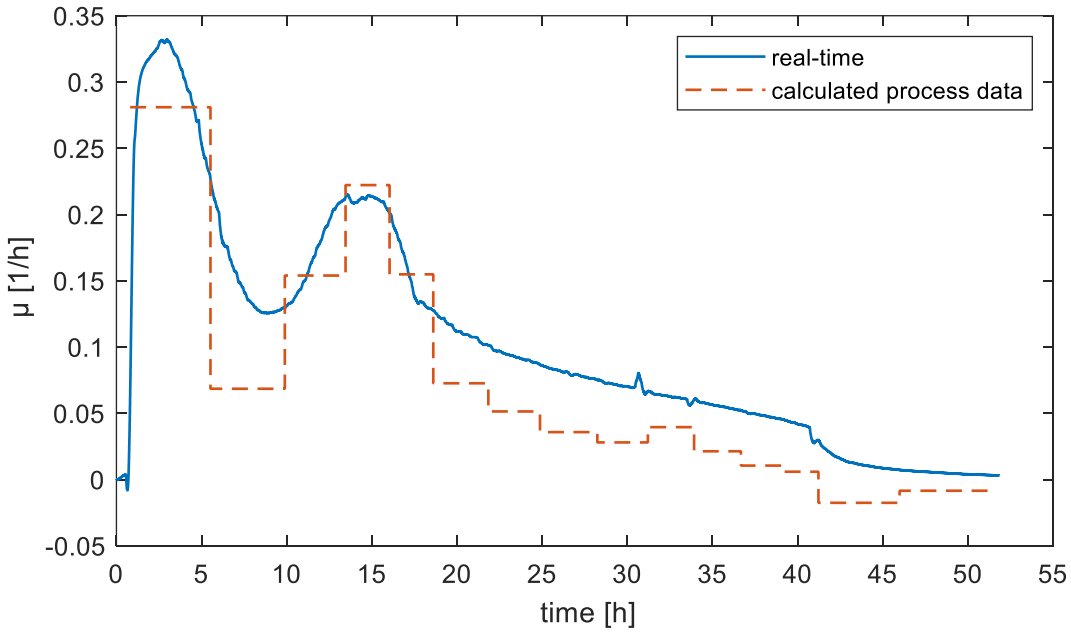

Figure 17: Comparison of calculated growth rate with process data and real-time growth rate of soft-sensor of a substrate-unlimited fed-batch process of C. glutamicum ATCC13032 (pOGOduet_mCherry) induced with 0.5 mM IPTG after 12 hours

The evaluation of the process data showed that the culture of the substrate-limited fed-batch process metabolized much less glucose compared to the substrate unlimited process (see Figure 18). This is not caused by the limitation of the substrate during the feeding, as the glucose concentration raised, and no more glucose was metabolized, which is indicating the bad process stability of this feeding strategy. In contrast to that, the biomass specific glucose uptake rate of both processes was in a similar range (see Figure 19). Thus, the higher amount of glucose that was metabolized was a result of the higher biomass concentration, which could be achieved with the unlimited feeding strategy (see Figure 21), due to the increased process stability.

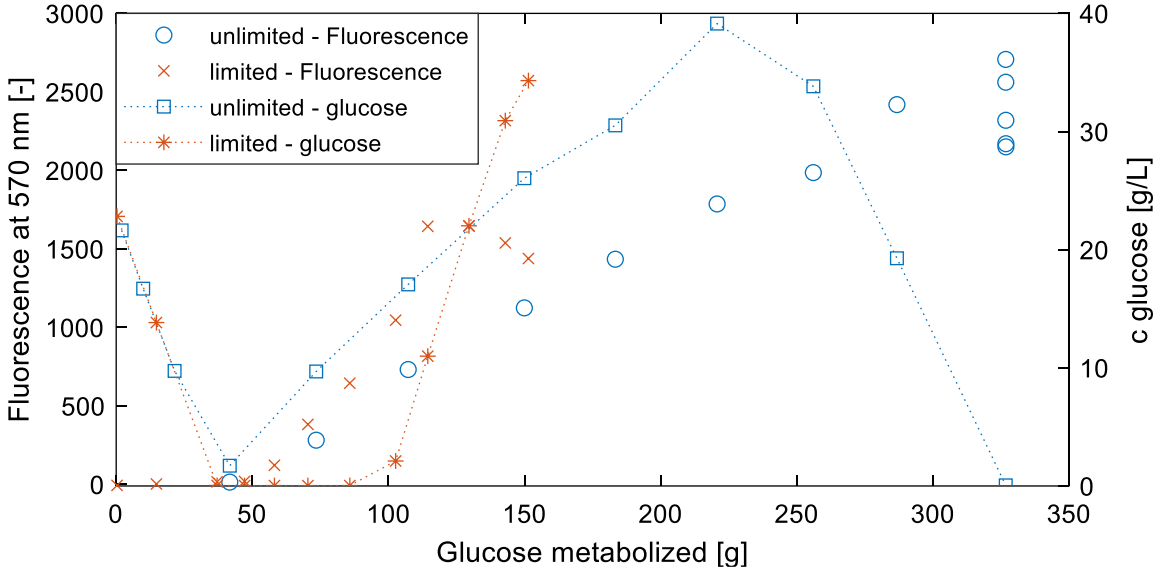

Figure 18: Comparison of fluorescence values depending on how much glucose was metabolized and corresponding glucose concentration values during substrate-limited and -unlimited fed-batch processes of C. glutamicum ATCC13032 (pOGOduet_mCherry), induced with 0.5 mM IPTG after 19 and 12 hours, respectively

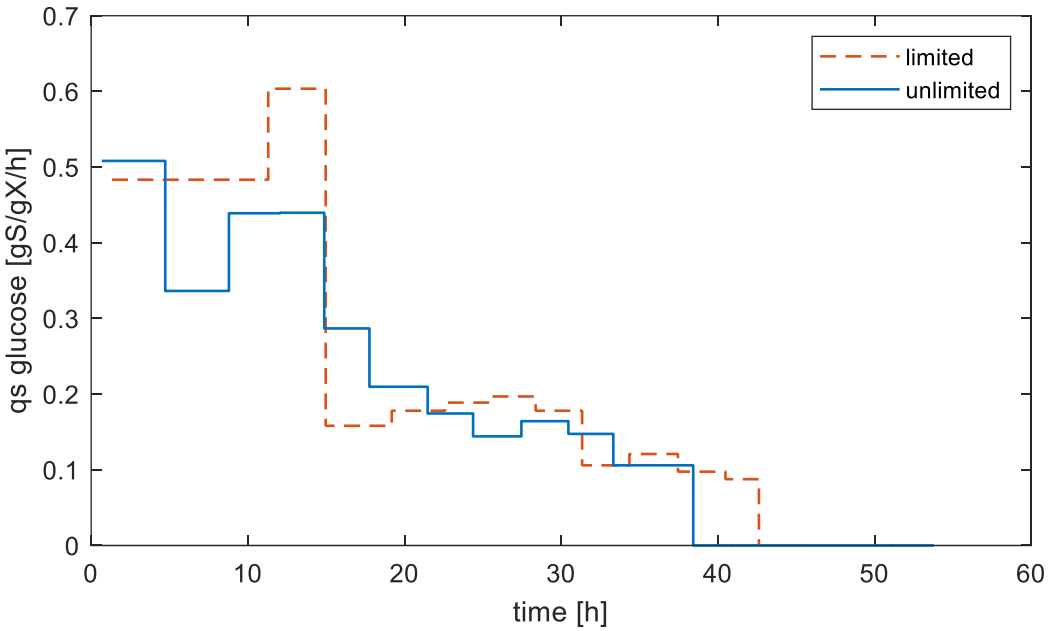

Figure 19: Comparison of glucose uptake rates of substrate-limited and -unlimited fed-batch processes of C. glutamicum ATCC13032 (pOGOduet_mCherry) induced with 0.5 mM IPTG after 19 and 12 hours, respectively

Figure 20 clearly shows that, although the glucose uptake rates of both processes were similar, the production rate of the limited fed-batch process decreased sharply and thus the production stopped sooner.

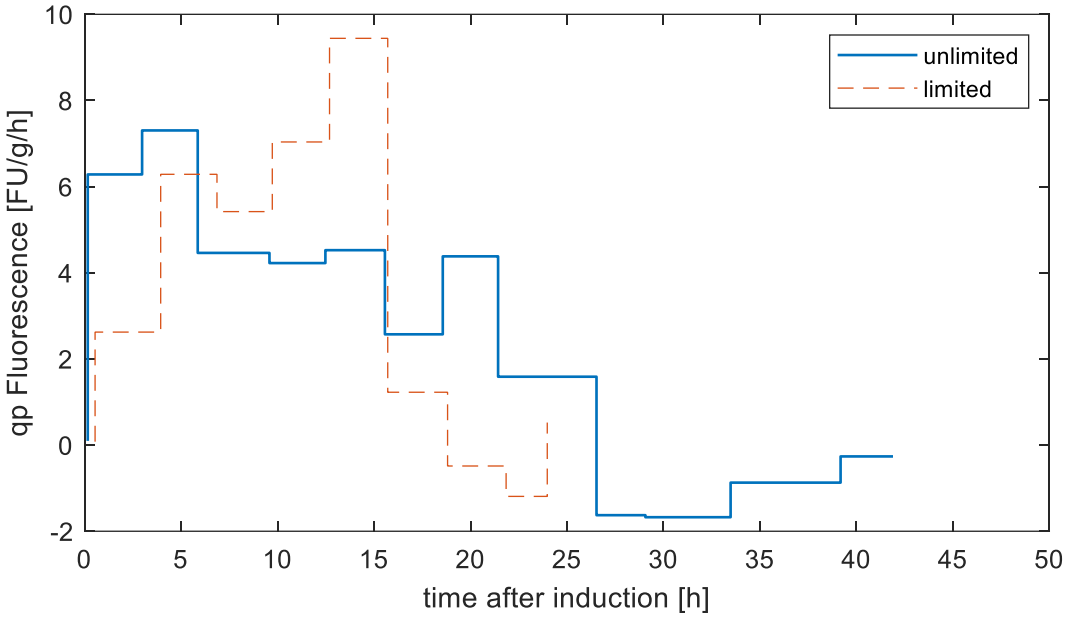

Figure 20: Comparison of time courses of production rates during a substrate-limited and a -unlimited fed-batch process of C. glutamicum ATCC13032 (pOGOduet_mCherry) induced with 0.5 mM IPTG

In Figure 21 the maximal achieved biomass concentrations and fluorescence values are compared. Both values were apparently higher for the substrate unlimited feeding strategy. As a consequence of the other results, also the space-time yield (equation (20)) is higher, which means that more product was produced within the same timeframe and reactor volume.

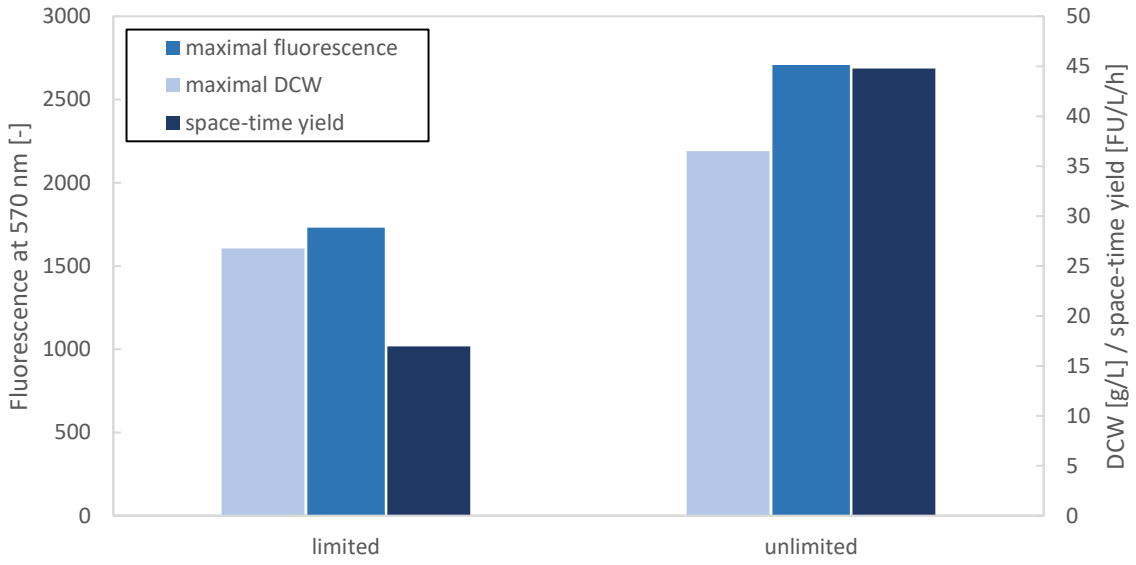

Figure 21: Comparison of maximal fluorescence and DCW which was reached during substrate-limited and -unlimited fed-batch process and the resulting space-time yields of C. glutamicum ATCC13032 (pOGOduet_mCherry) induced with 0.5 mM IPTG after 19 and 12 hours, respectively

The results of these cultivations showed that the substrate limitations did not affect the biomass specific glucose uptake rate but had a high effect on the maximal achievable biomass concentration and the production rate of mCherry. The unlimited substrate supply led to a

higher space-time yield and increased productivity compared to a substrate-limited fed-batch process. A drawback of the substrate unlimited process is that those processes are more complicated to control and many by-products could be produced due to overflow metabolism. During reduced growth, with high availability of the carbon source, higher amounts of intermediates are secreted from the cells. This phenomenon was observed for different microorganisms, among others *C. glutamicum* (Paczia et al., 2012). Krause et al. (2016) stated for *E. coli* that limiting the uptake rate and thus the growth rate via the feeding rate of the carbon sources leads to controlled cell physiology and process robustness. Since in this production process the unlimited substrate supply seems to be favorable for productivity, another way to increase the batch-to-batch reproducibility would be preferred. A solution could be the improvement of the application of the soft sensor to limit the deviations of the wanted substrate concentration. Changing substrate concentrations can lead to varying substrate inhibition effects or other alternating effects on the production rate of the product or by-products, or the growth, which should be avoided.

5.4 Comparison of different modeling approaches for biomass and substrate simulation

To simulate the time-dependent course of volume and the biomass and substrate concentration during the cultivations the following differential equations (21), (22), (23) were used in MATLAB (MathWorks, United States).

$$\frac{dV}{dt} = F_{in} - F_{out} \tag{21}$$

$$\frac{dX}{dt} = X * (\mu - \frac{F_{in}}{V}) \tag{22}$$

$$\frac{dS}{dt} = \frac{F_{in} * (S_{in} - S)}{V} - q_s * X \tag{23}$$

The growth rate was connected to the substrate uptake rate with a constant yield coefficient of substrate to biomass (Y_{xs}) according to equation (24).

$$\mu = q_s * Y_{X/S} \tag{24}$$

The model should be as straightforward as possible, it should achieve the model goal without overfitting due to too many parameters. Hence, the substrate uptake rate was first simulated according to a simple Monod kinetic, as described in section 3.4 according to equation (3).

As the results of the cultivations (section 4.4.3.2) showed, that the substrate uptake rate decreases with time during the process, several ways were tested to simulate this decrease. The used starting parameters can be seen in Table 15.

Table 15: Initial parameters for modeling substrate and biomass concentration (Sinner et al., 2019)

Parameter	Value	Unit
$q_{s,max}$	0.64	gS/gX/h
K_s	0.0949	gS/L
$Y_{x/s}$	0.527	gX/gS

As process data for simulation, the data of the cultivation of the limited glucose fed-batch process was used (section 4.4.3.2). As acceptance criteria for the NRSME, a widely used value in literature of 15 % for biomass and substrate concentration and the glucose uptake rate were chosen (Ulonska et al., 2018).

Version 1 - Glucose uptake rate decreases with the amount of biomass produced:

$$q_s = \frac{q_{s,max} * S}{S + K_S} * \frac{1}{e^{X*lag}} \quad (25)$$

Equation (25) describes the reduction of the uptake rate the more biomass is produced. To connect the rate with the biomass concentration a parameter called ‘lag’ was used. This simplified relationship could be a result of a changing maintenance coefficient during the process, due to the dependence of this parameter on the growth rate (Goma et al., 1979; van Bodegom, 2007). A similar approach has been used in the investigations of Mazzoleni et al. (2015), where the substrate uptake rate of *Saccharomyces cerevisiae* is dependent on among others the produced metabolites.

Table 16: Fitted parameters of simulation with a decrease of qs with biomass produced connected with a parameter called 'lag'

Parameter	Value	Unit
$q_{s,max}$	0.8197	gS/gX/h
K_s	0.0685	gS/L
$Y_{x/s}$	0.3387	gX/gS
lag	0.0057	1/gX

With parameter estimation, the final fitted parameters from Table 16 reveal the following simulations in Figure 22 (A).

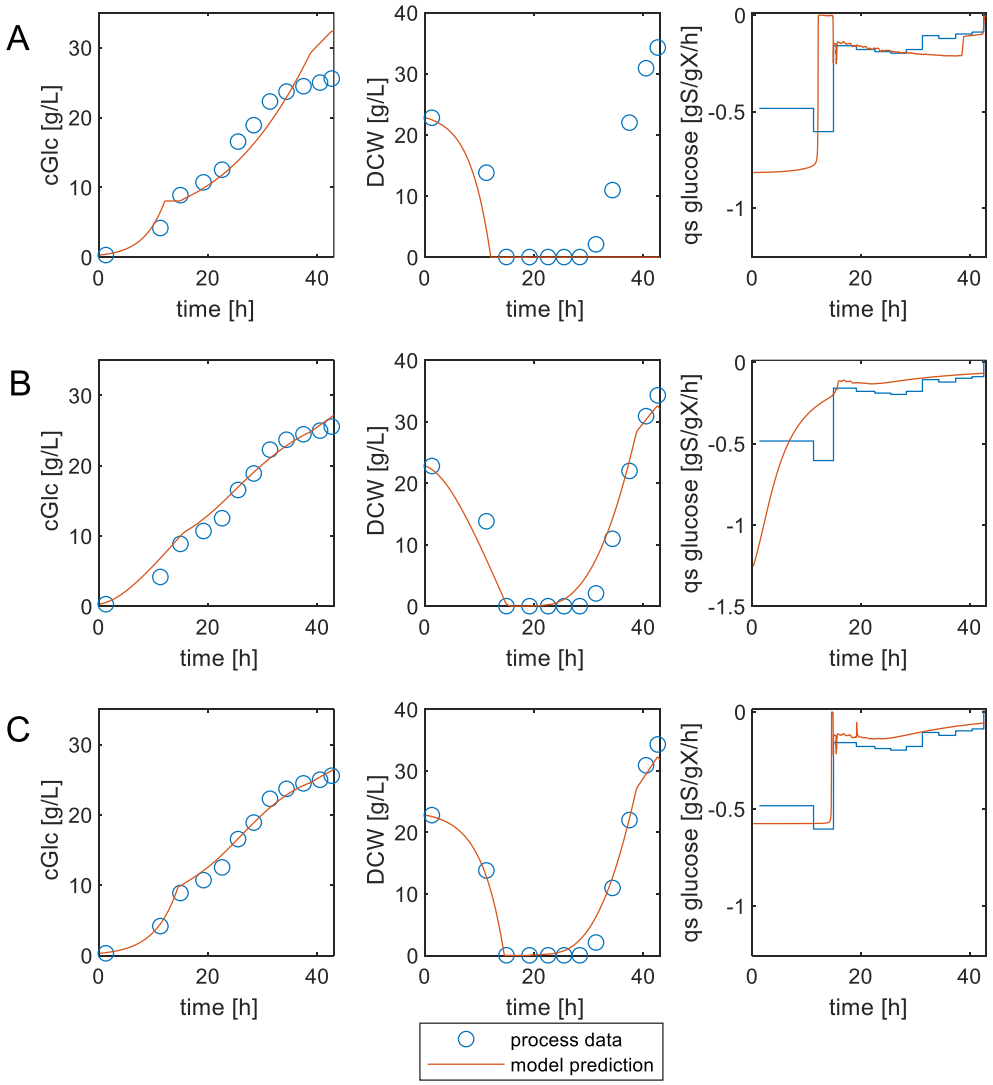

Figure 22: Simulation of DCW, glucose concentration, and q_s of a substrate-limited fed-batch process of C. glutamicum ATCC13032 (pOGOduet_mCherry) induced with 0.5 mM IPTG after 19 hours A: version 1 - decrease of q_s with biomass produced connected with a parameter called 'lag'; B: version 2 – starting with recombinant protein induction, decrease of qs with glucose metabolized with a non-competitive inhibition term; C: version 3 – starting with recombinant protein production, decrease of q_s with glucose metabolized connected with a parameter called 'lag'

Figure 22 (A) displays that after 30 hours q_s gets overestimated, which leads to too low substrate concentrations after 30 hours. The NRSME values for substrate, biomass, and substrate uptake rate were 44.8 %, 12.4 %, and 19.8 %, respectively. Thus, it seems that the produced biomass is not an adequate process variable to connect with the decrease of the substrate uptake rate in this case.

Version 2 - Inhibition term with glucose metabolized decreases glucose uptake rate:

$$q_S = \frac{q_{s,max} * S}{S + K_S} * \frac{K_i}{K_i + Glc_{met}} \quad (26)$$

Equation (26) utilizes a term similar to a non-competitive inhibition term with the amount of glucose that had been metabolized from the culture to simulate the decrease of the glucose uptake rate. The amount of glucose metabolized during the process was simulated with the aid of the glucose uptake rate. The term of the non-competitive inhibition was integrated similar to an approach of Daume et al. (2020). That the substrate uptake is not a constant but a time-dependent variable has been reported by Reichelt et al. (2017). They investigated, that the decrease of the uptake rate is strongly correlated to the metabolic activity of the culture and thus indicating the effect of the cumulated metabolized substrate.

Table 17: Fitted parameters of simulation with a decrease of qs with glucose metabolized with a non-competitive inhibition term

Parameter	Value	Unit
$q_{s,max}$	1.2565	gS/gX/h
K_s	0.0259	gS/L
$Y_{x/s}$	0.4297	gX/gS
K_i	7.1562	gS

With parameter estimation, the final fitted parameters from Table 17 reveal the simulations, which are displayed in Figure 22 (B).

The second version achieved NRSME values for substrate, biomass, and substrate uptake rate of 8.4 %, 5.3 %, and 34 %, respectively. Thus, this version achieved better simulations for biomass and substrate concentration. The simulation of the biomass concentration was approximate as the process data with a simulation error of about 8 %. The simulation of the substrate concentration showed at the beginning a too rapid decrease, which is caused by the overestimation of the uptake rate in the first 15 hours of the process. To overcome this overestimation, for the next version a connection with the induction phase was made, because

the process data showed that the uptake decreases only after the induction with IPTG. Reichelt et al. (2017) described in their publication the time dependence of the substrate uptake rate during the induction phase of an *E. coli* recombinant protein production process. After induction at 15 hours of process time, the simulation of the uptake rate, and thus the glucose concentration is approaching the process data. Thus, the connection of the rate decrease with the metabolized glucose seems to be a good approximation.

Version 3 - Glucose uptake rate decreases with the amount of glucose metabolized if culture is induced:

The decrease of the uptake rate due to the amount of glucose metabolized connected with an exponential parameter called 'lag', where the decrease starts when culture gets induced, is described by equation (27). The model parameter 'IPTG' is used as a switching parameter between the uninduced and induced state, thus the decrease of q_s starts with the induction of the culture. The model parameter 'lag' is used to connect the amount of glucose which is metabolized with the glucose uptake rate.

$$q_s = \frac{q_{S,max} * S}{S + K_S} * \frac{1}{1 + IPTG * e^{Glc\_met * lag}} \quad (27)$$

Table 18: Fitted parameters of simulation with a decrease of qs with glucose metabolized connected with a parameter called 'lag'

Parameter	Value	Unit
$q_{s,max}$	0.5764	gS/gX/h
K_s	0.0355	gS/L
$Y_{x/s}$	0.4167	gX/gS
lag	0.0172	1/gS

With parameter estimation, the final fitted parameters from Table 18 reveal the simulations, which are shown in Figure 22 (C).

The NRSME and RSME were calculated for the states biomass, substrate, and glucose uptake rate, the results are shown in Table 19. Those confirm the good simulation with NRSME of biomass and substrate below 5 %, compared with the standard deviation of biomass and substrate measurements of about 1 %. With this model, the set model goal of NRSME below 15 % was achieved.

Table 19: NRSME and RSME of biomass, substrate, and substrate uptake rate simulation with a decrease of q_s with glucose metabolized connected with a parameter called 'lag' of a substrate-limited fed-batch process of C. glutamicum ATCC13032 (pOGOduet_mCherry) induced with 0.5 mM IPTG after 19 hours

Parameter	NRSME [%]	RSME
X	3.5	0.89 g/L
S	4.99	1.71 g/L
q_s	7.96	0.049 g/g/h

Substrate and biomass concentration were also simulated for the substrate-unlimited fed-batch processes. In those experiments, the model with the q_s decrease with the glucose metabolized achieved only a bad simulation, which may be caused by the changed uptake behavior due to the unlimited substrate supply. As described in section 5.3, due to the different feeding strategies with unlimited substrate supply, better process stability could be achieved and different metabolic behavior was observed. The previously used model was not transferable, thus a different model structure was needed. A model with the simple Monod-kinetic according to equation (3) was used for the experiments with unlimited substrate supply. To find an optimal parameter set for several processes, multiple experiment fitting was used as described in section 4.10.1.

As an example, the simulations of the substrate-unlimited fed-batch processes with low (0.25 L/min) and high (1.6 L/min) aeration, both with 0.5 mL/L antifoam of section 4.4.3.3, are shown in Figure 23. The yielded optimal parameter set for the simulation of substrate and biomass concentrations for both processes is listed in Table 20. The fitted parameter of K_s was a remarkably high value, compared with literature values and the value achieved for the substrate limited fed-batch process (Sinner et al., 2019).

Table 20: Fitted parameters of simulation of substrate-unlimited fed-batch processes of C. glutamicum ATCC13032 (pOGOduet_mCherry) with low and high aeration both induced with 0.5 mM IPTG after 13 hours

Parameter	Value	Unit
$q_{s,max}$	0.8561	gS/gX/h
K_s	7.6766	gS/L
$Y_{x/s}$	0.2818	gX/gS

The simulation of the substrate-unlimited processes achieved worse NRSME values (Table 21) for the process states biomass, substrate, and glucose uptake rate, compared with the substrate-limited process (Table 19). Especially the substrate concentrations were strongly underestimated after 20 hours, due to the overestimation of the glucose uptake rate. The

decrease of the substrate uptake rate could not be simulated with the equation (27) of the substrate-limited process. Maybe the rate decrease is caused by other effects due to the infinite substrate supply. As Krause et al. (2016) stated for *E. coli,* the metabolism changes with different feed-strategies. Thus, an equation like described for the substrate-unlimited process have to be found to improve the simulation of the substrate concentration.

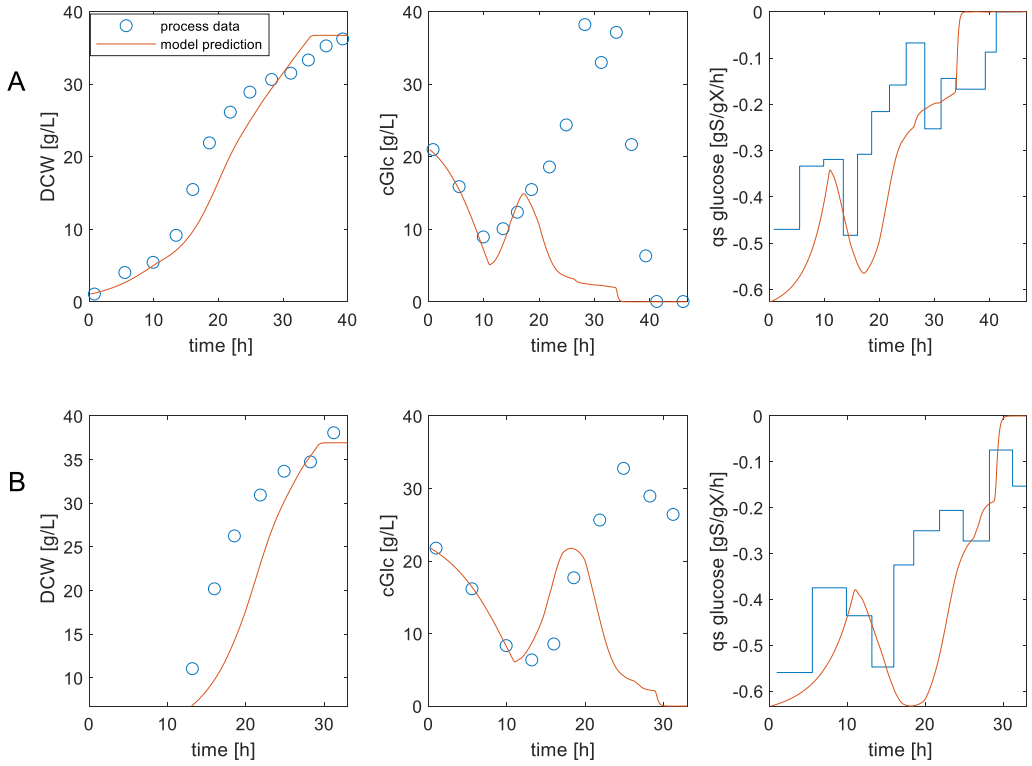

Figure 23: Simulation of glucose concentration, DCW, and q_S by multiple experiment parameter fitting of a substrate-unlimited fed-batch process of C. glutamicum ATCC13032 (pOGOduet_mCherry) with high (A) and low (B) aeration induced with 0.5 mM IPTG after 13 hours

Table 21: NRSME and RSME of biomass and substrate simulation with multiple experiment parameter fitting of substrate-unlimited fed-batch processes of C. glutamicum ATCC13032 (pOGOduet_mCherry) with high and low aeration induced with 0.5 mM IPTG after 13 hours

Process	Parameter	NRSME [%]	RSME [g/L]
High aeration	X	9.7	3.5
High aeration	S	45.8	17.5
Low aeration	X	14.1	5.5
Low aeration	S	45.2	14.8

The set NRSME limit of 15 % was achieved for the biomass concentration but could not be accomplished for the substrate concentration. Further improvements were not achievable

during the conduction of this thesis. Possible approaches for improvement would be using the metabolized glucose with another equation like the one described above with a non-competitive inhibition term (equation (26)). Figure 23 displays the decline of the uptake rate after induction, thus the switching parameter 'IPTG' should be included.

5.5 Model-based analysis of oxygen and carbon dioxide dynamics in bioprocesses

To test the hypothesis described in section 3.5, that different carbon dioxide concentrations would influence the stability and productivity of the recombinant protein production of *C. glutamicum* ATCC13032 (pOGOduet_mCherry), the model from section 5.4 was extended to describe the oxygen and carbon dioxide dynamics of the bioprocesses.

Simulations were based on the data of the glucose-unlimited fed-batch processes with high (1.6 L/min) and low (0.25 L/min) aeration with 0.5 mL/L antifoam (section 4.4.3.3). For straightforwardness, figures with the comparison of process data with conducted simulations are only shown for the glucose-unlimited fed-batch process with high aeration and 0.5 mL/L antifoam.

5.5.1 Oxygen uptake rate and carbon dioxide evolution rate

CER and OUR can be determined by gas balancing as an example by using an infrared analyzer to analyze the gas outlet and by knowing the composition of the gas flow inlet. Those two rates are important parameters for assessing metabolic activity during bioprocesses. Due to chemical and physical transfer limitations, differences between the observed carbon dioxide evolution rate (OCER) and the biological CER can occur (Figure 24). To calculate this real CER a mathematical model based on mass balance equations can be used. For this, it is also important to include the kinetics of desorption and absorption of carbon dioxide to complete the gas analysis method (Spérandio & Paul, 1997).

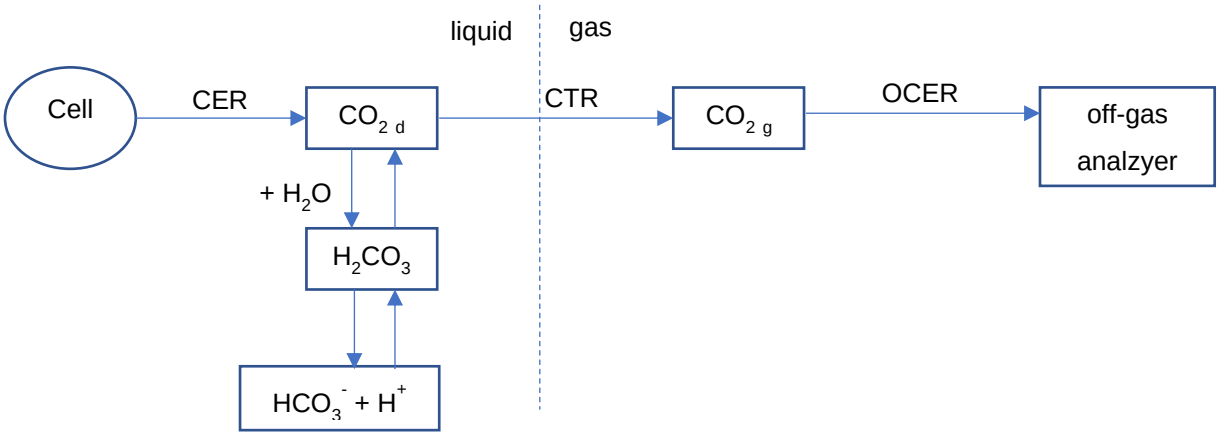

Figure 24: Representation of carbon dioxide states in the fermenter (adapted from Spérandio and Paul (1997))

In Figure 24 the different states in the liquid and the gas phase of carbon dioxide are represented. Microorganisms produce carbon dioxide which diffuses into the media (CER).

To model the CER and the OUR two different methods were tested:

1. With carbon mass balance and degree of reduction:

Mass balancing is a common strategy for bioprocess analysis (Bérangère et al., 2012). The CER can be calculated with such a mass balance, according to equation (28). It balances the carbon uptake from the substrate and the carbon usage for building up biomass. Thus, carbon which was metabolized, but not used for biomass growth, was counted as CER.

$$CER = \frac{q_s * X}{MW_{Glc}} * V - \frac{\mu * X}{MW_X} * V \quad (28)$$

To determine OUR equation (29) was used, which is similar to the calculation of CER. To convert the carbon moles to oxygen, the degree of reduction (DoR) was used. The concept of DoR is often used for more complex reactions, where additional information is required (Shuler & Kargi, 2008).

$$OUR = -\frac{1}{DoR_{O2}} * (\frac{DoR_X * \mu * X}{MW_X} * V - \frac{DoR_{GLc} * q_S * X}{MW_{GLc}} * V) \quad (29)$$

The degree of reduction (3.88) and the molecular weight per C-mole (29 g/C-mole) of biomass were calculated based on the elemental composition of *C. glutamicum* ATCC13032 grown on CGXII media (Eggeling & Bott, 2005).

2. Linked to the growth rate:

The second possibility to simulate the two rates is to connect the rates to the growth rate with a constant yield of CO_2 from biomass or the yield of biomass from oxygen (see equations (30) and (31)).

$$CER = \mu * Y_{CO2X} * X \quad (30)$$

$$OUR = -\mu * Y_{O2X} * X \quad (31)$$

The conversion yields were fitted with the process data to values for CO_2 of 0.037 $mol_{Carbon}/g_{Biomass}$ and for O_2 of 0.038 $mol_{Oxygen}/g_{Biomass}$ via multiple experiment parameter fitting for the glucose-unlimited fed-batch processes with high and low (2) aeration (section 4.4.3.3).

A drawback of this method is the risk of overfitting because due to the calculation two more parameters had to be fitted.

To compare those two methods the NRSME and RSME for the two rates were calculated. As process data for simulation, the data of the cultivation of the glucose-unlimited fed-batch process with high aeration (section 4.4.3.3) was used. The results are shown in Table 22.

Table 22: NRSME and RSME of CER and OUR simulations with mass balancing and growth rate linkage

Method	Parameter	NRSME [%]	RSME [mol/h]
Mass balance	CER	36.1	0.1
Mass balance	OUR	16	0.09
Growth rate linked	CER	34.7	0.09
Growth rate linked	OUR	15.4	0.09

Both methods achieved similar results of the calculated error between the process data and the simulations. Slightly better results were achieved with the second method, which connects the CER and the OUR with the growth rate, thus this method had been used for further extension of the model. Simulations of this method compared with the obtained process data are shown in Figure 25.

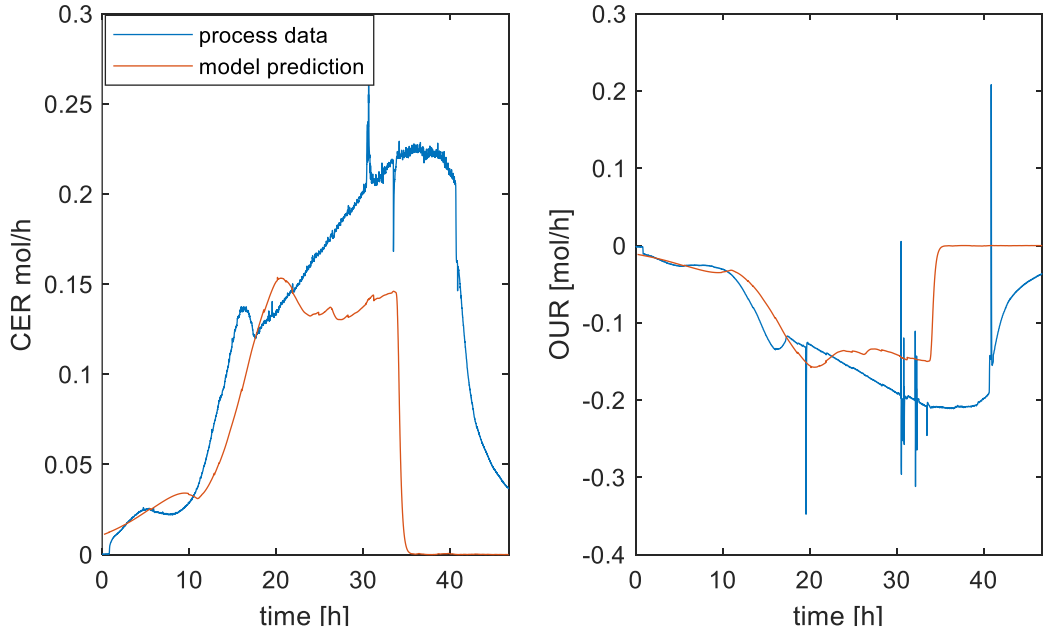

Figure 25: Comparison of process data and simulations of CER and OUR of a substrate-unlimited fed-batch process with high aeration of C. glutamicum ATCC13032 (pOGOduet_mCherry) induced with 0.5 mM IPTG after 13 hours; simulation was done with a connection of CER and OUR with the growth rate

In the first few hours, the simulations of both CER and OUR show small deviations to the process data. After approximately 20 hours, the simulations tend to show worse results, which could be caused by the induction after 13 hours. The started production process of mCherry could have influenced the yield between growth and OUR and CER respectively. Although the growth rate is slightly overestimated in this period, compared with the rate which was calculated from the process data (see Figure 26), the CER got underestimated, which led to the assumption that CO_2 formation is not only due to metabolic activity that results in biomass, but also caused by recombinant protein production. The same phenomenon was displayed during the simulation with the aid of mass balances and DoR because the stoichiometry was used under the assumption that the elemental biomass composition is not affected by intracellular protein accumulation. For further improvement of the model, the product formation should be included in the stoichiometry for the first method or the influence of the production onto the yield between CER and growth should be modeled. Thus, metabolic activity, which does not result in biomass can be included.

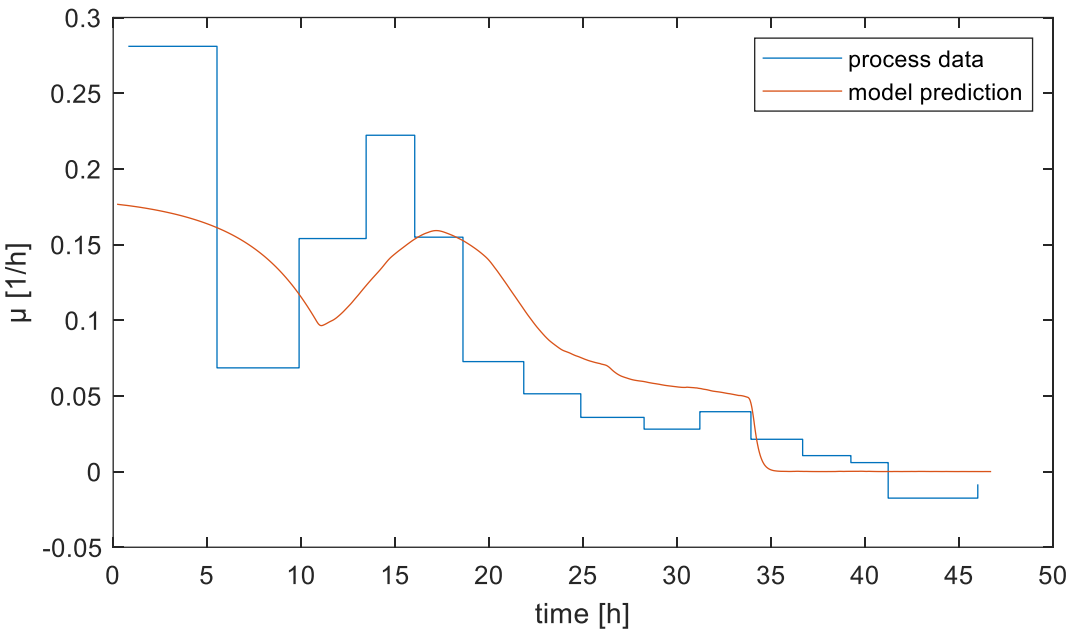

Figure 26: Comparison of process data and simulations of the growth rate of a substrate-unlimited fed-batch process with high aeration of C. glutamicum ATCC13032 (pOGOduet_mCherry) induced with 0.5 mM IPTG after 13 hours

After about 35 hours of process, the simulated growth rate gets zero (Figure 26), this leads to a sharp decrease of the simulated CER and OUR, although the process data showed a stop of metabolism activity only after 40 hours of the process. To improve the simulation of the last hours of the process, the simulation of biomass and substrate concentration, discussed in section 5.4, has to be enhanced.

5.5.2 Mass transfer coefficient and transfer rates

The mass transfer rates of oxygen (OTR) and carbon dioxide (CTR) can be calculated with equation (32) and (33). The driving force of both transfer rates is the difference between the equilibrium concentration according to Henry's law and the actual concentration in the liquid (see section 5.5.3).

$$CTR = kLa_{CO2} * (dCO_2{}^* - dCO_2) \quad (32)$$

$$OTR = kLa_{O2} * (dO_2{}^* - dO_2) \quad (33)$$

The mass transfer coefficient k_La of oxygen was determined according to section 4.8 for both reactors used during the conduction of this thesis. The results for the different tested conditions are shown in the following figures (Figure 27, Figure 28, Figure 29, Figure 30).

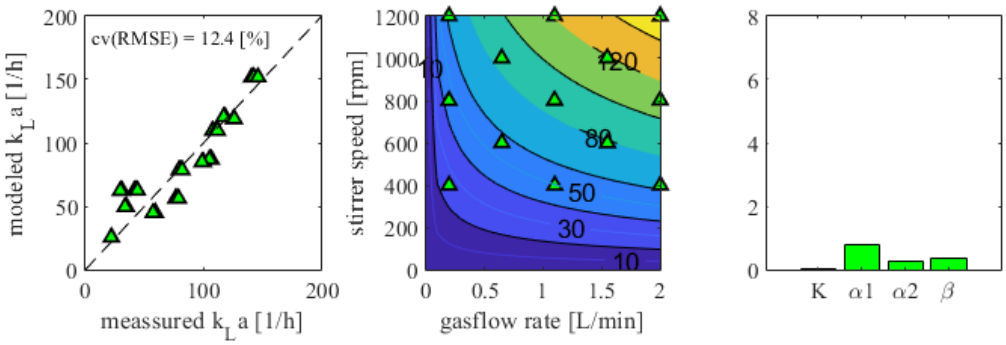

Figure 27: k_La results of the reactor (F20) with low antifoam concentration (0.05 mL/L)

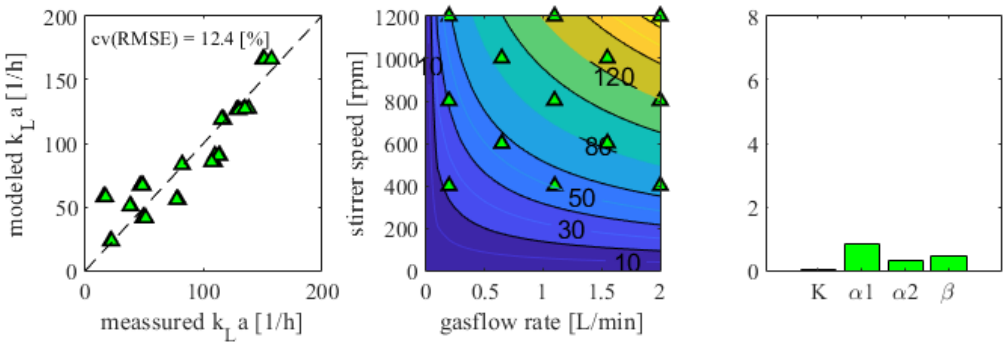

Figure 28: k_La results of the reactor (F20) with high antifoam concentration (0.5 mL/L)

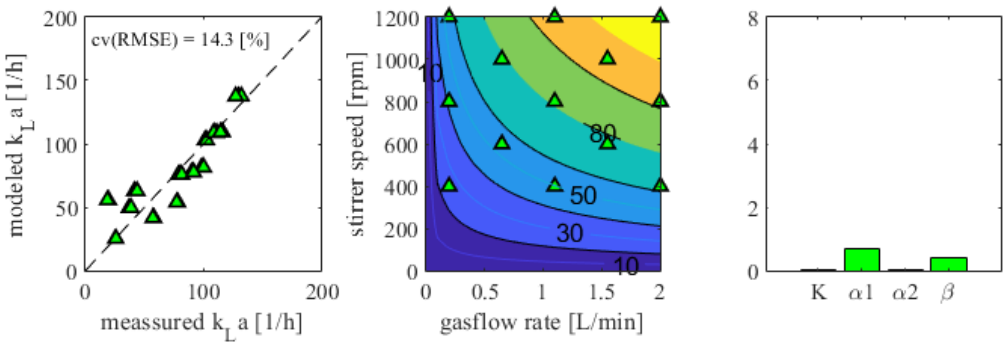

Figure 29: k_La results of the reactor (F10) with low antifoam concentration (0.05 mL/L)

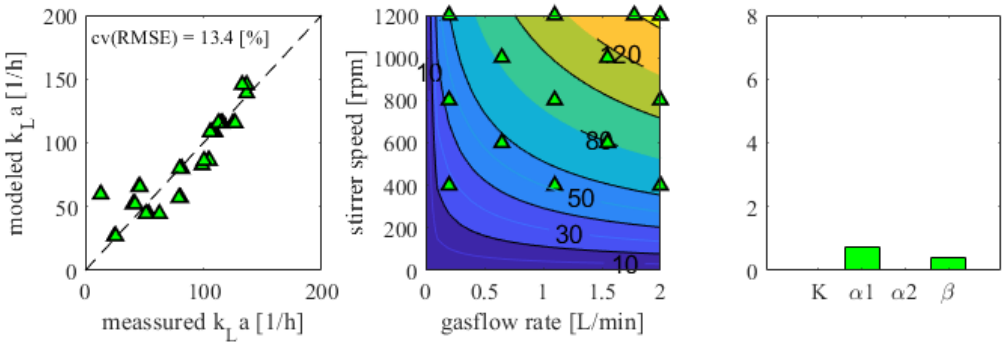

Figure 30: k_La results of the reactor (F10) with high antifoam concentration (0.5 mL/L)

The left diagrams of the four figures show, that the measured and the modeled k_La with the new fitted parameter resulted in similar values. In addition, it is shown that the measured triplicates had low deviations among each other. However, especially the small k_La values were more difficult to determine precisely. The diagrams in the middle show the k_La values with dependence on stirrer speed and gas flow rate. As expected, higher stirrer speed and higher gas flow rates increased the k_La value. It is shown that the two reactors, used in this study, display different k_La values, which is due to minor differences in the reactor structures, for example, positioning and type of baffles. In contrast to that, the antifoam concentration had a small influence on the k_La values, but mainly in the range of high stirrer speed and high gas flow rate. The right diagrams show the new fitted parameters, the comparison of the parameters of the different tested conditions can be seen in Figure 31.

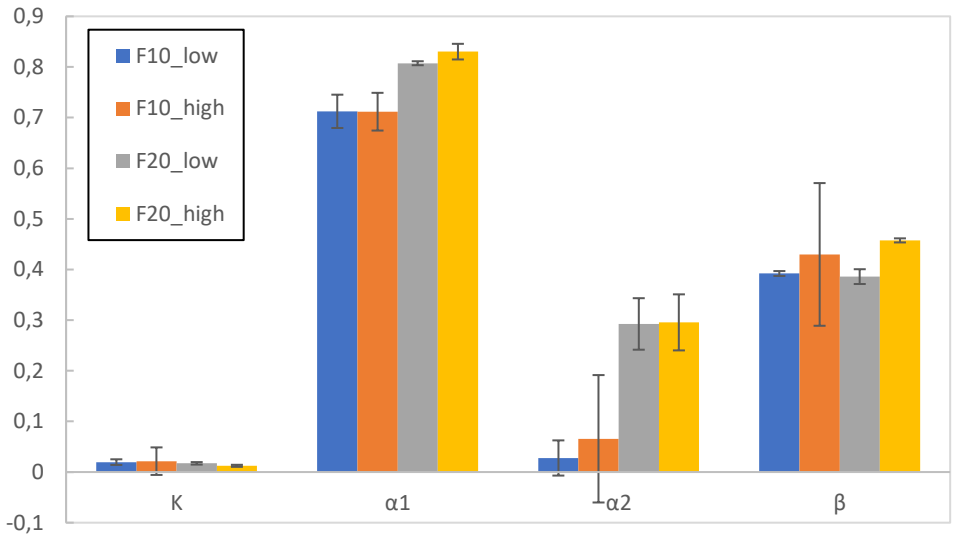

Figure 31: Comparison of kLa parameter determination of two different bioreactors (F10, F20) with each two different antifoam concentrations (high - 0.5 mL/L and low - 0.05 mL/L)

The standard deviations of the triplicate measurements for the Van't Riet parameters were low. The standard deviations of the reactor 'F10' with lower antifoam concentration displayed higher values, which is most probably due to microbial contamination during the last day of the series of experiments, which influenced the results. The determined values of the parameters were used for the simulation of the k_La and thus the OTR and the CTR of the processes could be simulated. If the obtained parameters were used directly for the simulation of the transfer rates, it resulted in too low dissolved oxygen concentrations compared with the process data. For this purpose, the parameters were fitted with the process data of CER, OUR, and molar fractions of oxygen and carbon dioxide in the off-gas, within allowed boundaries of the threefold of the standard deviations of the obtained parameter values. This was done for each process depending on the used reactor and antifoam concentration. The resulting parameters can be found in Table 23. Due to this procedure, the simulated (Figure 32) k_La values were much higher than those obtained in the diagrams above (Figure 29 and Figure 30). This shows that only slight deviations of the parameter values obtain large deviations of the resulted k_La value and therefore are highly sensitive on dynamic dissolved oxygen concentrations. This means that with the used method (section 4.8) it is hardly possible to obtain precisely parameter values that can be used for the simulations. However, the order of magnitude of the corresponding reactor parameters and possible k_La ranges could be assessed. The collinearity of the parameter of the Van't Riet equation is a major problem for the determination of the true set of parameters. For further improvement of the k_La determination, it would be beneficial to determine also the response time of the dissolved oxygen electrode, this value should be much smaller than 1 /k_La (Doran, 2013).

Table 23: Fitted model parameter for k_La calculation of substrate-unlimited fed-batch processes of C. glutamicum ATCC13032 (pOGOduet_mCherry) with 0.5 mL/L antifoam for high and low aeration both induced with 0.5 mM IPTG after 13 hours

	K	α1	α2	β
Low aeration (2)	0.0184	0.8767	0.1296	0.4467
High aeration	0.0384	0.7395	-0.0164	0.4327

The k_La for carbon dioxide was derived from the k_La of oxygen (see equation (34)). The two coefficients are proportionally linked to the ratio of diffusion coefficients for the two species in water (Spérandio & Paul, 1997).

$$kLa_{CO2} = kLa_{O2} * \sqrt{\frac{D_{CO2}}{D_{O2}}} = kLa_{O2} * 0.91 \qquad (34)$$

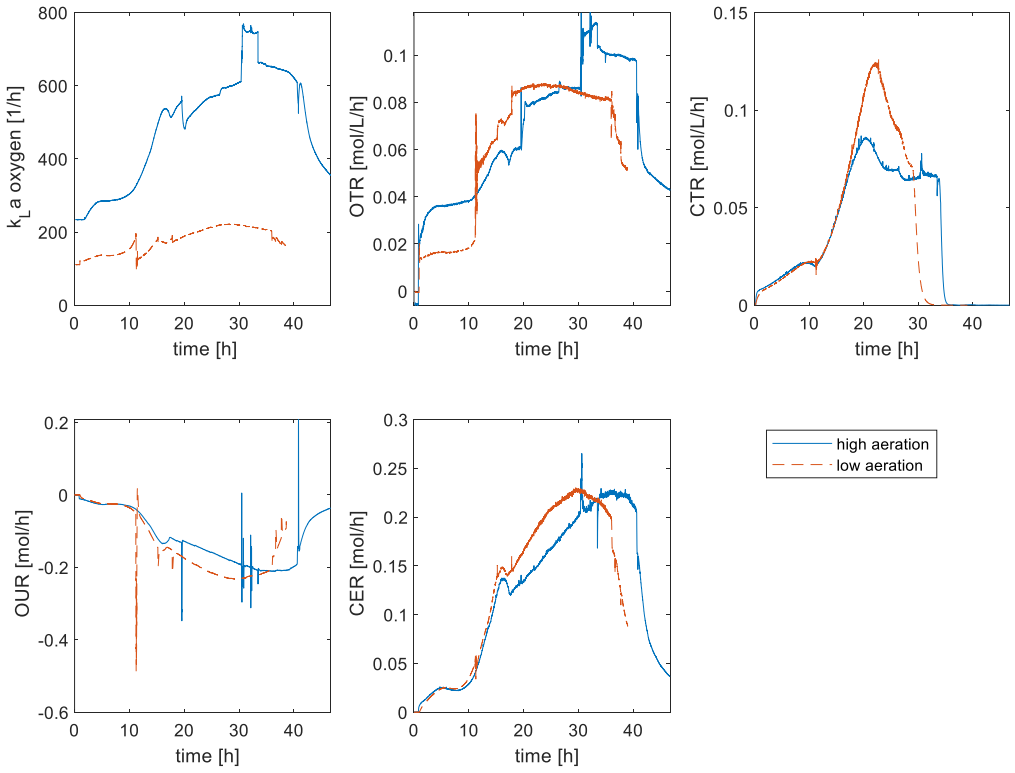

Figure 32: Comparison of simulated kLa, OTR, CTR, and process data of OUR, and CER of high and low aeration of substrate-unlimited fed-batch processes of C. glutamicum ATCC13032 (pOGOduet_mCherry) induced with 0.5 mM IPTG after 13 hours

As an illustration of the calculation of k_La, and subsequently OTR and CTR, the results of the processes of high and low (2) aeration of section 4.4.3.3 were presented in Figure 32. As the k_La value is dependent on the gas flow rate, the reactor with the lower aeration results in way lower k_La values. Although the k_La value of the process with the low aeration was lower, the

OTR and the CTR of both processes are in a comparable range. In the case of the OTR, this is due to the higher oxygen concentration in the gas flow, to obtain the oxygen saturation of 30 % (described in section 4.4.3.1). For CTR it is presumably due to higher carbon dioxide concentration in the medium which increased the transfer rate. Both the measured CER and the OUR are slightly higher for the bioprocess with lower aeration but in a comparable range. Due to a lower k_La combined with a higher CER, presumably higher dissolved carbon dioxide concentration could be reached, see following section 5.5.3.

5.5.3 Oxygen and carbon dioxide concentration in the liquid phase

Figure 24 (section 5.5.1) displays the several reactions of carbon dioxide to different states, like bicarbonate (equation (35) and (36)).

$$CO_2 + H_2O \underset{k_{-1}}{\overset{k_1}{\rightleftarrows}} H^+ + HCO_3^- \tag{35}$$

$$CO_2 + OH^- \underset{k_{-2}}{\overset{k_2}{\rightleftarrows}} HCO_3^- \tag{36}$$

The reaction rates are shown in the following equations (37) and (38) (Spérandio & Paul, 1997).

$$\begin{aligned} r_1 &= k_1\,[CO_2] - k_{-1}\,[HCO_3^-][H^+] \\ &= k_1\,[CO_2] - k_{-1}\,[HCO_3^-]10^{-pH} \end{aligned} \tag{37}$$

$$\begin{aligned} r_2 &= k_2\,[CO_2][OH^-] - k_{-2}\,[HCO_3^-] \\ &= k_2\,[CO_2]10^{pH-14} - k_{-2}\,[HCO_3^-] \end{aligned} \tag{38}$$

$$k_{-1} = \frac{k_1}{K_1} \tag{39}$$

$$k_{-2} = \frac{k_2}{K_2} \tag{40}$$

The regarding equilibrium constants are shown in equations (41) and (42). Those show that the equilibrium between CO_2 and HCO_3^- is highly dependent on the actual pH.

$$K_1 = \frac{[H^+][HCO_3^-]}{[CO_2]} \tag{41}$$

$$K_2 = \frac{[HCO_3^-]}{[OH^-][CO_2]} = \frac{K_1}{K_W} \tag{42}$$

At pH 7 more than 80 % of the carbon dioxide species are present as bicarbonate (Blombach & Takors, 2015). Thus, it is especially important to take the individual species into account for carbon dioxide calculations. As stated before, the bicarbonate concentration is highly dependent on the pH during the process, in comparison with CO_2, which is not influenced by the pH.

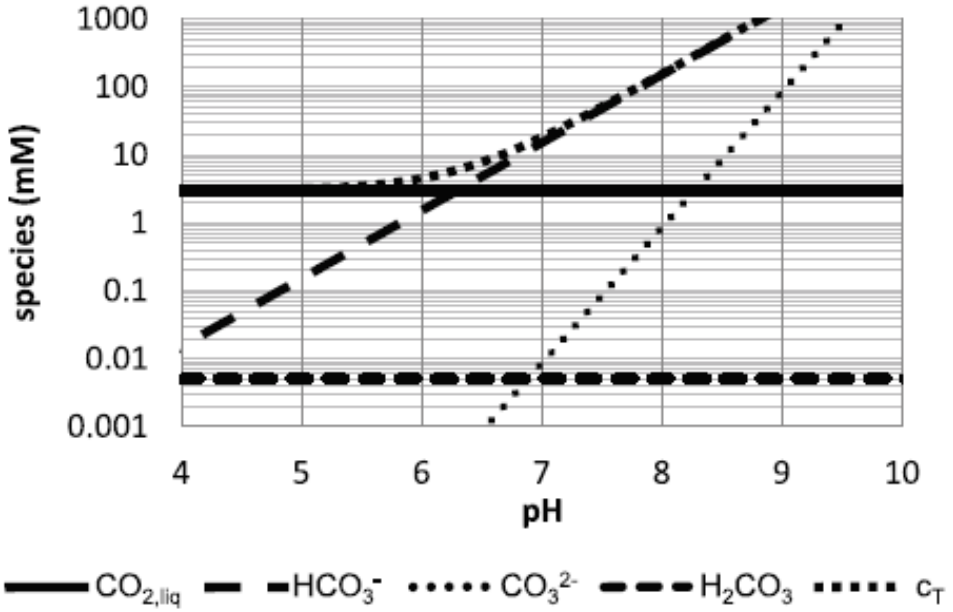

Figure 33: Species of carbon dioxide in water at atmospheric conditions at 25 °C depending on pH; ($CO_{2,liq}$ – concentration of dissolved carbon dioxide, HCO_3^- - concentration of bicarbonate, CO_3^{2-} - concentration of carbonate, H_2CO_3 – concentration of carbonic acid, c_T - total CO_2 dissolved in the suspension (Blombach & Takors, 2015)

The solubility of carbon dioxide is dependent on the partial pressure as described within Henry's law according to equation (43). With the assumption that the partial pressure of carbon dioxide is a product of the carbon dioxide fraction in the gas flow and the total pressure (equation (44)).

$$dCO_2{}^* = \frac{p_{CO_2}}{H} \tag{43}$$

$$p_{CO2} = p_{total} * y_{CO2} \tag{44}$$

The Henry constant is specific for the solute (carbon dioxide or oxygen) and is dependent on the temperature, which can be described by the Van't Hoff correlation, according to equation (45).

$$H = \frac{1}{H^0 * exp^{\Delta H^R * (\frac{1}{T} - \frac{1}{T_0})}} \tag{45}$$

Gas solubility is decreasing with increasing temperature. Dissolved carbon dioxide levels vary from 75 – 375 mg/L (pure water; 37°C), depending on the concentration in the gas phase. In comparison oxygen solubility is much lower, 7.5 – 8 mg/L at atmospheric conditions, depending on the medium composition (Blombach & Takors, 2015).

The carbon dioxide concentrations in the liquid were calculated according to equation (46). It includes the carbon dioxide, which is produced from the culture, the carbon dioxide which is transferred to the gas phase, and the forward and backward reactions of bicarbonate including the pH dependency (Kappelmann, 2018).

$$\frac{ddCO_2}{dt} = CER - CTR - (k_1 + k_2 * 10^{pH-14}) * dCO_2 + (k_{-2} + k_{-1} * 10^{-pH}) * dHCO_3^- \tag{46}$$

Dissolved bicarbonate concentrations were calculated according to equation (47), (Kappelmann, 2018).

$$\frac{ddHCO_3^-}{dt} = (k_1 + k_2 * 10^{pH-14}) * dCO_2 - (k_{-2} + k_{-1} * 10^{-pH}) * dHCO_3^- \tag{47}$$

As an illustration, Figure 34 demonstrates the simulation of the carbon dioxide and bicarbonate concentration of the high aeration process of the substrate-unlimited fed-batch process. As mentioned above dissolved carbon dioxide levels vary from 75 – 375 mg/L or 1.7 – 8.5 mmol/L in pure water at 37°C. Thus, the simulated values of dissolved carbon dioxide in the liquid were in a comparable range.

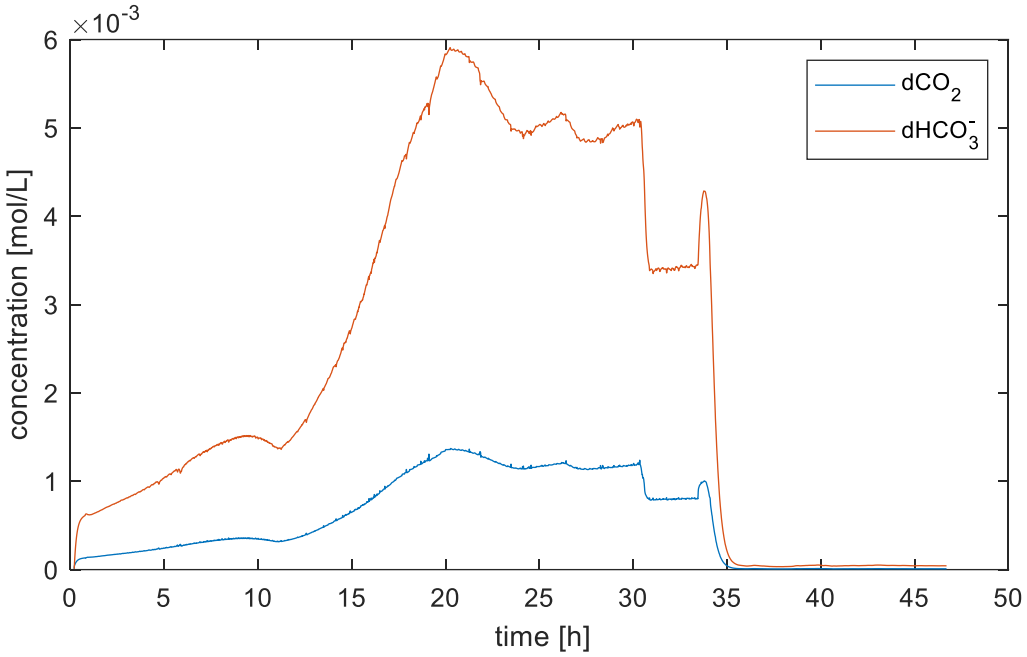

Figure 34: Comparison of dissolved carbon dioxide and bicarbonate of high aeration of substrate-unlimited fed-batch processes of C. glutamicum ATCC13032 (pOGOduet_mCherry) induced with 0.5 mM IPTG after 13 hours

For oxygen similar equations were used (equations (48),(49), and (50); (Kappelmann, 2018)), whereby the dissolved oxygen concentration was imported from the obtained process data because it is a process parameter, that is available in real-time and does not need to be simulated additionally.

$$dO_2{}^* = \frac{p_{O_2}}{H} \tag{48}$$

$$p_{O2} = p_{total} * y_{O2} \tag{49}$$

$$\frac{dO2}{dt} = OTR - OUR \tag{50}$$

5.5.4 Oxygen and carbon dioxide concentration in the gas phase

For parameter estimation of the dissolved carbon dioxide concentration, also the concentrations in the gas phase were simulated. For this issue, a mass flow balance was used to balance the mass transfer with the gas in- and outflow (equations (51) and (53)), (Kappelmann, 2018). To compare the gas concentrations with the obtained process data, the molar fraction was calculated from the partial pressure of oxygen and carbon dioxide, respectively (equations (52) and (54)). The partial pressures were calculated with the aid of the equations (55) and (56), which were used to calculate the gas hold up in the reactor and

the summed up gas flow rate. A ratio between gas hold up and reactor volume of 0.2 was used (Gouveia et al., 2003).

$$\frac{dpCO_2}{dt} = \left((CTR * V) - \frac{F_{gas} * pCO_2}{R * T} + \frac{p_{total} * \frac{y_{CO2\,in}}{100} * F_{air}}{R * T} \right) * \frac{R * T}{V_{air}} \quad (51)$$

$$y_{CO2\,out} = \left(\frac{pCO_2}{p_{total}}\right) * 100 \quad (52)$$

$$\frac{dpO_2}{dt} = \left((-OTR * V) - \frac{F_{gas} * pO_2}{R * T} + \frac{p_{total} * \frac{y_{O2\,in}}{100} * F_{air}}{R * T} + \frac{p_{total} * \frac{y_{O2\_O2in}}{100} * F_{O2}}{R * T} \right) * \frac{R * T}{V_{air}} \quad (53)$$

$$y_{O2\,out} = \left(\frac{pO_2}{p_{total}}\right) * 100 \quad (54)$$

$$V_{air} = \varepsilon * V \quad (55)$$

$$F_{gas} = F_{air} + F_{O2} \quad (56)$$

Figure 35 displays the good approximation which was reached with the simulation of both the molar fraction of carbon dioxide as well as of oxygen in the off-gas. As already mentioned for the CER simulation in section 5.5.1, due to the underestimation of the growth rate after 35 hours of the process (Figure 26), the CER was simulated as zero likewise and thus also the molar fraction of CO_2 decreases sharply after 35 hours in this simulation.

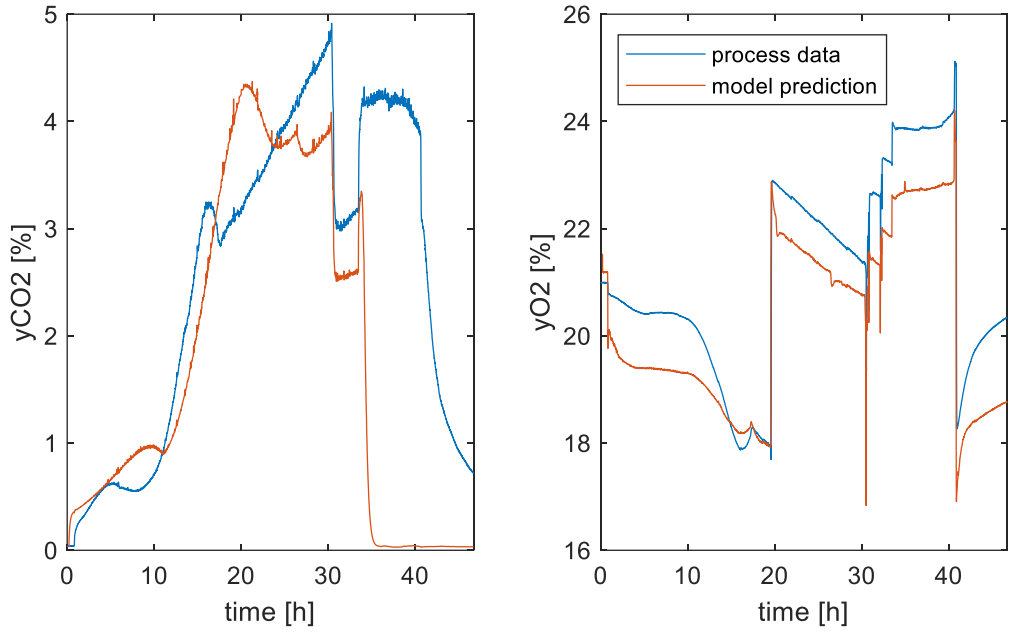

Figure 35: Comparison of process data and simulations of the molar fraction of oxygen and carbon dioxide in the off-gas of a substrate-unlimited fed-batch process with high aeration of C. glutamicum ATCC13032 (pOGOduet_mCherry) induced with 0.5 mM IPTG after 13 hours

The results of the error calculation of the simulated molar fractions compared with the process data are listed in Table 24. The off-gas value of oxygen was simulated with an error below 15 %, which was set as satisfying compared with other simulation literature. The carbon dioxide value was simulated with a higher error of about 30 %, mainly caused by the sharp decrease after 25 hours, due to the underestimation of the CER.

Table 24: NRSME and RSME of the simulation of the molar fraction of carbon dioxide and oxygen in the off-gas of a substrate-unlimited fed-batch process with high aeration of C. glutamicum ATCC13032 (pOGOduet_mCherry) induced with 0.5 mM IPTG after 13 hours

Parameter	NRSME %	RSME %
yCO_2	34.2	1.7
yO_2	13.6	1

A possible improvement of those simulations could be achieved by using real-time process data of CER, if available. Thus, the simulations of both off-gas values could be increased (Figure 36). The NRSME was reduced to 13.2 % and 8.4 % for carbon dioxide and oxygen, respectively.

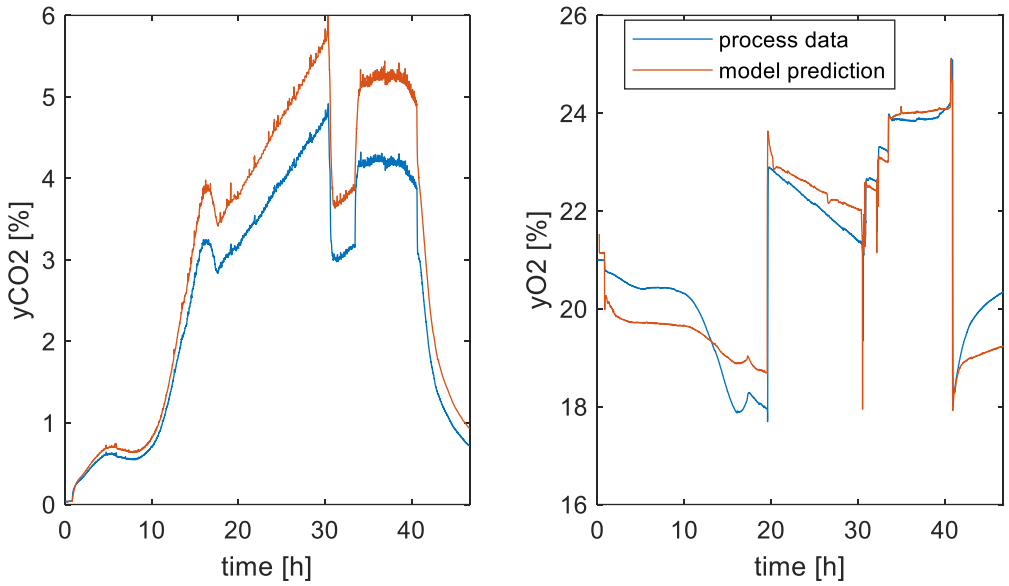

Figure 36: Comparison of process data and simulations of the molar fraction of oxygen and carbon dioxide in the off-gas by using the process data of CER of a substrate-unlimited fed-batch process with high aeration of C. glutamicum ATCC13032 (pOGOduet_mCherry) induced with 0.5 mM IPTG after 13 hours

5.6 Sensitivity analysis for selection of process parameters for affecting dissolved carbon dioxide concentration

To determine which process parameter was suitable to efficiently affect the dissolved carbon dioxide concentration a sensitivity analysis was conducted. Thus, no trial-and-error experiments were needed. As output variables carbon dioxide and bicarbonate were set, as possible process parameters pH, gas flow rate, stirrer speed, and temperature were chosen.

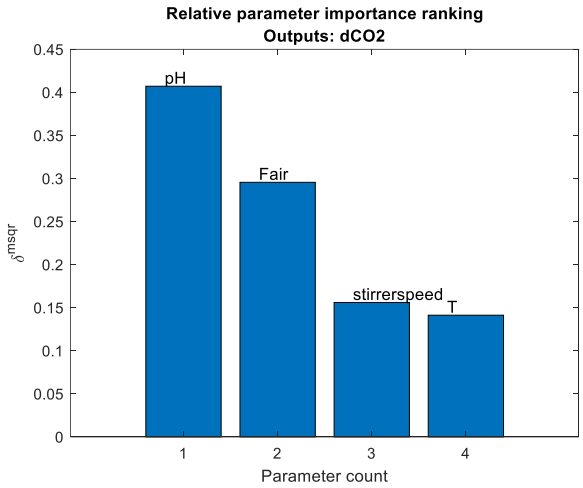

Figure 37: Sensitivity analysis for process parameter determination (1 pH, 2 gas flow rate, 3 stirrer speed, 4 temperature) for affecting carbon dioxide concentration

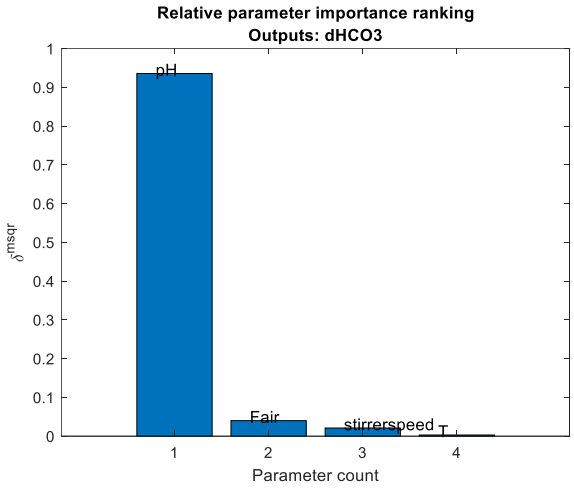

Figure 38: Sensitivity analysis for process parameter determination (1 pH, 2 gas flow rate, 3 stirrer speed, 4 temperature) for affecting bicarbonate concentration

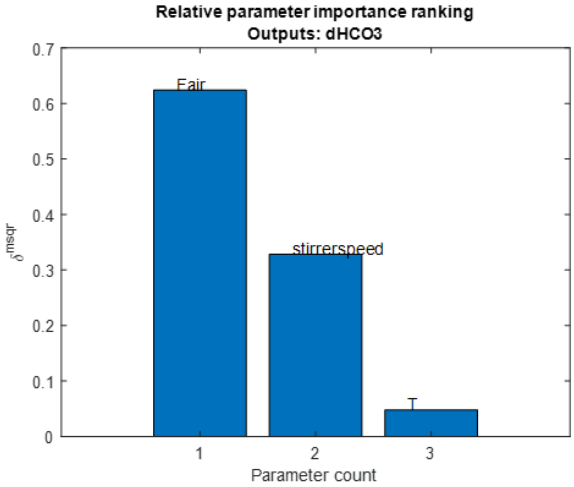

Figure 39: Sensitivity analysis for process parameter determination (1 gas flow rate, 2 stirrer speed, 3 temperature) for affecting bicarbonate concentration (2)

As Figure 37 and Figure 38 show, for CO_2 as well as HCO_3^- pH was the most sensitive process parameter. To select pH as the changing process parameter would have a main disadvantage namely, to affect not only the solubility but may also cell physiology and growth. In addition to that, the equations (46) and (47) show that the pH is mainly responsible for the distribution between CO_2 and HCO_3^-. Since it is not clear which species of those two would be positively contributing via anaplerotic reactions was another reason for not selecting pH as the changing process parameter.

Temperature and stirrer speed showed low sensitivity for the solubility of CO_2 and HCO_3^-. Temperature influences the solubility due to affecting the Henry constant, which is temperature-dependent (see equation (45)). Stirrer speed influences the mass transfer coefficient and thus the mass transfer of carbon dioxide from the liquid to the gas phase (see equations (9), (32), and (33)). Moreover, the temperature would most probably also affect the

metabolism, as Ohnishi et al. (2003) demonstrated for a L-lysine producing mutant of *C. glutamicum*. Thus, those process parameters were also not selected as changing parameters.

As the second sensitive process parameter, the gas flow rate was ascertained. Just as the stirrer speed, the gas flow rate affects the mass transfer of carbon dioxide and thus the concentration of CO_2 and HCO_3^-. Because the sensitivity analysis showed that the gas flow rate had a greater impact on the concentrations, the gas flow rate was chosen as the most promising process parameter to affect dissolved CO_2 concentration during the studied bioprocesses.

5.7 Impact of different aeration rates on growth and product formation during substrate-unlimited fed-batch processes

To compare the effect of different aeration strategies experiments, based on model-based process design in section 5.6, on the growth of *C. glutamicum*, the maximal achievable CDW of four processes were compared. Great differences displayed in the comparison of the maximal achieved DCW of the processes with different aeration strategies (Figure 40). The process with low aeration rate and high antifoam concentration (marked as low (2)) achieved a way higher DCW than the other processes. The lowest CDW was achieved with the process with low aeration but with low antifoam concentration (marked as low (1)).

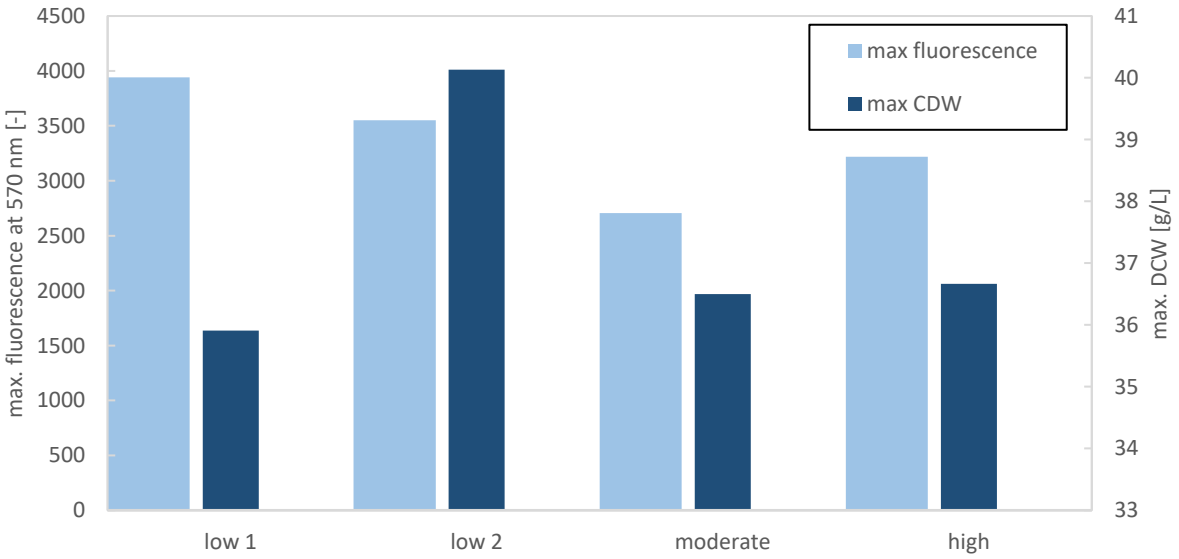

Figure 40: Comparison of maximal achieved fluorescence and DCW values of processes with different aeration rates of substrate-unlimited fed-batch processes of C. glutamicum ATCC13032 (pOGOduet_mCherry) (low (1) – 0.25 L/min, 0.05 mL/L antifoam, induced after 12 hours; moderate – 0.8 L/min, 0.05 mL/L antifoam induced after 15 hours; low (2) – 1.6 L/min, 0.5 mL/L antifoam, induced after 13 hours; high – 1.6 L/min, 0.5 mL/L antifoam, induced after 13 hours)

The different rates of glucose uptake rates, which are illustrated in Figure 41, gave some indications on the stability of the production processes. In the first hours after induction, all four processes showed a comparable uptake rate. The process with high aeration showed the earliest decrease in the uptake rate, but in contrast to that, it showed the latest decrease to zero. The process with low aeration and high antifoam concentration (low (2)) achieved higher uptake rates but decreased to zero the earliest. It seems like the high aeration process was longer stable but the process with low aeration (2) (both with high antifoam concentration) showed higher uptake rates and therefore achieved higher CDW (Figure 40) in a shorter period. The different used antifoam concentrations had a severe effect on growth. This result is in line with Routledge (2012), who observed that certain antifoams affect the growth rates of different organisms.

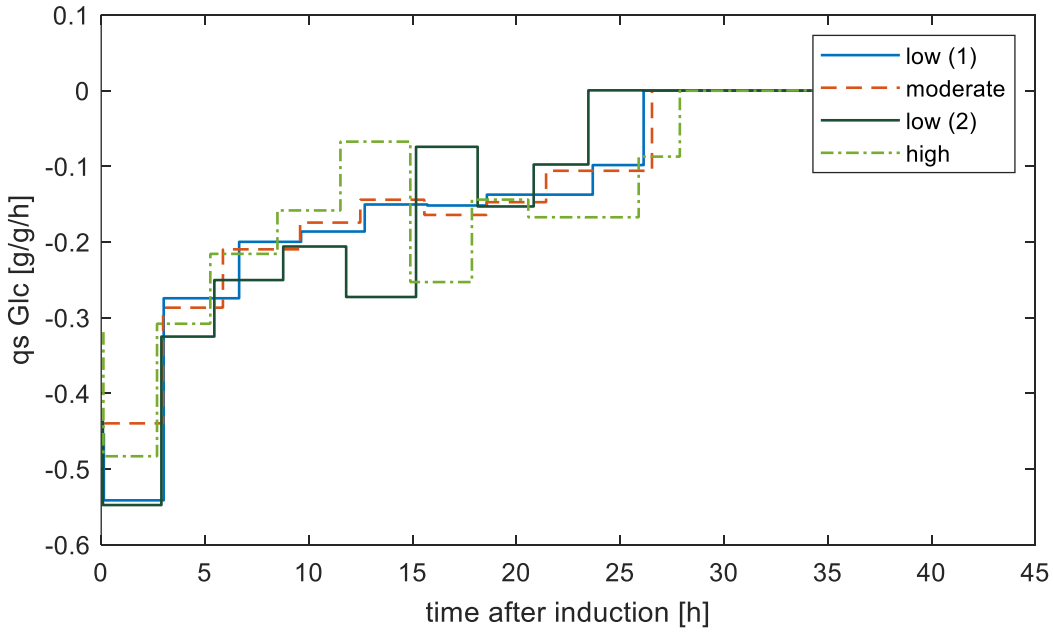

Figure 41: Comparison of glucose uptake rate after induction of different aeration strategies of substrate-unlimited fed-batch processes of C. glutamicum ATCC13032 (pOGOduet_mCherry) (low (1) – 0.25 L/min, 0.05 mL/L antifoam; moderate – 0.8 L/min, 0.05 mL/L antifoam; low (2) – 1.6 L/min, 0.5 mL/L antifoam; high – 1.6 L/min, 0.5 mL/L antifoam)

In Figure 42 the production rates of the different tested aeration rates are shown. The process with a low aeration rate and a low antifoam concentration showed most of the time the highest production rate. In addition to that, it also showed the longest production process stability. The process with a low aeration rate but with high antifoam concentration showed a lower production rate than the low (1) process and the production broke down earlier. This result indicates that also antifoam is an important factor for productivity of this production process, as antifoam influences the CO_2 and HCO_3^- concentration and thus maybe the productivity. The addition of antifoam highly affects the mass transfer of oxygen and presumably carbon dioxide, by affecting the surface tension of the gas bubbles (Doran, 2013). Likewise, Routledge (2012)

concluded that antifoams affecting the growth and also recombinant protein production differently, depending on the type and concentration of antifoam used. The process with low aeration and high antifoam concentration showed a similar production rate than the moderate and high aeration at the beginning of the induction, but after about 15 hours of induction, it showed a higher production rate. The processes with moderate and high aeration displayed similar production rates, but the high aeration process exhibited a longer stable production than the moderate aeration process.

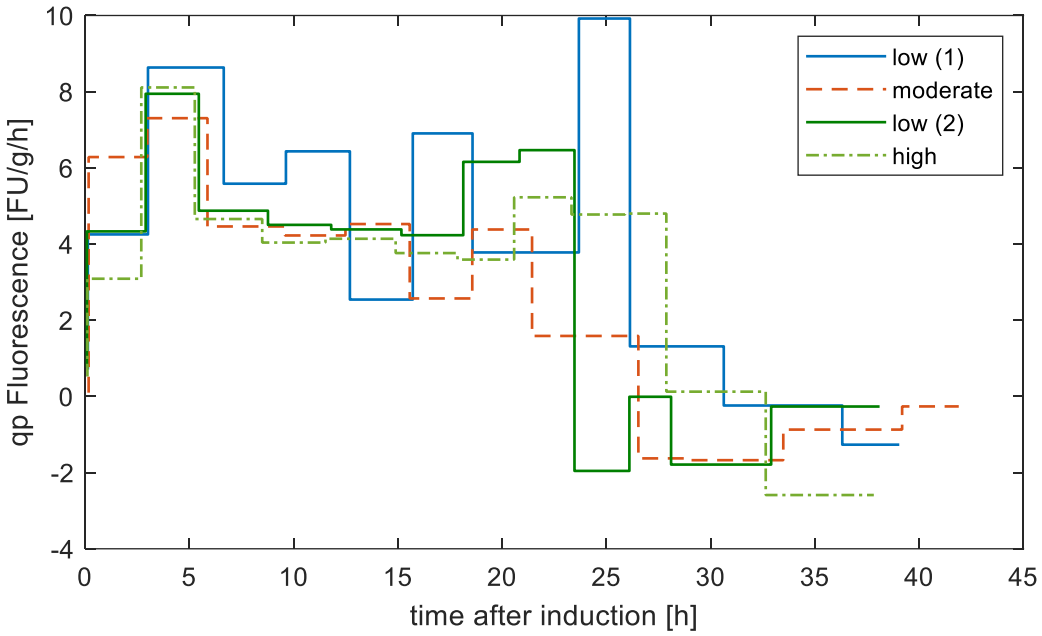

Figure 42: Comparison of production rates of processes with different aeration rates of substrate-unlimited fed-batch processes of C. glutamicum ATCC13032 (pOGOduet_mCherry) (low (1) – 0.25 L/min, 0.05 mL/L antifoam ; moderate – 0.8 L/min, 0.05 mL/L antifoam; low (2) – 1.6 L/min, 0.5 mL/L antifoam; high – 1.6 L/min, 0.5 mL/L antifoam)

The comparison of the maximal achieved fluorescence values (Figure 40), show that both processes with low aeration rate achieved the highest fluorescence values. Likewise, the highest biomass specific fluorescence value was achieved by the process with low aeration (1) (109.7 FU/gX). The processes with high antifoam concentration with low (2) and high aeration achieved comparable biomass specific fluorescence values (88.5 FU/gX and 87.8 FU/gX). As mentioned above the process with low aeration rate and low antifoam concentration displayed the highest production rate thus, it yielded the highest fluorescence value. The high aeration (high antifoam concentration) process achieved a higher fluorescence value than the moderate aeration (low antifoam concentration) process because as stated above it showed a longer stable production phase, this could be a result from the different aeration strategies or the different antifoam concentrations.

If the space-time yields (calculated with equation (20), results displayed in Figure 43) are compared, the moderate and the high aeration process show remarkably similar values. It

seems that those two aeration rates do not influence productivity, maybe because the achieved CO_2 and HCO_3^- concentrations are not different enough to obtain an effect on productivity. The highest space-time yield was achieved during the process, which displayed the highest simulated (section 5.5) dissolved carbon dioxide concentration (low aeration process with high antifoam concentration).

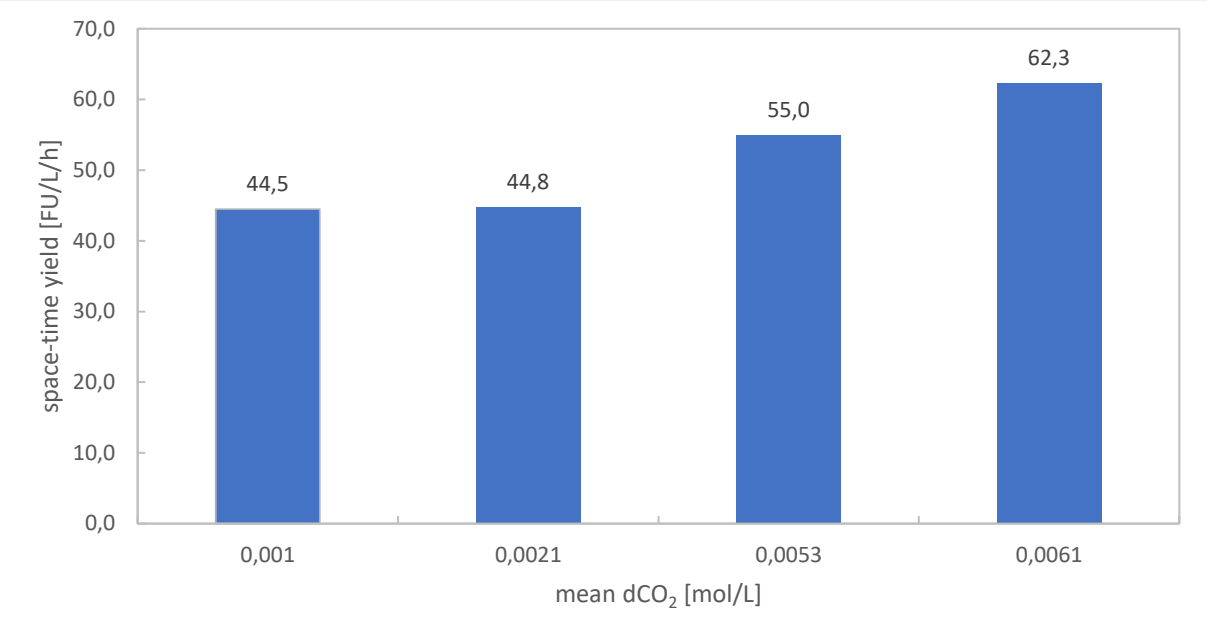

Figure 43: Space-time yields of processes with different aeration rates of substrate-unlimited fed-batch processes of C. glutamicum ATCC13032 (pOGOduet_mCherry) dependent on the achieved simulated mean of dissolved carbon dioxide (from left to right: high – 1.6 L/min, 0.5 mL/L antifoam, induced after 13 hours; moderate – 0.8 L/min, 0.05 mL/L antifoam induced after 15 hours; low (1) – 0.25 L/min, 0.05 mL/L antifoam, induced after 12 hours; low (2) – 1.6 L/min, 0.5 mL/L antifoam, induced after 13 hours)

Although the low aeration process with low antifoam concentration displayed a higher production rate, the low aeration process with high antifoam concentration returned a higher space-time yield value. The space-time yield of the low aeration (2) process was improved by 40 % compared to a standard bioprocess protocol (high aeration). The production rate was determined per g CDW, thus the lower production rate is also caused by the higher achieved CDW during this process. In conclusion, lower aeration rates positively affected the productivity of a mCherry production process in *C. glutamicum*. This was maybe due to higher CO_2 and HCO_3^- concentrations in the culture broth, which were used for anaplerotic reactions. Since in this thesis the dissolved carbon dioxide concentration was enhanced with lower aeration, other factors have to be investigated to verify the hypothesis. For example, the dissolved carbon dioxide concentration could be enhanced by increasing the carbon dioxide concentration in the inlet of the gas flow and other process parameters like stirrer speed and gas flow rate should be kept constant. Thus, influences like varying shear forces, due to different aeration rates could be excluded.

To analyze the protein production an SDS PAGE with time-course samples of the low aeration (1) and the moderate aeration process were conducted. The samples which were used are listed in Table 25.

Table 25: Lane identification of SDS PAGE of the time course of low aeration (1) and moderate aeration protein analysis

SDS PAGE lane	Process	Process time [h]	OD_{600}
1	Low aeration (1)	14	27.3
2	Moderate aeration	24	78.8
3	Low aeration (1)	24	82.7
4	Moderate aeration	30	94.8
5	Low aeration (1)	30	84.6
6	Moderate aeration	38	104.4
7	Low aeration (1)	38	69.2
8		Standard (10-250 kDa)	
9	Moderate aeration	45	75.1
10	Low aeration (1)	45	58.7

The resulting SDS PAGE (Figure 44) showed no identifiable bands in the section of 26.7 kDa (molecular weight of mCherry – see section 3.3) and no increase of bands in course of time were observable. These results may be caused by too low protein concentrations which were reached (detection limit of Coomassie blue staining is about 10 ng), or by incomplete cell lysis, as *C. glutamicum* is a highly stable gram-positive organism (see section 5.9). Maybe a purification step would be needed to enhance the mCherry concentration compared with other cellular proteins.

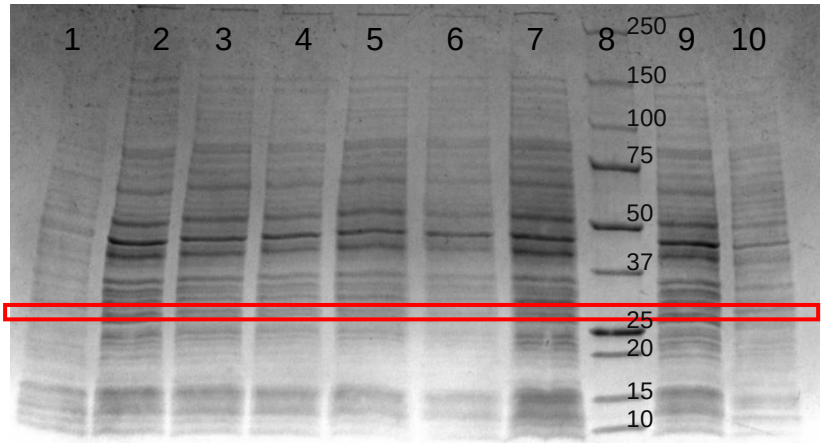

Figure 44: SDS PAGE - time course of low aeration (1) and moderate aeration process, marked section – about 27 kDa, expected observation of mCherry

5.8 Modeling of carbon dioxide influence on productivity

Due to the different results (see section 5.7), caused by the different antifoam concentrations that were used for the different aeration strategies, it was decided to model the influence of carbon dioxide on the productivity only with the data sets of the processes with high antifoam concentration (0.5 mL/L) and high (1.6 L/min gas flow rate) and low (0.25 L/min gas flow rate) aeration.

As described in section 5.5.3, the dissolved carbon dioxide and the bicarbonate were predicted with the model for both processes. As Figure 45 illustrates, the low aeration process displays about a ten-fold higher carbon dioxide and bicarbonate concentration than the high aeration process.

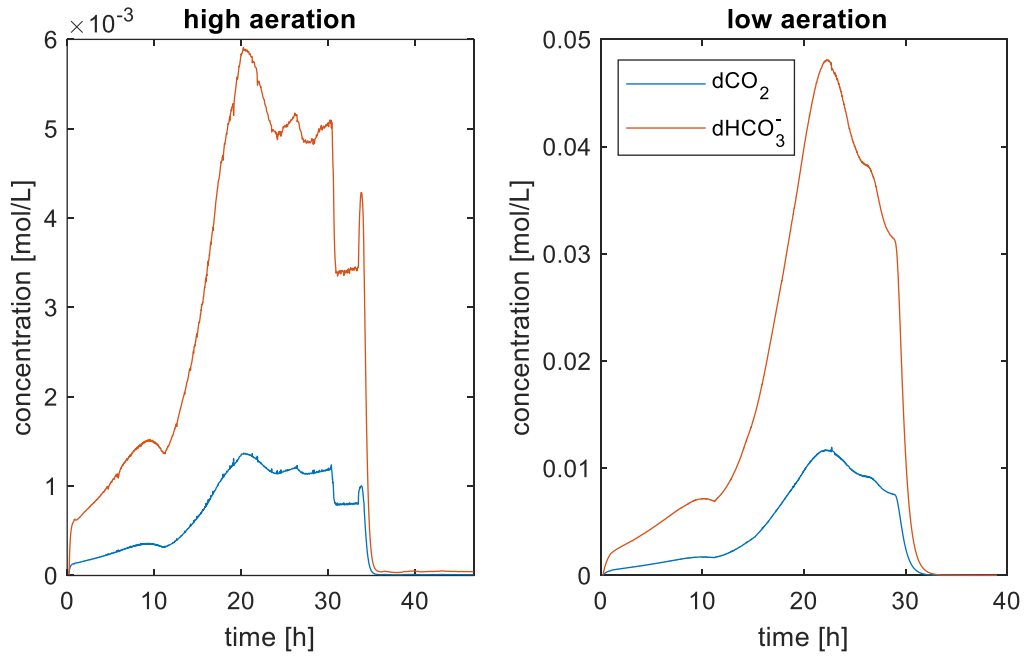

Figure 45: Comparison of dissolved carbon dioxide and bicarbonate of substrate-unlimited fed-batch processes of C. glutamicum ATCC13032 (pOGOduet_mCherry) with high (left diagram) and low (right diagram) aeration both induced with 0.5 mM IPTG after 13 hours

The first approach to model the production rate, was to connect it with the growth rate with the aid of a yield coefficient, according to equation (57). The model parameter 'IPTG' is used as a switching parameter between the uninduced and induced state, thus the production rate simulation started only after induction.

$$q_P = IPTG * q_X * Y_{P/X} \quad (57)$$

As an example, the simulation of the fluorescence values of the glucose-unlimited fed-batch process with high aeration from section 4.4.3.3 is shown in Figure 46. As described in section

5.5.1 for the CER, the production rate gets zero due to the underestimation of the growth rate after 35 hours of process time. This simulation leads to the assumption, that the recombinant production of mCherry in *C. glutamicum* ATCC13032 (pOGOduet_mCherry) is not growth rate connected, thus another model equation had to be found.

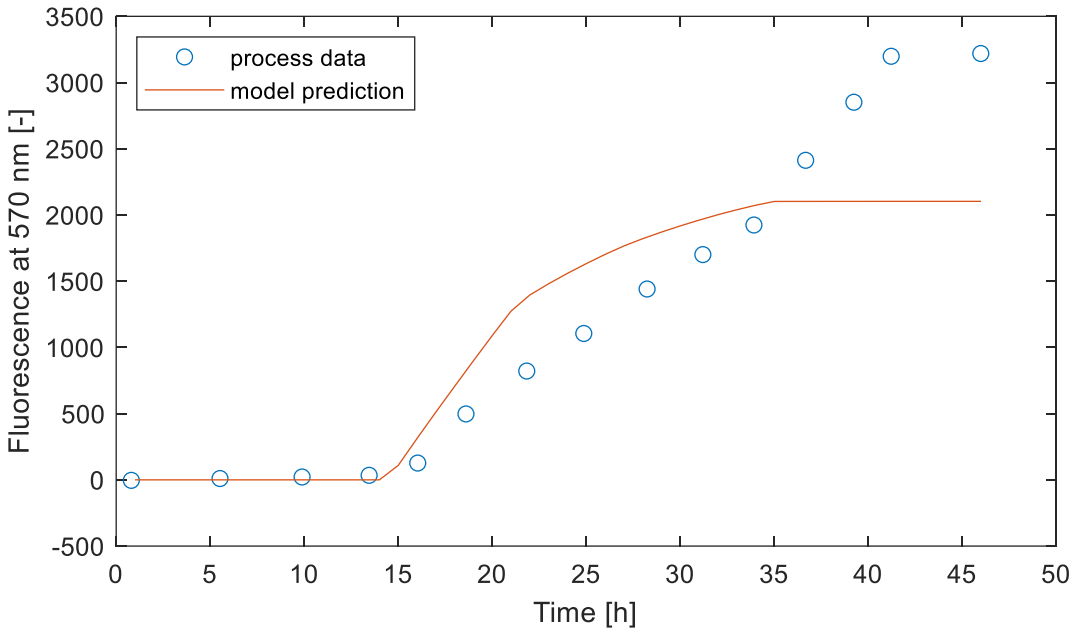

Figure 46: Comparison of process data and simulation of fluorescence values at 570 nm, where production rate is connected with the growth rate, of a glucose-unlimited fed-batch process of C. glutamicum ATCC13032 (pOGOduet_mCherry) with high aeration induced with 0.5 mM IPTG after 13 hours

The next version tried to implement the specific production rate $q_{p,0}$, which describes the production rate per g CDW, thus the more biomass would be built, the more product could be produced (equation (58)).

$$q_P = IPTG * q_{P,0} * X \qquad (58)$$

With the model equation (58), the fluorescence values of the processes could be simulated sufficiently. The calculated NRSME was 8.2 % for the high aeration process and 12.8 % for the low aeration process. Since, with multiple experiment fitting of the model parameter $q_{p,0}$ (5.067 1/g/h), at the process with low aeration the fluorescence values got underestimated compared with the one with high aeration, an equation had to be found to simulate the difference between those aeration strategies.

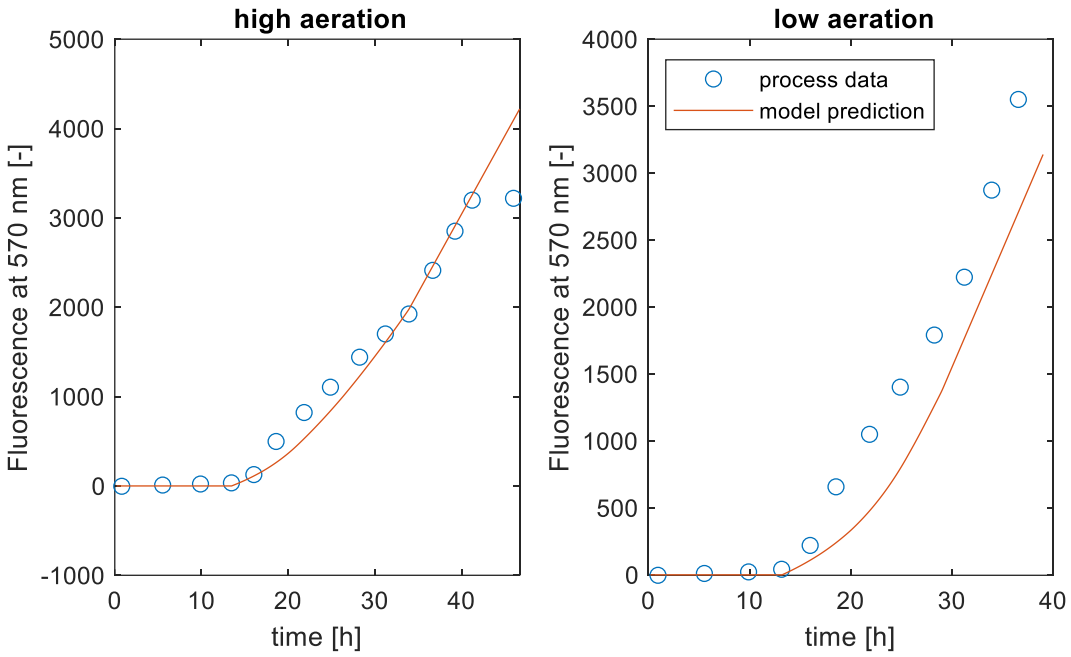

Figure 47: Comparison of process data and simulation of fluorescence values at 570 nm without carbon dioxide connection of a glucose-unlimited fed-batch process of C. glutamicum ATCC13032 (pOGOduet_mCherry) with high (left diagram) and low (right diagram) aeration, both induced with 0.5 mM IPTG after 13 hours

To test the hypotheses, that the dissolved carbon dioxide concentration is the relevant changing parameter, which influences the productivity, equation (59) was used for modeling. This equation includes a reversed inhibition term with the simulated dissolved carbon dioxide during the process, similar to the term mentioned in section 5.4 in equation (26). This should reflect the beneficial effect of carbon dioxide on the production rate.

$$q_P = IPTG * q_{P,0} * X * \frac{K_{CO2} + dCO_2}{K_{CO2}} \qquad (59)$$

With this approach, the calculated NRSME of the fluorescence results were 7.7 % for the high aeration process and 9.5 % for the low aeration process, and thereby accuracy was improved by 6 % and 25 %, respectively. This means an improvement for both process simulations compared with the model without a carbon dioxide connection. Both simulations are displayed in Figure 48.

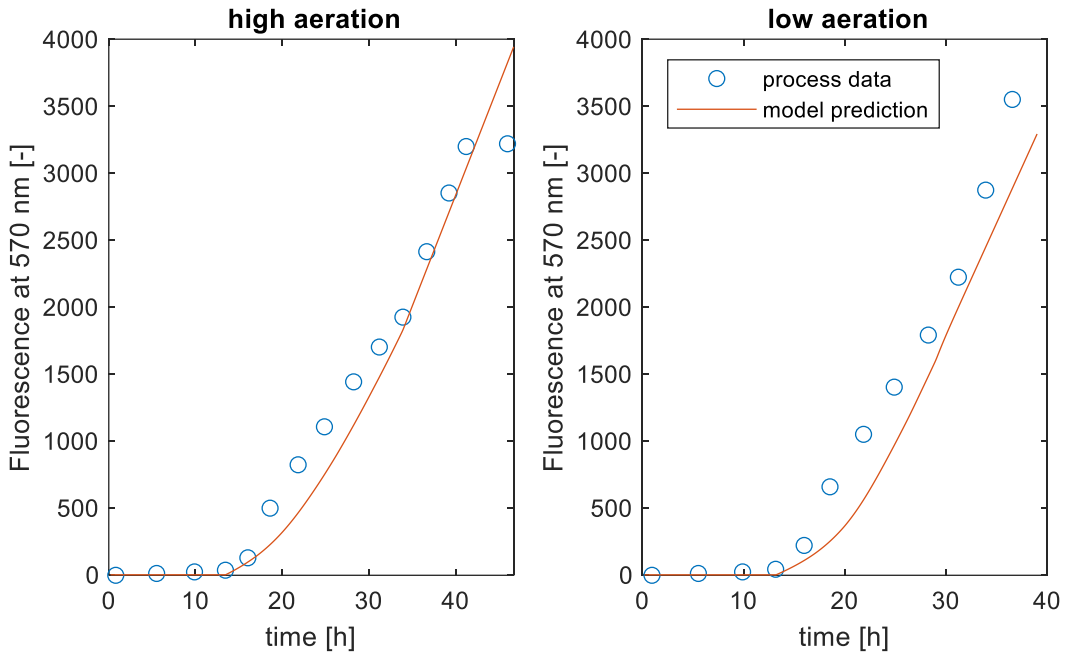

Figure 48:Comparison of process data and simulation of fluorescence values at 570 nm with carbon dioxide connection of a glucose-unlimited fed-batch process of C. glutamicum ATCC13032 (pOGOduet_mCherry) with high (left diagram) and low (right diagram) aeration, both induced with 0.5 mM IPTG after 13 hours

The simulation showed that the hypothesis of the connection between carbon dioxide concentration and productivity might be correct. With the incorporation of this connection, the simulation of the product values was improved.

Sakthiselvan et al. (2020) listed three different types of production rate relationships, growth-associated, non-growth associated, and mixed-growth associated. Equation (58) relates to the growth associated type, equation (59) would also presumably associated with the growth associated type but additionally including another factor on productivity. Another possibility would be the non-growth associated type, where a constant production rate would be implemented in the model, or the mixed type, where both would be combined.

5.9 Comparison of homogenization and sonication as cell disruption methods for C. glutamicum

To compare homogenization and sonication as cell disruption methods, an SDS PAGE with the supernatants and the pellets of the treated samples was conducted.

Figure 49 shows the SDS PAGE gel of the supernatants and Figure 50 the gel of the cell pellets of the different tested conditions. Thus, it was possible to compare the different conditions based on the protein fractions detectable in the supernatant. A higher amount of protein in the supernatant is referenced to better cell disruption.

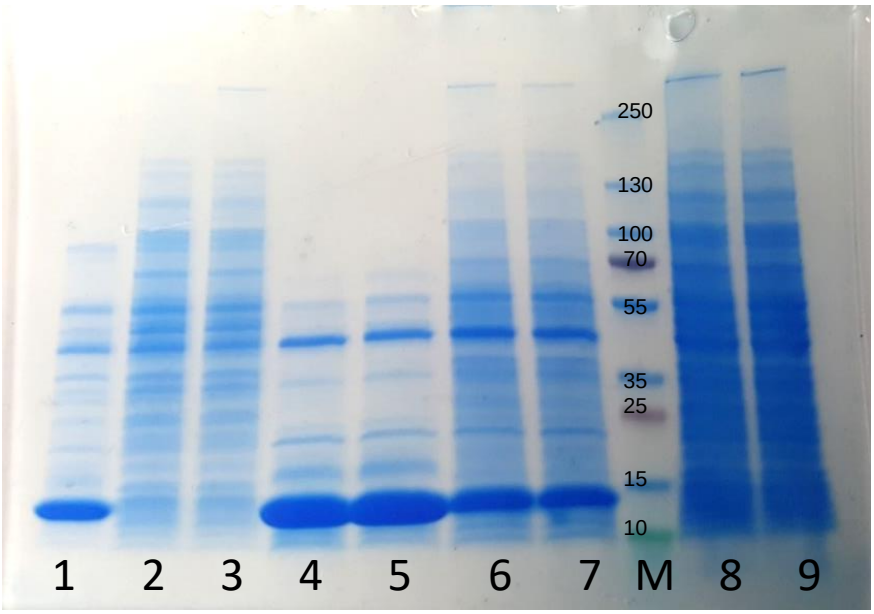

Figure 49: SDS PAGE gel of the supernatants of different tested conditions of cell disruption methods sonication and homogenization of C. glutamicum ATCC13032 cells. Lane 1 – 5 minutes homogenizer with 15 mg/mL lysozyme; Lane 2 – 20 minutes homogenizer; Lane 3 – 5 minutes homogenizer; Lane 4 – 30 minutes sonication with 15 mg/mL lysozyme; Lane 5 – 20 minutes sonication with 15 mg/mL lysozyme; Lane 6 – 30 minutes sonication with 5 mg/mL lysozyme; Lane 7 – 20 minutes sonication with 5 mg/mL lysozyme; Lane 8 – 45 minutes sonication; Lane 9 – 30 minutes sonication; Lane M - PageRuler Prestained marker 10-250 kDa (ThermoScientific, United States)

Lane 8 and 9, which are the samples from the cell disruption with 45 and 30 minutes sonication without lysozyme respectively, seemed to show the highest amount of protein in the supernatant fraction (Figure 49) compared with the other methods. But considering the 2.7 times higher dilution of the homogenization samples, the homogenization methods (20 and 5 minutes) without lysozyme had the best results (lane 2 and 3). The different used periods seemed to not affect the cell disruption efficiency as 45 and 30 minutes sonication and 20 and 5 minutes homogenization showed comparable results on the SDS PAGE gel.

Meissner et al. (2007) described in their work the cell lysis of *C. glutamicum* with sonication after incubation for 120 min with 15 mg/mL lysozyme. In contrast to that, in this experiment, it seems like the lysozyme had a negative influence. Figure 49 and Figure 50 display that fewer proteins were in the supernatant and more in the pellet. This could be caused by aggregation with lysozyme, leading to an insoluble protein complex, which gets separated during centrifugation with the cell membrane residues. The results of this study suggest not to add lysozyme for cell lysis of *C. glutamicum* to prevent aggregation of actual soluble protein fractions.

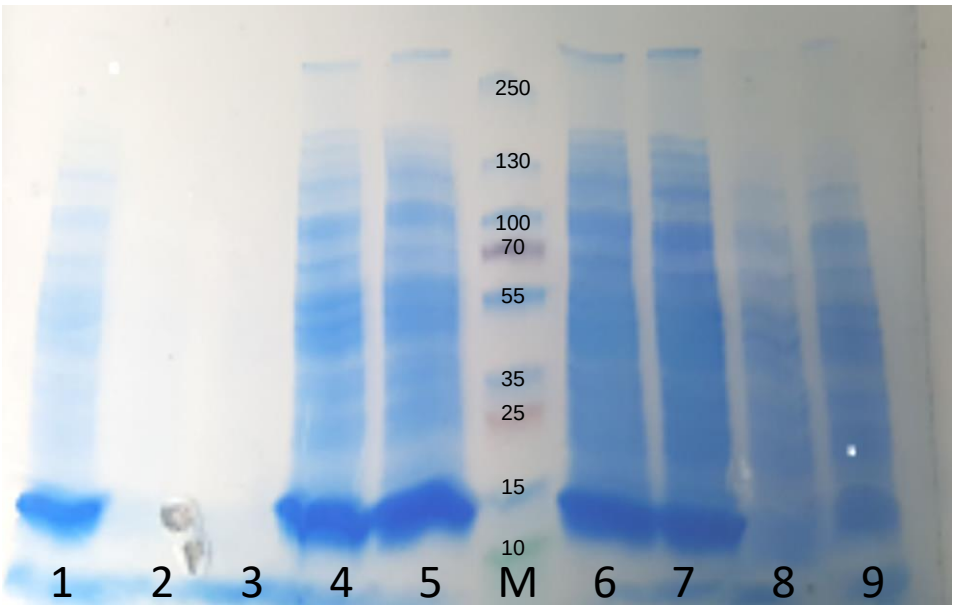

Figure 50: SDS PAGE gel of the pellets of different tested conditions of cell disruption methods sonication and homogenization of C. glutamicum ATCC13032 cells. Lane 1 – 5 minutes homogenizer with 15 mg/mL lysozyme; Lane 2 – 20 minutes homogenizer; Lane 3 – 5 minutes homogenizer; Lane 4 – 30 minutes sonication with 15 mg/mL lysozyme; Lane 5 – 20 minutes sonication with 15 mg/mL lysozyme; Lane 6 – 30 minutes sonication with 5 mg/mL lysozyme; Lane 7 – 20 minutes sonication with 5 mg/mL lysozyme; Lane 8 – 45 minutes sonication; Lane 9 – 30 minutes sonication; Lane M - PageRuler Prestained marker (ThermoScientific, United States)

Although homogenization showed a better yield on the SDS PAGE, sonication was chosen as the cell disruption method for later protein analysis of cultivation samples, due to the higher sample dilution which is needed for homogenization. The minimal sample volume was 15 mL for sonication and 40 mL for homogenization. Small concentrations of proteins were expected and therefore a higher dilution would not have been preferable. Moreover, the sonication method is better reproducible, due to sample handling. During homogenization, it came to sample losses caused by manual rinsing of the homogenizer between each sample. It might be that other cell disruption methods would lead to a more sufficient cell disruption, like disruption with a bead mill. The bead mill approach has been successfully used for *C. glutamicum* from Jansen et al. (2020). As mentioned in this publication, this would be also a good approach for a more automated cell disruption, compared with the sonication lance.

6 Summary and conclusion

Corynebacterium glutamicum is a commonly used host for metabolite production, like amino acids, but is not very established for recombinant protein production. To overcome the current translational or transcriptional limitations of protein production, several approaches to increase the productivity and stability of a recombinant protein production process of *Corynebacterium glutamicum* ATCC13032 (pOGOduet_mCherry) were investigated.

One approach for process improvement was to test various inducer concentrations to investigate possible transcriptional limitations. Those investigations showed no indication of effects neither on the productivity nor on the process stability under the tested conditions. Those results led to the assumption that the recombinant mCherry production process with *Corynebacterium glutamicum* ATCC13032 (pOGOduet_mCherry) is limited by translational and not by transcriptional effects. For further examination, experiments under oxygen-unlimited conditions have to be done, since mCherry maturation is oxygen dependent and oxygen limitations during the bioprocess could have influenced the findings.

To investigate hypotheses regarding energy supply limitations during a recombinant protein production process, two approaches were tested. On the one hand, the effect of unlimited substrate supply and on the other hand the exploitation of anaplerotic reactions were analyzed.

For the first approach, an unlimited and a state-of-the-art substrate limited feeding strategy were compared. It had been shown that the unlimited substrate supply led to increased productivity and a raised space-time yield from 17 FU/L/h to 45 FU/L/h. Since varying substrate concentrations could lead to batch-to-batch variations, an improvement of the used soft-sensor would be recommended. This could be achieved by including the product and by-products into the used simplified stoichiometry.

The exploitation of anaplerotic reactions to increase the yield of recombinant protein production processes with *Corynebacterium glutamicum* ATCC13032 was investigated. Acetate and carbon dioxide as substrates for anaplerotic reactions, to support the metabolism during the increased protein production, were examined. The influence of carbon dioxide or acetate by exploiting anaplerotic reactions on product yields and growth of *Corynebacterium glutamicum* during amino acid or organic acid productions has been investigated before but it was not reported for recombinant protein production previously.

Acetate was used as co-substrate with glucose, and it was tested if it would have a beneficial effect on the productivity or stability of the process, compared with glucose as the sole carbon source. The tested ratio of 0.3:1 acetate to glucose, showed a negative influence on the stability as well as on the productivity of the substrate limited fed-batch process. It has been

previously reported that different acetate to glucose ratios had different effects on the metabolite production process, thus may also in this case another ratio could have led to a beneficial effect and screening could be successful.

To investigate the effect of carbon dioxide a model-based approach was conducted. For in-silico design of the optimal process conditions, a quantitative and dynamic model was developed. To improve the simulation of the process variables biomass and substrate concentration of a substrate-limited fed-batch process, an equation to decrease the glucose uptake rate after induction with the metabolized glucose were included. With this approach, both variables could be predicted with a normalized root-mean-square error below 5 %. Unfortunately, this kinetic description could not be used for the substrate-unlimited processes, presumably caused by different effects of the substrate concentrations on cell metabolism. The biomass concentrations could be predicted with a normalized root-mean-square error below 15 % and the substrate concentration about 45 %. The unsatisfactory simulation of the substrate was caused by an overestimation of the glucose uptake rate after the induction. To improve the model, an equation has to be found to decrease the glucose uptake rate in the right manner. Further improvement was not achievable in course of this thesis.

For the model-based design of the optimal process conditions of the recombinant protein production process, it was necessary to build a model for simulating the dynamics of carbon dioxide in the liquid and the gas phase of the bioreactor and hence investigating the effect of high dissolved carbon dioxide concentrations. To estimate the dissolved carbon dioxide and bicarbonate concentrations, several equations for predicting the carbon evolution rates, transfer rates, and the off-gas concentration were built in the model. The simulated values coincide with the process data. Bigger deviations at the end of the process were caused by the underestimation of the growth rate. It has been shown that the carbon evolution rate is not only growth-connected but also production-related. Thus, for further improving, the production rate has to be included in the equations of the carbon evolution rate simulation. If the carbon evolution rate is available in real-time during the processes, those process data can be used to improve the simulations. The predicted values for the dissolved carbon dioxide concentrations were in a comparable range with literature values. Moreover, the good estimation of the off-gas values of carbon dioxide as well as oxygen, which are directly dependent on the simulated concentrations in the liquid, verifies the model. The model was useful for designing targeted experiments by estimating the different dissolved carbon dioxide levels, which were achieved with different aeration strategies.

The compiled model was used to find the most promising process parameter to affect the dissolved carbon dioxide concentration and to design the optimal testing conditions. Thus, time-consuming trial-and-error experiments were avoided. Various experiments with varying

aeration strategies should investigate the effects on the production and stability of the process by influencing the degassing of the carbon dioxide produced from the bacteria. It has been shown that different antifoam concentrations (0.5 mL/L or 0.05 mL/L) had a great influence on both, may be caused by influencing the transfer rates of oxygen and carbon dioxide, and thereby influencing the carbon dioxide concentration in the liquid. The highest fluorescence values and the highest space-time yields were achieved by the processes with low aeration (0.25 L/min). The space-time yield was improved by 40 % compared with the process with high aeration (1.6 L/min). This is hypothesized to be caused by higher concentrations of dissolved carbon dioxide, which could be used by the microorganism via anaplerotic reactions.

To investigate the effect of the dissolved carbon dioxide concentration on productivity, the initial model was adapted. Different equations were tested to simulate the fluorescence values of mCherry production processes with high (1.6 L/min) and low (0.25 L/min) aeration. It has been shown that the prediction of the fluorescence values could be improved by the integration of a reversed inhibition term with the predicted dissolved carbon dioxide into the production rate equation by 6 % and 25 %, respectively. This promotes the hypothesis that raised carbon dioxide concentrations in the culture medium lead to higher productivity of the mCherry process with *Corynebacterium glutamicum* ATCC13032 (pOGOduet_mCherry).

7 Outlook

The investigations show promising results for the hypothesis, that higher dissolved carbon dioxide concentrations can lead to increased productivity of a recombinant protein production process with *Corynebacterium glutamicum*. With the constructed model, which includes the effect of the dissolved carbon dioxide effect on the production rate, further model-assisted optimization of the production process would be possible in future work. Thus, the process conditions can be designed to attain a minimal degassing of the microbially produced carbon dioxide and achieving maximal productivity. The simulations of the model could be verified and improved with the aid of a dissolved carbon dioxide concentration sensor. This approach could enhance the productivity of further recombinant protein production processes with *Corynebacterium glutamicum* on defined media.

It was shown that unlimited substrate supply would be beneficial for the productivity of a recombinant mCherry production process with *Corynebacterium glutamicum*, but varying substrate concentrations could negatively affect the process repeatability. Thus, the used soft-sensor could be improved by the integration of the product and by-products into the stoichiometry to increase the accuracy of the prediction of the substrate concentration and hereby increasing the process robustness by advanced model-based feeding control enabling constant substrate concentration levels during induction conditions.

8 References

Bastin, G. (1990). *On-line Estimation and Adaptive Control of Bioreactors*. *Process Measurement and Control*. Elsevier Science. http://search.ebscohost.com/login.aspx?direct=true&scope=site&db=nlebk&AN=893327

Bastin, G., & van Impe, J. F. (1995). Nonlinear and Adaptive Control in Biotechnology: A Tutorial. *European Journal of Control*, *1*(1), 37–53. https://doi.org/10.1016/S0947-3580(95)70006-1

Becker, J., & Wittmann, C. (2012). Systems and synthetic metabolic engineering for amino acid production - the heartbeat of industrial strain development. *Current Opinion in Biotechnology*, *23*(5), 718–726. https://doi.org/10.1016/j.copbio.2011.12.025

Bérangère, F., Laurent, P., Agns, P., & Claude-Gilles, D. (2012). Methodology for Bioprocess Analysis: Mass Balances, Yields and Stoichiometries. In A. Innocenti (Ed.), *Stoichiometry and Research - The Importance of Quantity in Biomedicine.* InTech. https://doi.org/10.5772/34673

Blombach, B., Buchholz, J., Busche, T., Kalinowski, J., & Takors, R. (2013). Impact of different CO2/HCO3- levels on metabolism and regulation in Corynebacterium glutamicum. *Journal of Biotechnology*, *168*(4), 331–340. https://doi.org/10.1016/j.jbiotec.2013.10.005

Blombach, B., & Takors, R. (2015). Co2 - Intrinsic Product, Essential Substrate, and Regulatory Trigger of Microbial and Mammalian Production Processes. *Frontiers in Bioengineering and Biotechnology*, *3*, 108. https://doi.org/10.3389/fbioe.2015.00108

BlueSens gas sensor GmbH. (n.d.). *BlueInOne Ferm*. Retrieved September 23, 2020, from https://www.bluesens.com/us/products/gas-analyzers/blueinone-ferm?r=1&cHash=82443a314a55ae15a28cf814418581d2

Boer, H. A. de, Comstock, L. J., & Vasser, M. (1983). The tac promoter: A functional hybrid derived from the trp and lac promoters. *Proceedings of the National Academy of Sciences of the United States of America*, *80*(1), 21–25. https://doi.org/10.1073/pnas.80.1.21

Carroll, P., Muttucumaru, D. G. N., & Parish, T. (2005). Use of a tetracycline-inducible system for conditional expression in Mycobacterium tuberculosis and Mycobacterium smegmatis. *Applied and Environmental Microbiology*, *71*(6), 3077–3084. https://doi.org/10.1128/AEM.71.6.3077-3084.2005

Date, M., Itaya, H., Matsui, H., & Kikuchi, Y. (2006). Secretion of human epidermal growth factor by Corynebacterium glutamicum. *Letters in Applied Microbiology*, *42*(1), 66–70. https://doi.org/10.1111/j.1472-765X.2005.01802.x

Daume, S., Kofler, S., Kager, J., Kroll, P., & Herwig, C. (2020). Generic Workflow for the Setup of Mechanistic Process Models, *2095*, 189–211. https://doi.org/10.1007/978-1-0716-0191-4_11

Doran, P. M. (2013). *Bioprocess engineering principles* (2nd ed.). Academic Press. http://www.sciencedirect.com/science/book/9780122208515

Eggeling, L., & Bott, M. (2005). *Handbook of Corynebacterium glutamicum*. CRC Press. https://doi.org/10.1201/9781420039696

Fromm, H. J., & Hargrove, M. (2012). *Essentials of Biochemistry*. Springer-Verlag Berlin Heidelberg. http://site.ebrary.com/lib/alltitles/docDetail.action?docID=10652586 https://doi.org/10.1007/978-3-642-19624-9

Goldbeck, O., & Seibold, G. M. (2018). Construction of pOGOduet - An inducible, bicistronic vector for synthesis of recombinant proteins in Corynebacterium glutamicum. *Plasmid*, *95*, 11–15. https://doi.org/10.1016/j.plasmid.2018.01.001

Goma, G., Moletta, R., & Novak, M. (1979). Comments on the "Maintenance coefficient" changes during alcohol fermentation. *Biotechnology Letters*, *1*(10), 415–420. https://doi.org/10.1007/BF01388078

Gouveia, E. R., Hokka, C. O., & Badino-Jr, A. C. (2003). The effects of geometry and operational conditions on gas holdup, liquid circulation and mass transfer in an airlift reactor. *Brazilian Journal of Chemical Engineering*, *20*(4), 363–374. https://doi.org/10.1590/S0104-66322003000400004

Graaf, A. A., Eggeling, L., & Sahm, H. (2001). Metabolic engineering for L-lysine production by Corynebacterium glutamicum. *Advances in Biochemical Engineering/biotechnology*, *73*, 9–29. https://doi.org/10.1007/3-540-45300-8_2

Grünberger, A., van Ooyen, J., Paczia, N., Rohe, P., Schiendzielorz, G., Eggeling, L., Wiechert, W., Kohlheyer, D., & Noack, S. (2013). Beyond growth rate 0.6: Corynebacterium glutamicum cultivated in highly diluted environments. *Biotechnology and Bioengineering*, *110*(1), 220–228. https://doi.org/10.1002/bit.24616

Hadj Sassi, A., Deschamps, A. M., & Lebeault, J. M. (1996). Process analysis of l-lysine fermentation with Corynebacterium glutamicum under different oxygen and carbon dioxide supplies and redox potentials. *Process Biochemistry*, *31*(5), 493–497. https://doi.org/10.1016/0032-9592(95)00087-9

Hermann, T. (2003). Industrial production of amino acids by coryneform bacteria. *Journal of Biotechnology*, *104*(1-3), 155–172. https://doi.org/10.1016/S0168-1656(03)00149-4

Inui, M., Kawaguchi, H., Murakami, S., Vertès, A. A., & Yukawa, H. (2004). Metabolic engineering of Corynebacterium glutamicum for fuel ethanol production under oxygen-deprivation conditions. *Journal of Molecular Microbiology and Biotechnology*, *8*(4), 243–254. https://doi.org/10.1159/000086705

Jansen, R. P., Müller, M. F., Schröter, S. E., Kappelmann, J., Klein, B., Oldiges, M., & Noack, S. (2020). Parallelized disruption of prokaryotic and eukaryotic cells via miniaturized and automated bead mill. *Engineering in Life Sciences*, *20*(8), 350–356. https://doi.org/10.1002/elsc.202000002

Kalinowski, J., Bathe, B., Bartels, D., Bischoff, N., Bott, M., Burkovski, A., Dusch, N., Eggeling, L., Eikmanns, B. J., Gaigalat, L., Goesmann, A., Hartmann, M., Huthmacher, K., Krämer, R., Linke, B., McHardy, A. C., Meyer, F., Möckel, B., Pfefferle, W., . . . Tauch, A. (2003). The complete Corynebacterium glutamicum ATCC 13032 genome sequence and its impact on the production of l-aspartate-derived amino acids and vitamins. *Journal of Biotechnology*, *104*(1-3), 5–25. https://doi.org/10.1016/S0168-1656(03)00154-8

Kappelmann, J. (2018). *Tandem Massenspektrometrie getriebene Untersuchung der anaplerotischen Reaktionen in Corynebacterium glutamicum* [, RWTH Aachen University]. DataCite.

Kinoshita, S., Udaka, S., & Shimono, M. (1957). Studies on the amino acid fermentation. *The Journal of General and Applied Microbiology*, *3*(3), 193–205. https://doi.org/10.2323/jgam.3.193

Krause, M., Neubauer, A., & Neubauer, P. (2016). The fed-batch principle for the molecular biology lab: Controlled nutrient diets in ready-made media improve production of recombinant proteins in Escherichia coli. *Microbial Cell Factories*, *15*(1), 110. https://doi.org/10.1186/s12934-016-0513-8

Lambert, T. (n.d.). *mCherry at FPbase*. Retrieved September 23, 2020, from https://www.fpbase.org/protein/mcherry/

Lee, J.-Y., Na, Y.-A., Kim, E., Lee, H.-S., & Kim, P. (2016). The Actinobacterium Corynebacterium glutamicum, an Industrial Workhorse. *Journal of Microbiology and Biotechnology*, *26*(5), 807–822. https://doi.org/10.4014/jmb.1601.01053

Lee, M. J., & Kim, P. (2018). Recombinant Protein Expression System in Corynebacterium glutamicum and Its Application. *Frontiers in Microbiology*, *9*, 2523. https://doi.org/10.3389/fmicb.2018.02523

Liu, L., Yang, H., Shin, H.-D., Li, J., Du, G., & Chen, J. (2013). Recent advances in recombinant protein expression by Corynebacterium, Brevibacterium, and Streptomyces: From transcription and translation regulation to secretion pathway selection. *Applied Microbiology and Biotechnology*, *97*(22), 9597–9608. https://doi.org/10.1007/s00253-013-5250-x

Liu, Y., Schulze-Makuch, D., Vera, J.-P. de, Cockell, C., Leya, T., Baqué, M., & Walther-Antonio, M. (2018). The Development of an Effective Bacterial Single-Cell Lysis Method Suitable for Whole Genome Amplification in Microfluidic Platforms. *Micromachines*, *9*(8), 367. https://doi.org/10.3390/mi9080367

MathWorks Deutschland. (n.d.–a). *Find minimum of unconstrained multivariable function using derivative*. Retrieved September 23, 2020, from https://de.mathworks.com/help/matlab/ref/fminsearch.html

MathWorks Deutschland. (n.d.–b). *Outlier removal using Hampel identifier*. Retrieved September 23, 2020, from https://de.mathworks.com/help/signal/ref/hampel.html

Mazzoleni, S., Landi, C., Cartenì, F., Alteriis, E. de, Giannino, F., Paciello, L., & Parascandola, P. (2015). A novel process-based model of microbial growth: Self-inhibition in Saccharomyces cerevisiae aerobic fed-batch cultures. *Microbial Cell Factories*, *14*(1), 109. https://doi.org/10.1186/s12934-015-0295-4

Meissner, D., Vollstedt, A., van Dijl, J. M., & Freudl, R. (2007). Comparative analysis of twin-arginine (Tat)-dependent protein secretion of a heterologous model protein (GFP) in three different Gram-positive bacteria. *Applied Microbiology and Biotechnology*, *76*(3), 633–642. https://doi.org/10.1007/s00253-007-0934-8

Michel, A., Koch-Koerfges, A., Krumbach, K., Brocker, M., & Bott, M. (2015). Anaerobic growth of Corynebacterium glutamicum via mixed-acid fermentation. *Applied and Environmental Microbiology*, *81*(21), 7496–7508. https://doi.org/10.1128/AEM.02413-15

Mitsuhashi, S., Ohnishi, J., Hayashi, M., & Ikeda, M. (2004). A gene homologous to beta-type carbonic anhydrase is essential for the growth of Corynebacterium glutamicum under atmospheric conditions. *Applied Microbiology and Biotechnology*, *63*(5), 592–601. https://doi.org/10.1007/s00253-003-1402-8

Neuromics. (n.d.). *mCherry Fluorescence Protein Marker or Antibody*. Retrieved September 23, 2020, from https://www.neuromics.com/RA22117

Ohnishi, J., Hayashi, M., Mitsuhashi, S., & Ikeda, M. (2003). Efficient 40 degrees C fermentation of L-lysine by a new Corynebacterium glutamicum mutant developed by genome breeding. *Applied Microbiology and Biotechnology*, *62*(1), 69–75. https://doi.org/10.1007/s00253-003-1254-2

Okino, S., Inui, M., & Yukawa, H. (2005). Production of organic acids by Corynebacterium glutamicum under oxygen deprivation. *Applied Microbiology and Biotechnology*, *68*(4), 475–480. https://doi.org/10.1007/s00253-005-1900-y

Okino, S., Suda, M., Fujikura, K., Inui, M., & Yukawa, H. (2008). Production of D-lactic acid by Corynebacterium glutamicum under oxygen deprivation. *Applied Microbiology and Biotechnology*, *78*(3), 449–454. https://doi.org/10.1007/s00253-007-1336-7

Paczia, N., Nilgen, A., Lehmann, T., Gätgens, J., Wiechert, W., & Noack, S. (2012). Extensive exometabolome analysis reveals extended overflow metabolism in various microorganisms. *Microbial Cell Factories*, *11*(1), 122. https://doi.org/10.1186/1475-2859-11-122

Paegle, L., & Ruklisha, M. (2003). Lysine synthesis control in Corynebacterium glutamicum RC 115 in mixed substrate (glucose-acetate) medium. *Journal of Biotechnology*, *104*(1-3), 123–128. https://doi.org/10.1016/S0168-1656(03)00143-3

Razak, M. A., & Viswanath, B. (2015). Optimization of fermentation upstream parameters and immobilization of Corynebacterium glutamicum MH 20-22 B cells to enhance the production of L-lysine. *3 Biotech*, *5*(4), 531–540. https://doi.org/10.1007/s13205-014-0252-7

Regmi, C. K., Bhandari, Y. R., Gerstman, B. S., & Chapagain, P. P. (2013). Exploring the diffusion of molecular oxygen in the red fluorescent protein mCherry using explicit oxygen molecular dynamics simulations. *The Journal of Physical Chemistry. B*, *117*(8), 2247–2253. https://doi.org/10.1021/jp308366y

Reichelt, W. N., Brillmann, M., Thurrold, P., Keil, P., Fricke, J., & Herwig, C. (2017). Physiological capacities decline during induced bioprocesses leading to substrate accumulation. *Biotechnology Journal*, *12*(7). https://doi.org/10.1002/biot.201600547

Remington, S. J. (2006). Fluorescent proteins: Maturation, photochemistry and photophysics. *Current Opinion in Structural Biology*, *16*(6), 714–721. https://doi.org/10.1016/j.sbi.2006.10.001

Rittmann, D., Lindner, S. N., & Wendisch, V. F. (2008). Engineering of a glycerol utilization pathway for amino acid production by Corynebacterium glutamicum. *Applied and Environmental Microbiology*, *74*(20), 6216–6222. https://doi.org/10.1128/AEM.00963-08

Routledge, S. J. (2012). Beyond de-foaming: The effects of antifoams on bioprocess productivity. *Computational and Structural Biotechnology Journal*, *3*, e201210014. https://doi.org/10.5936/csbj.201210014

Sakthiselvan, P., Sudharsan Meenambiga, S., & Madhumathi, R. (2020). Kinetic Studies on Cell Growth. In B. Vikas & M. Fasullo (Eds.), *Cell growth.* IntechOpen. https://doi.org/10.5772/intechopen.84353

Sasaki, M., Jojima, T., Inui, M., & Yukawa, H. (2010). Xylitol production by recombinant Corynebacterium glutamicum under oxygen deprivation. *Applied Microbiology and Biotechnology*, *86*(4), 1057–1066. https://doi.org/10.1007/s00253-009-2372-2

Shu, X., Shaner, N. C., Yarbrough, C. A., Tsien, R. Y., & Remington, S. J. (2006). Novel chromophores and buried charges control color in mFruits. *Biochemistry*, *45*(32), 9639–9647. https://doi.org/10.1021/bi060773l

Shuler, M. L., & Kargi, F. (2008). *Bioprocess engineering: Basic concepts* (2. ed., 14. print). *Prentice Hall PTR international series in the physical and chemical engineering sciences*. Prentice Hall PTR.

Sinner, P., Kager, J., Daume, S., & Herwig, C. (2019). Model-based Analysis and Optimisation of a Continuous Corynebacterium glutamicum Bioprocess Utilizing Lignocellulosic Waste. *IFAC-PapersOnLine*, *52*(26), 181–186. https://doi.org/10.1016/j.ifacol.2019.12.255

Solle, D., Hitzmann, B., Herwig, C., Pereira Remelhe, M., Ulonska, S., Wuerth, L., Prata, A., & Steckenreiter, T. (2017). Between the Poles of Data-Driven and Mechanistic Modeling for Process Operation. *Chemie Ingenieur Technik*, *89*(5), 542–561. https://doi.org/10.1002/cite.201600175

Spérandio, M., & Paul, E. (1997). Determination of carbon dioxide evolution rate using on-line gas analysis during dynamic biodegradation experiments. *Biotechnology and Bioengineering*, *53*(3), 243–252. https://doi.org/10.1002/(SICI)1097-0290(19970205)53:3<243::AID-BIT1>3.0.CO;2-I

Srivastava, P., & Deb, J. K. (2005). Gene expression systems in corynebacteria. *Protein Expression and Purification*, *40*(2), 221–229. https://doi.org/10.1016/j.pep.2004.06.017

Ulonska, S., Kroll, P., Fricke, J., Clemens, C., Voges, R., Müller, M. M., & Herwig, C. (2018). Workflow for Target-Oriented Parametrization of an Enhanced Mechanistic Cell Culture Model. *Biotechnology Journal*, *13*(4), e1700395. https://doi.org/10.1002/biot.201700395

van Bodegom, P. (2007). Microbial maintenance: A critical review on its quantification. *Microbial Ecology*, *53*(4), 513–523. https://doi.org/10.1007/s00248-006-9049-5

van Waveren, H. (1999). *Good modelling practice handbook*. *Nota: nr. 99.036*. STOWA; Rijkswaterstaat-RIZA; SDU, afd. SEO/RIZA [etc. distr.].

Van't Riet, K. (1979). Review of Measuring Methods and Results in Nonviscous Gas-Liquid Mass Transfer in Stirred Vessels. *Industrial & Engineering Chemistry Process Design and Development*, *18*(3), 357–364. https://doi.org/10.1021/i260071a001

Wendisch, V. F., Graaf, A. A. de, Sahm, H., & Eikmanns, B. J. (2000). Quantitative determination of metabolic fluxes during coutilization of two carbon sources: Comparative analyses with Corynebacterium glutamicum during growth on acetate and/or glucose. *Journal of Bacteriology*, *182*(11), 3088–3096. https://doi.org/10.1128/jb.182.11.3088-3096.2000

Yim, S. S., An, S. J., Choi, J. W., Ryu, A. J., & Jeong, K. J. (2014). High-level secretory production of recombinant single-chain variable fragment (scFv) in Corynebacterium glutamicum. *Applied Microbiology and Biotechnology*, *98*(1), 273–284. https://doi.org/10.1007/s00253-013-5315-x

9 List of figures

Figure 1: Central metabolism of C. glutamicum (Blombach & Takors, 2015); ACC, acetyl-CoA carboxylase; AHAIR, acetohydroxyacid isomeroreductase; AHAS, acetohydroxyacid synthase; AK, acetate kinase; AlaT, alanine aminotransferase; AvtA, valine-pyruvate aminotransferase; CA, carbonic anhydrase; DHAD, dihydroxy acid dehydratase; GDH, glutamate dehydrogenase; GPDH, glucose-6P dehydrogenase; ICD, isocitrate dehydrogenase; MalE, malic enzyme; ODHC, 2-ketoglutarate dehydrogenase complex; ODx, oxaloacetate decarboxylase; PCx, pyruvate carboxylase; PDHC, pyruvate dehydrogenase complex; PEP phosphoenolpyruvate; PEPCk, PEP carboxykinase; PEPCx, PEP carboxylase; PGDH, 6P-gluconate dehydrogenase; PK, pyruvate kinase; PQO, pyruvate:quinone oxidoreductase; PTA, phosphotransacetylase; TA, transaminase B; TPP, thiamine pyrophosphate 9

Figure 2: Fluorescence spectra of mCherry (Lambert, n.d.) 11

Figure 3: Roadmap of the thesis 15

Figure 4: Simplified bioreactor setup with measurements of temperature, pH, and dO_2 and with off-gas analysis and at-line analysis of biomass, substrate, and product. Temperature is controlled with a heating and cooling jacket, the pH with acid and base pumps, and the dO2 with the gas flow controller and the stirrer speed. 22

Figure 5: Feed rate of the substrate-limited fed-batch process with glucose and acetate 23

Figure 6: Feed rate of the substrate-limited fed-batch process with glucose 23

Figure 7: Signal to noise ratio of a fluorescence spectra, calculated with an uninduced and an induced sample of a recombinant mCherry bioprocess with C. glutamicum ATCC13032 26

Figure 8: Design of experiments for the determination of the mass transfer coefficient of bioreactors 30

Figure 9: Comparison of fluorescence measurements values of supernatants and whole broth samples of shake flask cultivation with C. glutamicum ATCC13032 (pOGOduet_mCherry) with 0.5 mM IPTG for determination of product location 33

Figure 10: Time course of CDW measurements of shake flask cultivation of C. glutamicum ATCC13032 (pOGOduet_mCherry) with different inducer concentrations (500 µM, 1000 µM, 200 µM, 100 µM, 20 µM, and 0 µM IPTG) 34

Figure 11: Time course of fluorescence measurements at 570 nm of shake flask cultivation of C. glutamicum ATCC13032 (pOGOduet_mCherry) with different inducer concentrations (500 µM, 1000 µM, 200 µM, 100 µM, 20 µM, and 0 µM IPTG) 34

Figure 12: Comparison of maximal reached fluorescence values at 570 nm of shake flask cultivation of C. glutamicum ATCC13032 (pOGOduet_mCherry) with different inducer concentrations (500 µM, 1000 µM, 200 µM, 100 µM, 20 µM, and 0 µM IPTG) 35

Figure 13: Time course of growth rate and substrate uptake rates of glucose and acetate during substrate-limited fed-batch processes of C. glutamicum ATCC13032 (pOGOduet_mCherry) with and without acetate as co-substrate both induced with 0.5 mM IPTG after 19 hours 36

Figure 14: Time course of production rate during substrate-limited fed-batch processes of C. glutamicum ATCC13032 (pOGOduet_mCherry) with and without acetate as co-substrate both induced with 0.5 mM IPTG after 19 hours 37

Figure 15: Evaluation of the effect of acetate as co-substrate on growth, the maximal fluorescence value, and the space-time yield during substrate-limited fed-batch processes of C. glutamicum ATCC13032 (pOGOduet_mCherry) both induced with 0.5 mM IPTG after 19 hours 37

Figure 16: Schematic overview of the procedure of real-time control of substrate-unlimited feeding strategy.....38

Figure 17: Comparison of calculated growth rate with process data and real-time growth rate of soft-sensor of a substrate-unlimited fed-batch process of C. glutamicum ATCC13032 (pOGOduet_mCherry) induced with 0.5 mM IPTG after 12 hours.....39

Figure 18: Comparison of fluorescence values depending on how much glucose was metabolized and corresponding glucose concentration values during substrate-limited and -unlimited fed-batch processes of C. glutamicum ATCC13032 (pOGOduet_mCherry), induced with 0.5 mM IPTG after 19 and 12 hours, respectively.....40

Figure 19: Comparison of glucose uptake rates of substrate-limited and -unlimited fed-batch processes of C. glutamicum ATCC13032 (pOGOduet_mCherry) induced with 0.5 mM IPTG after 19 and 12 hours, respectively.....40

Figure 20: Comparison of time courses of production rates during a substrate-limited and a -unlimited fed-batch process of C. glutamicum ATCC13032 (pOGOduet_mCherry) induced with 0.5 mM IPTG.....41

Figure 21: Comparison of maximal fluorescence and DCW which was reached during substrate-limited and -unlimited fed-batch process and the resulting space-time yields of C. glutamicum ATCC13032 (pOGOduet_mCherry) induced with 0.5 mM IPTG after 19 and 12 hours, respectively 41

Figure 22: Simulation of DCW, glucose concentration, and q_s of a substrate-limited fed-batch process of C. glutamicum ATCC13032 (pOGOduet_mCherry) induced with 0.5 mM IPTG after 19 hours A: version 1 - decrease of q_s with biomass produced connected with a parameter called 'lag'; B: version 2 – starting with recombinant protein induction, decrease of qs with glucose metabolized with a non-competitive inhibition term; C: version 3 – starting with recombinant protein production, decrease of q_s with glucose metabolized connected with a parameter called 'lag'.....44

Figure 23: Simulation of glucose concentration, DCW, and q_s by multiple experiment parameter fitting of a substrate-unlimited fed-batch process of C. glutamicum ATCC13032 (pOGOduet_mCherry) with high (A) and low (B) aeration induced with 0.5 mM IPTG after 13 hours.....48

Figure 24: Representation of carbon dioxide states in the fermenter (adapted from Spérandio and Paul (1997)).....49

Figure 25: Comparison of process data and simulations of CER and OUR of a substrate-unlimited fed-batch process with high aeration of C. glutamicum ATCC13032 (pOGOduet_mCherry) induced with 0.5 mM IPTG after 13 hours; simulation was done with a connection of CER and OUR with the growth rate 51

Figure 26: Comparison of process data and simulations of the growth rate of a substrate-unlimited fed-batch process with high aeration of C. glutamicum ATCC13032 (pOGOduet_mCherry) induced with 0.5 mM IPTG after 13 hours.....52

Figure 27: k_La results of the reactor (F20) with low antifoam concentration (0.05 mL/L) 53

Figure 28: k_La results of the reactor (F20) with high antifoam concentration (0.5 mL/L).....53

Figure 29: k_La results of the reactor (F10) with low antifoam concentration (0.05 mL/L) 54

Figure 30: k_La results of the reactor (F10) with high antifoam concentration (0.5 mL/L).....54

Figure 31: Comparison of kLa parameter determination of two different bioreactors (F10, F20) with each two different antifoam concentrations (high - 0.5 mL/L and low - 0.05 mL/L) 55

Figure 32: Comparison of simulated kLa, OTR, CTR, and process data of OUR, and CER of high and low aeration of substrate-unlimited fed-batch processes of C. glutamicum ATCC13032 (pOGOduet_mCherry) induced with 0.5 mM IPTG after 13 hours 56

Figure 33: Species of carbon dioxide in water at atmospheric conditions at 25 °C depending on pH; ($CO_{2,liq}$ – concentration of dissolved carbon dioxide, HCO_3^- - concentration of bicarbonate, CO_3^{2-} - concentration of carbonate, H_2CO_3 – concentration of carbonic acid, c_T - total CO_2 dissolved in the suspension (Blombach & Takors, 2015).....58

Figure 34: Comparison of dissolved carbon dioxide and bicarbonate of high aeration of substrate-unlimited fed-batch processes of C. glutamicum ATCC13032 (pOGOduet_mCherry) induced with 0.5 mM IPTG after 13 hours.....60

Figure 35: Comparison of process data and simulations of the molar fraction of oxygen and carbon dioxide in the off-gas of a substrate-unlimited fed-batch process with high aeration of C. glutamicum ATCC13032 (pOGOduet_mCherry) induced with 0.5 mM IPTG after 13 hours 62

Figure 36: Comparison of process data and simulations of the molar fraction of oxygen and carbon dioxide in the off-gas by using the process data of CER of a substrate-unlimited fed-batch process with high aeration of C. glutamicum ATCC13032 (pOGOduet_mCherry) induced with 0.5 mM IPTG after 13 hours.....63

Figure 37: Sensitivity analysis for process parameter determination (1 pH, 2 gas flow rate, 3 stirrer speed, 4 temperature) for affecting carbon dioxide concentration.....63

Figure 38: Sensitivity analysis for process parameter determination (1 pH, 2 gas flow rate, 3 stirrer speed, 4 temperature) for affecting bicarbonate concentration 64

Figure 39: Sensitivity analysis for process parameter determination (1 gas flow rate, 2 stirrer speed, 3 temperature) for affecting bicarbonate concentration (2).....64

Figure 40: Comparison of maximal achieved fluorescence and DCW values of processes with different aeration rates of substrate-unlimited fed-batch processes of C. glutamicum ATCC13032 (pOGOduet_mCherry) (low (1) – 0.25 L/min, 0.05 mL/L antifoam, induced after 12 hours; moderate – 0.8 L/min, 0.05 mL/L antifoam induced after 15 hours; low (2) – 1.6 L/min, 0.5 mL/L antifoam, induced after 13 hours; high – 1.6 L/min, 0.5 mL/L antifoam, induced after 13 hours).....65

Figure 41: Comparison of glucose uptake rate after induction of different aeration strategies of substrate-unlimited fed-batch processes of C. glutamicum ATCC13032 (pOGOduet_mCherry) (low (1) – 0.25 L/min, 0.05 mL/L antifoam; moderate – 0.8 L/min, 0.05 mL/L antifoam; low (2) – 1.6 L/min, 0.5 mL/L antifoam; high – 1.6 L/min, 0.5 mL/L antifoam) 66

Figure 42: Comparison of production rates of processes with different aeration rates of substrate-unlimited fed-batch processes of C. glutamicum ATCC13032 (pOGOduet_mCherry) (low (1) – 0.25 L/min, 0.05 mL/L antifoam ; moderate – 0.8 L/min, 0.05 mL/L antifoam; low (2) – 1.6 L/min, 0.5 mL/L antifoam; high – 1.6 L/min, 0.5 mL/L antifoam) 67

Figure 43: Space-time yields of processes with different aeration rates of substrate-unlimited fed-batch processes of C. glutamicum ATCC13032 (pOGOduet_mCherry) dependent on the achieved simulated mean of dissolved carbon dioxide (from left to right: high – 1.6 L/min, 0.5 mL/L antifoam, induced after 13 hours; moderate – 0.8 L/min, 0.05 mL/L antifoam induced after 15 hours; low (1) – 0.25 L/min, 0.05 mL/L antifoam, induced after 12 hours; low (2) – 1.6 L/min, 0.5 mL/L antifoam, induced after 13 hours).....68

Figure 44: SDS PAGE - time course of low aeration (1) and moderate aeration process, marked section – about 27 kDa, expected observation of mCherry 69

Figure 45: Comparison of dissolved carbon dioxide and bicarbonate of substrate-unlimited fed-batch processes of C. glutamicum ATCC13032 (pOGOduet_mCherry) with high (left diagram) and low (right diagram) aeration both induced with 0.5 mM IPTG after 13 hours ...70

Figure 46: Comparison of process data and simulation of fluorescence values at 570 nm, where production rate is connected with the growth rate, of a glucose-unlimited fed-batch process of C. glutamicum ATCC13032 (pOGOduet_mCherry) with high aeration induced with 0.5 mM IPTG after 13 hours 71

Figure 47: Comparison of process data and simulation of fluorescence values at 570 nm without carbon dioxide connection of a glucose-unlimited fed-batch process of C. glutamicum ATCC13032 (pOGOduet_mCherry) with high (left diagram) and low (right diagram) aeration, both induced with 0.5 mM IPTG after 13 hours....72

Figure 48:Comparison of process data and simulation of fluorescence values at 570 nm with carbon dioxide connection of a glucose-unlimited fed-batch process of C. glutamicum ATCC13032 (pOGOduet_mCherry) with high (left diagram) and low (right diagram) aeration, both induced with 0.5 mM IPTG after 13 hours....73

Figure 49: SDS PAGE gel of the supernatants of different tested conditions of cell disruption methods sonication and homogenization of C. glutamicum ATCC13032 cells. Lane 1 – 5 minutes homogenizer with 15 mg/mL lysozyme; Lane 2 – 20 minutes homogenizer; Lane 3 – 5 minutes homogenizer; Lane 4 – 30 minutes sonication with 15 mg/mL lysozyme; Lane 5 – 20 minutes sonication with 15 mg/mL lysozyme; Lane 6 – 30 minutes sonication with 5 mg/mL lysozyme; Lane 7 – 20 minutes sonication with 5 mg/mL lysozyme; Lane 8 – 45 minutes sonication; Lane 9 – 30 minutes sonication; Lane M - PageRuler Prestained marker 10-250 kDa (ThermoScientific, United States) 74

Figure 50: SDS PAGE gel of the pellets of different tested conditions of cell disruption methods sonication and homogenization of C. glutamicum ATCC13032 cells. Lane 1 – 5 minutes homogenizer with 15 mg/mL lysozyme; Lane 2 – 20 minutes homogenizer; Lane 3 – 5 minutes homogenizer; Lane 4 – 30 minutes sonication with 15 mg/mL lysozyme; Lane 5 – 20 minutes sonication with 15 mg/mL lysozyme; Lane 6 – 30 minutes sonication with 5 mg/mL lysozyme; Lane 7 – 20 minutes sonication with 5 mg/mL lysozyme; Lane 8 – 45 minutes sonication; Lane 9 – 30 minutes sonication; Lane M - PageRuler Prestained marker (ThermoScientific, United States) 75

10 List of tables

Table 1: Media composition 2TY 16

Table 2: Media composition CGXII 17

Table 3: Media composition base 17

Table 4: Media composition acid 17

Table 5: Media composition phosphate-buffered saline 18

Table 6: Media composition trace elements solution 18

Table 7: Media composition 4xLaemli buffer....18

Table 8: Media composition 10xSDS running buffer 19

Table 9: Media composition Coomassie brilliant blue staining solution 19

Table 10: Media composition Coomassie destaining solution....19

Table 11: Media composition lysis buffer....20

Table 12: Shake flask cultivation conditions with different inducer concentrations 21

Table 13: Cell disruption methods – tested conditions of homogenization 27

Table 14: Cell disruption methods – tested conditions of sonication 28

Table 15: Initial parameters for modeling substrate and biomass concentration (Sinner et al., 2019) 43

Table 16: Fitted parameters of simulation with a decrease of qs with biomass produced connected with a parameter called 'lag' 44

Table 17: Fitted parameters of simulation with a decrease of qs with glucose metabolized with a non-competitive inhibition term 45

Table 18: Fitted parameters of simulation with a decrease of qs with glucose metabolized connected with a parameter called 'lag' 46

Table 19: NRSME and RSME of biomass, substrate, and substrate uptake rate simulation with a decrease of q_s with glucose metabolized connected with a parameter called 'lag' of a substrate-limited fed-batch process of C. glutamicum ATCC13032 (pOGOduet_mCherry) induced with 0.5 mM IPTG after 19 hours 47

Table 20: Fitted parameters of simulation of substrate-unlimited fed-batch processes of C. glutamicum ATCC13032 (pOGOduet_mCherry) with low and high aeration both induced with 0.5 mM IPTG after 13 hours 47

Table 21: NRSME and RSME of biomass and substrate simulation with multiple experiment parameter fitting of substrate-unlimited fed-batch processes of C. glutamicum ATCC13032 (pOGOduet_mCherry) with high and low aeration induced with 0.5 mM IPTG after 13 hours 48

Table 22: NRSME and RSME of CER and OUR simulations with mass balancing and growth rate linkage 51

Table 23: Fitted model parameter for k_La calculation of substrate-unlimited fed-batch processes of C. glutamicum ATCC13032 (pOGOduet_mCherry) with 0.5 mL/L antifoam for high and low aeration both induced with 0.5 mM IPTG after 13 hours 56

Table 24: NRSME and RSME of the simulation of the molar fraction of carbon dioxide and oxygen in the off-gas of a substrate-unlimited fed-batch process with high aeration of C. glutamicum ATCC13032 (pOGOduet_mCherry) induced with 0.5 mM IPTG after 13 hours .62

Table 25: Lane identification of SDS PAGE of the time course of low aeration (1) and moderate aeration protein analysis 69

Table 26: List of chemicals 90

Table 27: List of equipment 92

11 Attachments

11.1 Chemicals

Table 26: List of chemicals

Chemical	Company	Article number
3-morpholino propane sulfonacid (MOPS)	Carl Roth, Germany	6979.4
Agar, Bacteriological European Type (Ingredient) for microbiology	AppliChem, Germany	402302.121
Ammonia solution 25 %	Carl Roth, Germany	5460.2
Ammonium sulfate	Carl Roth, Germany	9218.2
Biotin	Carl Roth, Germany	3822.3
Bromophenol	Carl Roth, Germany	3215.1
Calcium chloride dihydrate	Carl Roth, Germany	5239.3
cOmplete Mini, EDTA free	Roche, Switzerland	11836170001
Copper(II) sulfate pentahydrate	Carl Roth, Germany	8175.1
D(+) glucose monohydrate	Carl Roth, Germany	6887.5
Dipotassium hydrogen phosphate	Carl Roth, Germany	P749.3
Disodium hydrogen phosphate dihydrate	Carl Roth, Germany	T877.1
EDTA (Ethylenediaminetetraacetic acid disodium salt dihydrate)	Carl Roth, Germany	8043.1
Glycerol	Carl Roth, Germany	7530.6
Hydrochloric acid 32 %	Carl Roth, Germany	X896.1
IPTG	Carl Roth, Germany	2316.4
Iron(II) sulfate heptahydrate	Carl Roth, Germany	P015.2
Kanamycin sulfate	Carl Roth, Germany	T832.2
Magnesium sulfate heptahydrate	Carl Roth, Germany	8283.3
Manganese sulfate monohydrate	Carl Roth, Germany	7347.1

Chemical	Company	Article number
Nickel(II) chloride hexahydrate	De Haën, Germany	31462
Phosphoric acid 85 %	Carl Roth, Germany	9079.3
Polypropylene glycol P 2,000	SigmaAldrich, United States	81380
Potassium chloride	Carl Roth, Germany	HN02.3
Potassium dihydrogen phosphate	Carl Roth, Germany	3904.3
Sodium acetate	Carl Roth, Germany	6773.2
Sodium chloride	Carl Roth, Germany	3957.2
SDS (*sodium dodecyl sulfate)*	Carl Roth, Germany	2326.5
Tris (tris(hydroxyethyl)amino methane)	Carl Roth, Germany	4855.2
Tryptone (Ingredient) for microbiology	AppliChem, Germany	103682.121
Urea	Carl Roth, Germany	X999.3
Yeast extract	Carl Roth, Germany	2363.5
Zinc sulfate heptahydrate	Carl Roth, Germany	T884.1

11.2 Equipment

Table 27: List of equipment

Device	Company	Type	Specifications
Analytical balance (1)	Mettler Toledo, Switzerland	ME204	max= 220 g d= 0.0001 g
Analytical balance (2)	Sartorius, Germany	TE214S	max= 210 g d= 0.0001 g
Balance	Sartorius, Germany	Extend	max= 8200 g d= 0.1 g
Balance	KERN & Sohn, Germany	KMS-TM	max= 35 kg d= 1 g
Balance Feed	Mettler Toledo, Switzerland	MS8001	max= 8200 g d= 0.1 g
Balance	Sartorius, Germany	CPA34001S	max= 34000 g d= 0.1 g
Balance	KERN & Sohn, Germany	KMS-TM	max= 15 kg d= 0.5 g
Balance reactor	Sartorius, Germany	SIWSDCS-1-35-H	max= 35 kg d= 0.1 g
Balance	Mettler Toledo, Switzerland	PM600	max= 6100 g d= 0.1 g
Sonication	Bandelin, Germany	Sonoplus	-
Sonication lance	Bandelin, Germany	UW 2070	-
Power supply (SDS PAGE)	BIO-RAD, United States	PowerPac Basic	-
Molecular Imager® Gel Doc™ XR System	BIO-RAD, United States	Universal Hood II	-
Photometer	ThermoScientific, United States	Genesys 20	-
Cedex Bio HT Analyzer	Roche, Switzerland	-	-
Fluorescence spectrometer	TECAN, Austria	Infinite M200 PRO	-
Centrifuge	Sigma, USA	3-18KS	-
Centrifuge	Sigma, USA	3-18K	-
Centrifuge	HERMLE Labortechnik GmbH, Germany	Z 36 HK	Max. speed: 30000 1/min

Device	Company	Type	Specifications
Rotary shaker	Infors HT, Switzerland	Multitron Standard	-
dO_2 sensor for Labfors 5	Infors HT, Switzerland	Visiferm Arc 325	-
pH electrode for Labfors 5	Mettler Toledo, Switzerland	32899	diameter: 12 mm, length: 325 mm
Biomass sensor for Labfors 5	Fogale Nanotech, France	iBiomass System 465	DN12, 420 mm
Labfors 5 reactor	Infors HT, Switzerland	Labfors 5 (3.5 L glass vessel)	volume: 3.5 L, stirrer: double 6-blade disc, microbial configuration
Offgas analyzer	BlueSens, Germany	BlueInOne Ferm	-
Offgas analyzer	BlueSens, Germany	BlueInOne Vary	-
Lucullus PIMS	Securecell, Switzerland	-	-
MATLAB	MathWorks, United States	R2019b	-